UiT The Arctic University of Norway

Faculty of Biosciences, Fisheries and Economics
Department of Arctic and Marine Biology

Sympagic-pelagic coupling and vertical export in two seasonally ice-covered fjords

Study of the physical and biological drivers in the sub-Arctic Ramfjorden (Norwegian mainland) and the Arctic Van Mijenfjorden (Svalbard archipelago) during early spring bloom.

Lucie Hélène Marie Goraguer
BIO-3950 Master's thesis in Biology, June 2020

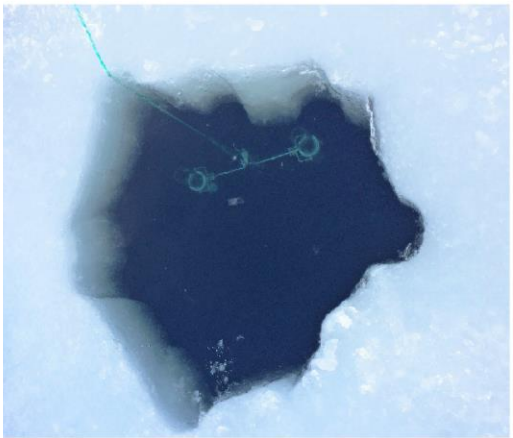

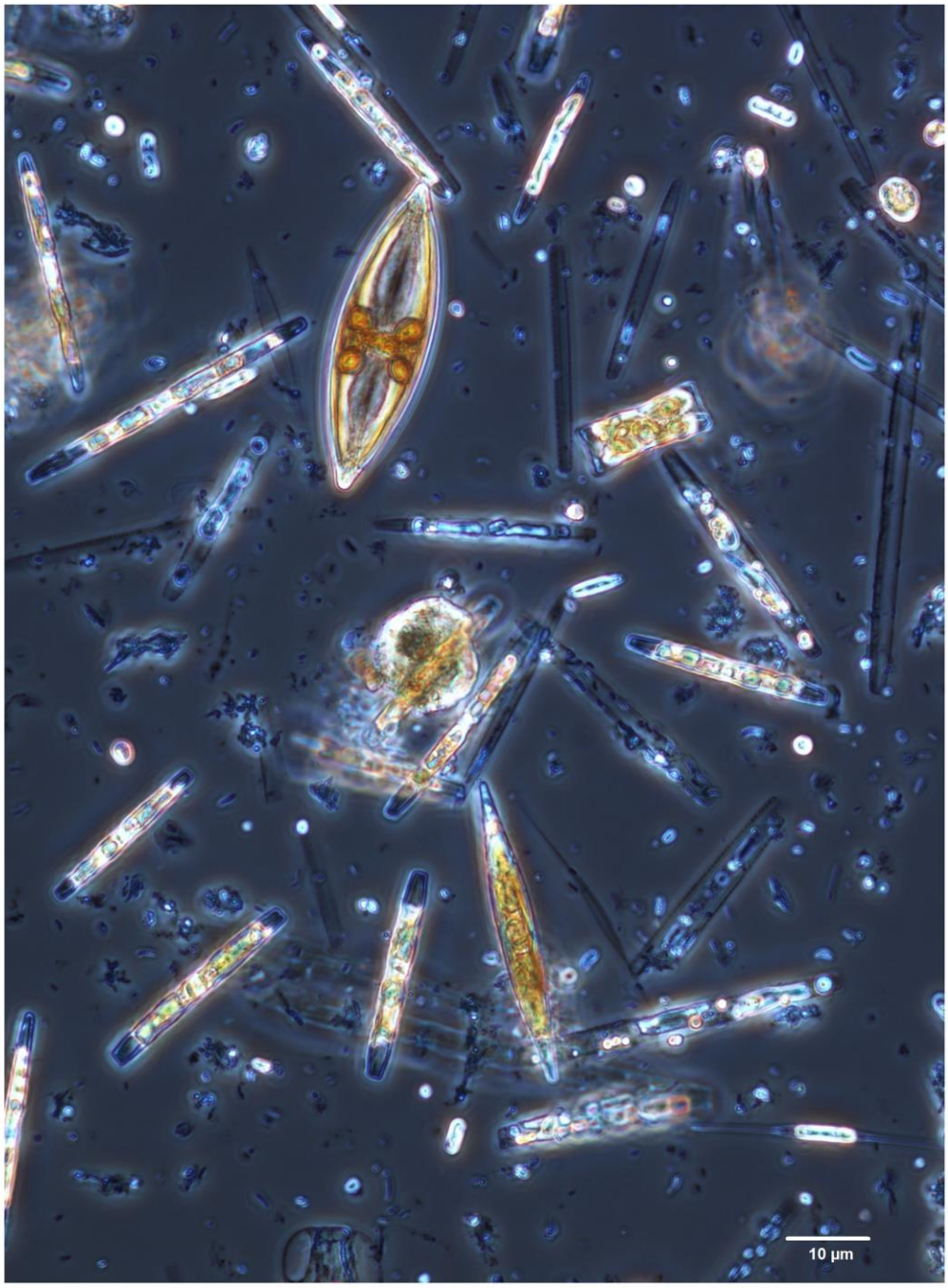

Frontpage - main picture: Sea-ice algae under 400x magnification; left top picture: Ramfjorden station; middle: sediment trap into ice hole; bottom: Colony of *Nitzschia frigida/neofrigida*. © Lucie Goraguer 2019/2020

Table of Contents

Abstract 5
Acknowledgements 6
Abbreviations 7
1 Introduction 1
1.1 Arctic fjords and their hydrography 1
1.2 Sea-ice ecosystem and Arctic spring bloom in fjords 2
1.3 Export of organic material 4
1.4 A changing Arctic coastal system 5
1.5 Aims of investigation & sampling area 6
2 Material and methods 8
2.1 Sampling sites 8
2.1.1 Ramfjorden 9
2.1.2 Van Mijenfjorden 10
2.2 Physical observations 11
2.2.1 Meteorology 11
2.2.2 Snow and sea-ice 11
2.2.3 Hydrographic measurements and observations 13
2.3 Biological observations 15
2.3.1 Sea-ice 15
2.3.2 Water column 21
2.3.3 Sinking biomass 22
3 Results 25
3.1 Physical and hydrographic data 25
3.1.1 Meteorology 25
3.1.2 Snow and sea-ice 25
3.1.3 Water column 27
3.2 Biological data 32
3.2.1 Ice cores 32
3.2.2 Water column 36
3.2.3 Vertical export of biomass 40
4 Discussion 48
4.1 Ramfjorden 48
4.1.1 Ice ecosystem 48
4.1.2 Water column 52
4.1.3 Downward export 56

4.2 Van Mijenfjorden 59
4.2.1 Ice ecosystem 59
4.2.2 Water column 63
4.2.3 Downward export 66
4.3 Fjords comparison 69
5 Conclusion 73
6 References 74
7 Appendix 81

Abstract

Fjords are important high latitudes ecosystems, many have beside planctonic ones, a unique ecosystem associated with seasonal ice cover. During the development of the spring season conditions, two major type of primary producers contribute highly to the biomass production: sea-ice algae inhabiting brine channels and bottom surface of the ice (sympagic algae) and phytoplankton, living in the water column (pelagic algae). The biomass produced by algae is the base of the food web in the fjord ecosystem and is commonly exported to the benthic realm and sequestered at the sea floor. It is still not resolved 1) if autotrophic biomass in the sea-ice, and suspended in or exported from the water column differ in fjords on a short time scale, and 2) how physical processes drive the sympagic-pelagic coupling and sinking biomass in fjords on different latitudes. This study compared the seasonally ice-covered sub-Arctic, Ramfjorden (RMF, 69 °N, 19 °E) in March 2019 with the high Arctic, Van Mijenfjorden (VMF, 77 °N, 16 °E) in April 2019 during the early spring bloom to investigate these questions. Physical oceanographic and meteorologic data, ice cores and water column samples were collected as well as deployment of short-term sediment trap brought together with the chlorophyll *a* (Chl *a*), particulate organic carbon and nitrogen (POC and PON) concentration and the algal community composition in the ice and water column. This revealed that the two fjord systems differed with regard to sympagic-pelagic coupling and export of biomass. Ramfjorden was more impacted by river run-off than Van Mijenfjorden, the truly Arctic fjord. The sea-ice in Ramfjorden was fresher and hold a lower autotrophic biomass and a less rich sea-ice algae community, than the thicker and more saline sea-ice in Van Mijenfjorden. Thus, while the export in Ramfjorden was driven by pelagic species, in the high Arctic Van Mijenfjorden a tighter coupling between the sympagic, pelagic system and the vertical export was found. The short time scale, meteorological and hydrographical factors (e.g., air temperature and under-ice currents) seemed important drivers on the sea-ice, suspended and sinking biomass. In conclusion, the sympagic-pelagic coupling and the link to the vertical export of biomass seems to be very different in seasonally ice-covered fjords on different latitudes and in fjords with unlike freshwater impact.

Key words: sympagic-pelagic coupling, export, vertical flux, suspended biomass, fjord, Arctic, sub-Arctic, sea-ice, microalgae, spring bloom

Acknowledgements

While sea-ice algae are confined to the brine channels whithin the sea-ice, humans are confined to our habitat and facing an uncertain future. Thankfully, during this challenging time and since the beginning of the master, Ingrid, you have supported and guided me through these long processes called master thesis and life. Thank you very much your motivation, your patience and the endless time you have given me. I am very grateful to you. Thank you a lot Angelika for all the help with the fieldwork, the data processing, and all the time you dedicated to me and my project. Thank you Janne for arranging the course and fieldwork on Svea, and giving me the opportunity to study this incredible fjord Van Mijenfjorden. Without you, this project would not have been possible, thank you for introducing me to your respective field of study. Thank you to Józef, to introduce me to this fantastic protists world of the inverted bottom at IOPAN, for the endless hours of microscoping and the knowledge you have imparted to me. Thank you Anna and Agnieszka for your taxonomic help with the protists discussion. Thank you to all the researchers, professors and students during the field and lab work in Ramfjorden and in Van Mijenfjorden. Thank you Bernhard and Daniel for the support in the field and data processing. Thank you Emma for the help and the shared work during the fieldwork.

Abbreviations

ADCP	Acoustic Doppler Current Profiler
ArW	Arctic Water
AW	Atlantic Water
CET	Central European Time
Chl *a*	Chlorophyll *a*
CTD	Conductivity Temperature Depth
DMS	Degrees Minutes Seconds
FSW	Filtered Sea Water
FYI	First-Year Ice
IOPAN	Institute of Oceanology of the Polish Academy of Sciences
MET	Norwegian Meteorological Institute
MYI	Multi-Year Ice
NCC	Norwegian Coastal Current
Phaeo	Phaeophytin
POC	Particulate Organic Carbon
PON	Particulate Organic Nitrogen
RMF	Ramfjorden
UiT	The Arctic University of Norway
UNIS	The University Centre in Svalbard
UTC	Universal Time Coordinated
VMF	Van Mijenfjorden
WCW	Winter-Cooled Water
WSC	West Spitsbergen Current

1 Introduction

1.1 Arctic fjords and their hydrography

Fjords are high-latitude estuaries resulting from the retreat of glaciers and important features of coastlines in the northern and southern hemispheres (Syvitski et al., 1987). By being the link between the land and the ocean, fjords are unique ecosystems along sub-Arctic and Arctic continental shelves (Cottier et al., 2010; Eilertsen et al., 1981).

Fjords are classified by climate regime (after Domack and Mcclemen, 1996), glacier regime (after Hambrey, 1994), and physical features of the fjord (after Howe et al., 2010). They are categorized by three different climate regimes: polar, sub-polar, and temperate (Howe et al., 2010). Characteristics for polar fjords are the permanent ice-cover and presence of a glacier. The current study will focus on sub-polar fjords with mean summer temperature above 0 °C, and seasonal land-fast ice coverage with or without presence of glaciers (Domack and Mcclemen, 1996; Howe et al., 2010). Fjord in the temperate zone, in turn, do not experience seasonal ice cover, but presence of glacier (Howe et al., 2010). All types of fjords are characterised by their unique oceanography. Strongly related to seasonality, water circulation in fjords can have direct influence on exported materials (Cottier et al., 2010). Fjords topography, as the presence of sill at the entrance or shoal, regulate the cross shelf water exchange, by reducing the overall volume of water flowing in, from the coast or from the open ocean (Cottier et al., 2010). Moreover, the width of the fjord determines the rotational dynamics by the Coriolis effect. This effect is limited in narrow fjords, and the bathymetry, plus length influence as well the water masses origin (Cottier et al., 2010). The fjord setting and water circulation conditions are also driven by other topographical conditions, such as runoffs from tidewater glaciers, terrestrial terminating glaciers, and rivers run-off (freshwater discharges) (Skarðhamar and Svendsen, 2010).

In high latitude fjords, the vertical circulation pattern changes seasonally. During summer, these fjords most commonly have a layer structure (Cottier et al., 2010). The top layer is a fresh layer flowing out of the fjord, the intermediate is a saline layer flowing into the fjord and the deepest layer is an isolated layer/basin of high density (Cottier et al., 2010; Inall and Gillibrand, 2010). In contrast, during winter, when temperatures are low, the water masses are overturned by thermal convection. This important process of water masses mixing can also lead to material resuspension (Cottier et al., 2010; Zajączkowski et al., 2010). High latitude fjords may experience the presence of seasonal land-fast ice formation, which can result in the production

of brine. When released, the brine initiates an haline convective overturning, resulting in the homogenisation of the water mass (Cottier et al., 2010). During the period when the fjord is covered by the seasonal land-fast sea-ice, fjord circulation is mostly dependent on ocean tides and freshwater discharges as wind is hindered (Cottier et al., 2010; Luneva et al., 2015). The tides, a periodic motion of the water along the coastlines, in Arctic are mostly semi-diurnal, i.e., two low and high tides each day (Bowditch, 2002; Cottier et al., 2010; Kowalik, 2005). The moon is the most influential body contributing to the M2 tidal constituents (period 12.42 h) (Bowditch, 2002; Kowalik, 2005). The tidal current, defined as horizontal movement of the water, contributes to the vertical and water masses mixing. This can induces the transportation of organic materials and nutrients by lateral advection and resuspension of sedimented material (Inall and Gillibrand, 2010; Kowalik, 2005; Luneva et al., 2015; Thornton and McManus, 1994). During the end of spring, the land-fast ice melts and eventually breaks. This, combined with snow melt, rainfall, river, and increased glacial discharge due to increasing air temperature, leads to the following stratification with a fresher warmer water layer forming (Cottier et al., 2010; Meire et al., 2016).

1.2 Sea-ice ecosystem and Arctic spring bloom in fjords

The biomass production in high latitude fjords is strongly affected by the seasonality, with the Arctic winter being characterized by low biological activity due to the polar night (Leu et al., 2011). However, it has been revealed that despite the absence of photosynthetic activity, there is relatively important biological activity of higher trophic levels during the polar night (Berge et al., 2015). During the unfavourable conditions of absent light, phytoplankton and ice algae are persisting as dormant or active stage suspended in the water column, on the sea floor, and in surrounding older ice (when present) until the light level is sufficient to trigger their growth (Kauko et al., 2018; Sakshaug et al., 2009; Vader et al., 2014).

The algae spring bloom in Arctic fjords is characterized as an high algal concentration, and the onset of this bloom is usually fixed in time (Eilertsen and Taasen, 1984). The spring bloom starts from mid-March and lasts until May/June with often a peak in late April/early May in coastal areas of northern Norway and of West Spitsbergen (Eilertsen et al., 1989; Eilertsen and Taasen, 1984; Hodal et al., 2012).The onset and intensity of the bloom usually depends on the actual conditions. Beside higher solar insolation, which is the dominant factor in high-latitude ecosystems, others factors can be relevant, such as the sea-ice break up, the vertical mixing,

and sometimes, but not always, the presence of stratification (Eilertsen, 1993; Eilertsen and Taasen, 1984; Leu et al., 2015; Sakshaug et al., 2009).

Two major types of primary producers contribute to the algae spring bloom in polar regions: sea-ice algae and phytoplankton. Sea-ice algae live within the ice, mostly in the brine channels, at the surface of the ice, as interior community, or even at the underside of the sea-ice with highest abundance found in the lowermost section of the ice (Horner et al., 1992; Thomas, 2012). The brine channels are established during the ice formation, when the ice matrix dissolves locally due to downward flow of salt expulsion, or brine drainage (Horner et al., 1992). Apart from ice algae, the brine channels are also a habitat for many others sympagic (ice-associated) organisms, e.g., virus, bacteria, fungi, and meiofauna as amphipods, copepods, rotifers, nematodes (Bluhm et al., 2017; Horner et al., 1992)

The Arctic spring bloom develops in three distinct phases (Leu et al., 2015). During the first stage (pre-bloom), the solar irradiance is not sufficient to trigger photosynthetic activity, the community is therefore net heterotrophic. At this stage, the low light level is mainly controlled by ice thickness and snow cover with the latter having strong vertical light extinction coefficient (Perovich, 1990). Although very weak irradiance, specialized ice-algae begin to grow under and within sea-ice (Hancke et al., 2018; Leu et al., 2011). The second stage of the Arctic spring bloom starts when the light level reaching the ice bottom is sufficient to trigger exponential growth and considerable biomass of sea-ice algae, with a system becoming net autotrophic (Leu et al., 2015). The sympagic-pelagic-benthic coupling remains limited due to low flux of sinking material (Leu et al., 2015). Finally, the third stage (post-bloom) starts after the onset of ice melting, with increase of irradiance and temperature into the water column (Leu et al., 2015). The sea-ice algae are, at this point, flushed out of the ice and could continue to growth in the upper water column, sink at greater depths or being grazed (Riebesell et al., 1991). The sea-ice algae bloom is followed by the phytoplankton pelagic bloom and both contribute strongly in sustaining higher trophic levels in the fjords. Especially organic carbon formation and export from surface waters to the oceanic bottom through the sympagic-pelagic-benthic coupling is important in high-latitude fjord ecosystems (Meire et al., 2016; Søreide et al., 2013).

1.3 Export of organic material

The sinking of biomass is a key process of the biological carbon pump by which the photosynthetically fixed particulate organic carbon (POC) sinks from the photic zone to greater depth and possibly, to the benthic realm (Legendre et al., 1992). In general, the vertical carbon export is attenuated with depth by biological and physical transformations and the strongest carbon flux attenuation is found in the upper 200 m of the water column (Wassmann et al., 2003). The sea-ice algae are the main contributors of the POC in coastal first year ice (FYI) (Riedel et al., 2008). However, marine POC also consists of other living material as meiofauna, zooplankton, phytoplankton, heterotrophic bacteria, and detritus (Legendre and Michaud, 1999). The organic matter has different origin, e.g., marine, estuarine, or terrestrial, and the Redfield POC/PON ratio (Redfield et al., 1963) can give a rough idea of the origins. Marine organic matter usually has a POC/PON ratio of 6-9 while terrestrial biomass (e.g., plant fragments) tend to have a POC/PON ratio > 12 (Bianchi, 2006; Thornton and McManus, 1994). A commonly used proxy for the phytoplankton biomass is the photosynthetic pigment chlorophyll *a* (Chl *a*) and its degradation product phaeophytin (Phaeo) (Yentsch, 1965). The POC/PON ratios and additionally the POC/Chl *a* ratios allow to distinguish the algal material contribution and the algae physiological state. High ratio POC/PON and POC/Chl *a* are typical for microalgae with high light acclimation or of microalgae with nitrogen deficiency (Demers et al., 1989; Gosselin et al., 1990; Michel et al., 1996). The POC/Chl *a* ratio of 45 was, for example typically found in healthy algal cells (Passow, 1991) and a ratio of 15 - 180 has been suggested for ice algae (Gosselin et al., 1990). Finally, the ratio Chl *a*/Phaeo allows to estimate the proportion of decomposition products from algal material (Yentsch, 1965).

The spring bloom intensity and its composition of sea-ice algae and phytoplankton drive the strength of the vertical carbon export (Lalande et al., 2016; Søreide et al., 2013). Throughout the spring, the sea-ice species composition changes from heterotrophic protists, including flagellates and dinofagellates, to autotrophic protists with pennate over the centric diatoms (Arrigo, 2014; Von Quillfeldt, 2000). The centric diatoms are often dominant in the phytoplankton bloom, accompanied by pennate, and followed in late summer by the heterotroph protists dominance (Ratkova and Wassmann, 2005; Wassmann et al., 1999). These successions have significant influence in the marine ecosystems through the substantial carbon source for the sympagic and pelagic grazers, as well as the benthic realms (Søreide et al., 2013).

The intensity of the biomass downward flux is further determined by the changing community composition, because the sinking velocity tend to be species-specific (Passow, 1991). The physiologic state of algae can also modify the sinking velocity (e.g., dead cells with higher sinking velocity than senescent diatoms cells and resting stages) and physical transformations as formation of aggregates of particles can enhance the sinking velocity (Miklasz and Denny, 2010; Passow, 1991; Smayda, 1971). The aggregation rates are species specific and healthy cell tend to remain unaggregated (Leventer, 2008). Furthermore, sinking velocity seems independent from particle and shape sources (e.g., different species composition) and aggregation size (Iversen and Ploug, 2010), but another study found the opposite (Laurenceau-Cornec et al., 2015), therefore research is still ongoing. During the post-bloom situation, the more abundant zooplankton population retains the biomass flux by their strong grazing on the algae, even though export can now be mediated by fast-sinking faecal pellets and active downward transport of biomass by vertical migration (Lundsgaard, 1999; Michel et al., 1996; Turner, 2002). Furthermore, the physical processes, as the physical oceanography along with climatic forcing, influence highly the vertical particles flux through episodic event on short time scales (e.g., daily) or on longer scale (e.g., monthly) (Wassmann et al., 1996). The exported flux is impacted by direct mechanisms, as by advection of water masses and mixing, and indirect mechanisms, as the changing algae community composition resulting from effect of freshwater discharge, wind effect, ice cover, etc. (Wassmann et al., 1996). The investigation of the magnitude and composition of algae together with the shape of particles and physical processes allow a better understanding of the potential drivers of the exported material.

1.4 A changing Arctic coastal system

The Arctic recently has experienced a considerable increase in air and sea surface temperature. Consequently, the future of the Arctic sea-ice seems uncertain in the next few decades (Granskog et al., 2016; Wassmann and Reigstad, 2011). Multi-year ice (MYI) has decreased by more than 50 % in the last three decades and nowadays it only tends to cover one third of the Arctic Ocean (Kwok, 2018). The changes in sea-ice cover, that is to say the increase of the seasonal sea-ice, or FYI, over the MYI, will impact the amplification process of Arctic warming. In addition, changes in the surface albedo and ice temperature will cause positive feedback associated with melting of snow and ice (Screen and Simmonds, 2010). All these physical changes will then also affect the productivity, biogeochemical cycle, sympagic-pelagic

and pelagic-benthic coupling in the Arctic (Kwok, 2018; Søreide et al., 2013; Wassmann and Reigstad, 2011).

In the sub-Arctic, the increasing temperature will most likely also influence the spatial and temporal occurrence of the seasonal land-fast ice, which has already been observed in Svalbard fjords with a shorter seasonal ice cover period, or even with fjord becoming year-round ice free (Granskog et al., 2016; Osuch and Wawrzyniak, 2017; Wiedmann et al., 2016). The shrinking and disappearance of seasonal ice will strongly impact the whole fjord ecosystems (Granskog et al., 2016) by affecting the timing, the duration, the magnitude and the composition (e.g., shift in small-sized phytoplankton under warmer conditions) of the algal bloom (Lalande et al., 2016; Leu et al., 2015; Li et al., 2009). Reducing ice and snow thickness will increase light transmittance into the water column which can trigger an earlier spring bloom and lead to a mismatch between the primary producers and secondary producers (Søreide et al., 2010) . The ongoing changes may also impact the downward export of biogenic matter, which will probably reduce the strength of the sympagic-pelagic-benthic coupling and hence the role of carbon sequestration of the fjord ecosystem (Lalande et al., 2016; Smith et al., 2015; Wiedmann et al., 2016). These changes may modify at longer temporal scale, the climate regulation due to high burial of the organic carbon into fjords (Screen, 2014; Smith et al., 2015).

1.5 Aims of investigation & sampling area

The aim of this study was to identify the important drivers of the vertical sinking biomass in two seasonally ice-covered fjords during the early spring bloom. The central focus was therefore on studying the main drivers as the sympagic ecosystem, the pelagic realm, and the composition of the sinking biomass. In addition, this study wanted to characterize to which extent the meteorological drivers, sea-ice physics and the hydrography in the water column drive the downward biomass flux.

The investigation was conducted in two fjords, Ramfjorden, mainland Norway (69 °N), and Van Mijenfjorden, Svalbard (77 °N). These fjords possess similar geomorphologic characteristics (e.g., a shallow sill) and seasonal characteristics (e.g., seasonal land-fast ice cover) and there were therefore well suited for a comparison of the sympagic and pelagic ecosystem over a latitudinal gradient.

The objectives of this study were in particular:

1) To investigate if episodic events on short time scales (e.g., changing currents and weather) can influence on the biomass in ice, in water column and exported
2) To investigate which driver in the sympagic or pelagic system predominatly influences the quality and quantity of sinking biomass in each of the two fjords
3) To study the sympagic-pelagic coupling and the biomass export in two fjords on different latitudes and investigate if similar/different ecological mechanisms can be found in both systems

The hypotheses of this study are:

- In both fjords, the biomass in the sea-ice and the water column and the vertically exported biomass will not differ considerably on a very short time sampling (few days)
- The biomass flux will be mostly related with the water column and impacted by the hydrographical parameters (e.g., higher currents under the sea-ice resulting in a higher biomass flux)
- Both fjords are, due to their similar geomorphology and sampled during (early) spring, characterized by similar concentrations of biomass in the sea-ice and the water column and a similar vertical biomass export

2 Material and methods

2.1 Sampling sites

The fieldwork of the present study was conducted in the inner part of two high latitude fjords, Ramfjorden (RMF, 69 °N, 19 °E), mainland Norway, in March 2019 and in Van Mijenfjorden (VMF, 77 °N, 16 °E), Svalbard, in April 2019 (Table 1). The latter work was done in conjunction with the "Ecosystems in Ice-Covered Water" (AB-330) fieldwork course at The University Centre of Svalbard (UNIS). For each fjord, sampling was conducted twice at the same location. RMF1/VMF1 refer in the following to the first day of sampling and RMF2/VMF2 the second day in each fjord (Table 1). The sampling schedule for the different measurements collected and instruments deployed are presented in the Table 2.

Table 1 Overview of the stations name, locations, maximum bottom depths (m), sampling date, and station label.

Station	Latitude-Longitude (DMS)	Station depth (m)	Sampling date	Label
Ramfjorden (RMF)	69°32'45.528" N 19°11'10.464" E	57.6	14.03.2019– 15.03.2019 18.03.2019 – 19.03.2019	RMF1 RMF2
Van Mijenfjorden (VMF)	77° 50' 56.4" N 16° 42' 21.599" E	55.0	26.04.2019 – 27.04.2019 28.04.2019 – 29.04.2019	VMF1 VMF2

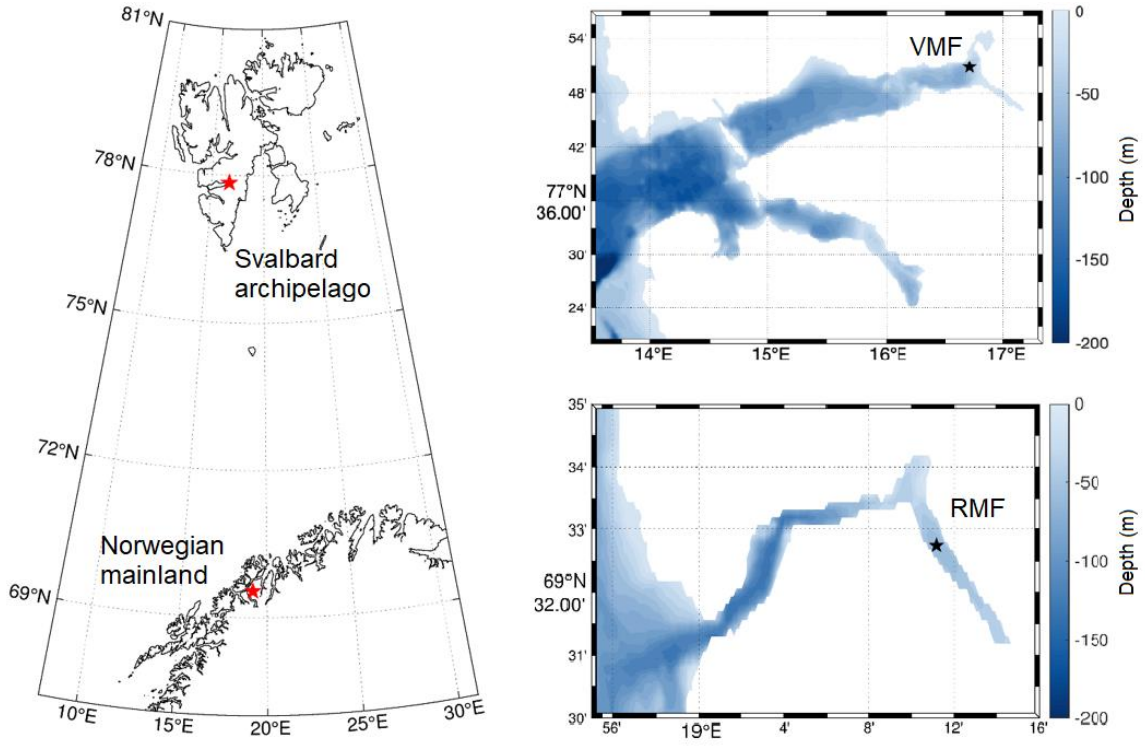

Figure 1. Map showing Ramfjorden and Van Mijenfjorden. The overview map to the left shown Northern Norway in the south and Svalbard archipelago in the north with red stars marking the fjords location. The detailed maps on the right shows VMF (top) and RMF (bottom) stations (black starts) with including bathymetry depth gradient (m). Note the different scale in latitude and longitude gradient.

Table 2. Sampling schedule for the different measurements collected and instruments deployed at the station in Ramfjorden (RMF) and in Van Mijenfjorden (VMF).

Station	Sampling date	Label	CTD deployment	ADCP deployment	Ice core sample	Water column sample	Sediment trap deployment
Ramfjorden (RMF)	14.03.	RMF1	13:13	Deployment: 14:20	14.03.	11:00	Deployment: 14:03
	15.03.	RMF1		Recovery: 09:00			Recovery: 10:00
	18.03.	RMF2	14:15	Deployment: 12:00	18.03.	11:00	Deployment: 13:15
	19.03.	RMF2		Recovery: 15:00			Recovery: 13:45
Van Mijenfjorden (VMF)	26.04.	VMF1	09:10	Deployment: 09:00	26.04.	12:00	Deployment: 14:22
	27.04.	VMF1		ADCP in water			Recovery: 13:30
	28.04.	VMF2		ADCP in water		12:00	Deployment: 17:00
	29.04.	VMF2	14:30	Recovery: 14:00	29.04.		Recovery: 14:20

Vertical hydrographical profiles were taken with a CTD (Conductivity, Temperature, Depth) sonde. The ADCP (Acoustic Doppler Current Profiler) recorded the currents under the sea-ice. All times presented in the table are given in Central European Time (CET), which corresponds to the Universal Time Coordinated (UTC) + 1 h.

2.1.1 Ramfjorden

Ramfjorden is a side fjord of Balsfjorden, in the proximity of Tromsø, Troms and Finnmark county in Northern Norway. Ramfjorden is a narrow fjord with a length of 14 km and a width of about 1 km. It has two main basins. The outer basins is approximately 120 m deep and separated by a sill (25 m) from the inner basin (maximum depth 54 m). Ramfjorden is separated from Balsfjorden by a shallow sill (approximately 28 m deep) (Noji et al., 1993). Balsfjorden is a long and wider fjord (57 km long and average width of 3.5 km). It is winding and with a single-basin. Balsfjorden is separated from the surrounding coastal waters by narrow opening straights and sounds with shallow sills (10-35 m deep) (Hopkins et al., 1989; Reigstad and Wassmann, 1996). It is influenced by the northward flowing Norwegian Coastal Current (NCC), with temperature of 3-5 °C and salinity of 34.8 (Eilertsen and Skarðhamar, 2006) The tides and freshwater inflow from rivers run-off play an important role for the mixing of water masses and water exchange in Balsfjorden (Eilertsen et al., 1981), and as well in Ramfjorden. Due to its location, Balsfjorden is one of the coldest fjords in Norway (Lutter et al., 1989) and Ramfjorden, its sidearm, tends to be ice-covered from November to April. During the winter

2018/2019, when this field study was conducted, Ramfjorden showed a large ice cover area reaching to the outer part of the angle of the arm-shape fjord (Fig. 1).

2.1.2 Van Mijenfjorden

Van Mijenfjorden is located on the west coast of Spitsbergen and it is the second largest fjord system in western Svalbard, with length of 70 km and width of 5-14 km (Gerland and Hall, 2006; Skarðhamar and Svendsen, 2010). It consists of two main basins. The outer basins is 115 m deep and separated by 45 m deep sill from the inner basin of 74 m deep (Skarðhamar and Svendsen, 2010). The entrance of the fjord is almost closed off by a shallow sill (34 m) and Akseløya island (Gerland and Hall, 2006). This geomorphology promotes a longer period of ice cover in Van Mijenfjorden than in other fjords on western Svarbard, because it hinders swell and sea-ice drifting away (Gerland and Hall, 2006). Van Mijenfjorden tends to be ice-covered between November and May/June (Høyland, 2009; Skarðhamar and Svendsen, 2010). The West Spitsbergen Current (WSC) outside Van Mijenfjorden transports warm (>3 °C) and saline (> 34.9) Atlantic water (AtW) which reach the fjord through the narrow strait, Akselsundet passage, (500 m wide and 12 m deep) in the north of Akseløya Island (Cottier et al., 2005; Skarðhamar and Svendsen, 2010). The influx is therefore weak and follow the southern shore of the fjord eastwards by circulating anticlockwise (Gerland and Hall, 2006). Van Mijenfjorden has various freshwater inputs. There are two glaciers calving; Fridtjovbreen in the north of Akselsundet and Paulabreen in Rindersbukta, south branch of the fjord (Skarðhamar and Svendsen, 2010), and lots of rivers entering the fjord. The largest river drains into the fjord from the largest ice-free valley on Svalbard, Reindalen (Skarðhamar and Svendsen, 2010), and in Braganzavagen, the bay in North-East of Van Mijenfjorden (Shestov et al., 2015). The freshwater entering the fjord influence the circulation pattern, and result, especially during the melting season, in lower salinity surface waters (Skarðhamar and Svendsen, 2010). The tides in Van Mijenfjorden have an amplitude of about 50 cm and act with approximately one hour delay compared to the tides prediction in Svalbard (Table A, for tidal prediction chart), due of the inflow and outflow through the narrow straits around Akseløya Island limiting the water masses exchanges (Skarðhamar and Svendsen, 2010).

2.2 Physical observations

2.2.1 Meteorology

The air temperature was recorded by using a hand-held thermometer (TD20, VWR, USA), approximately at mid-day during each sampling. The average daily: temperature (in °C), precipitation (in mm), snow depth (in cm), wind speed (in m s^{-1}) and wind direction (in degrees) were retrieved from eKlima, an open-access climate database (Meteorologisk institutt (MET), 2020) (Table A2). The MET Norway has different stations for Northern Norway and Svalbard. The data were collected from two stations for both sampling areas. In Troms and Finmark county data were used from Breivikeidet station (#91020, 69° 38' 12.12"N, 19° 30' 37.08"E, north-east of Ramfjorden station) and at Tromsø airport (#90490, 69° 40' 36.1194"N, 18° 54' 47.8794”E). On Svalbard, the data were collected from the meteorological station in Sveagruva (#99760, 77° 52' 59.88"N, 16° 43' 0.1194"E, at the head of Van Mijenfjorden) and at the airport in Longyearbyen (#99840, 78° 14' 43.08"N, 15° 30' 5.4"E). In addition, daily estimates (in m^3 s^{-1}) of the river freshwater discharge into Ramfjorden were retrieved from the Norwegian Water Resources and Energy Directorate through their updated data series from all catchment areas in Norway (NVE, 2020). These data series use measured water flows to estimate the total run off along the coastline within each catchment area. Data was extracted in March 2020 (Fig. A1).

2.2.2 Snow and sea-ice

The snow depth was determined at three arbitrary points at the sampling stations by placing a ruler through the snow cover down to the ice. The ice thickness was measured by measuring the length of each extracted ice core with a measurement tape. The freeboard, defined as the distance between the sea water surface and the ice surface, was measured with a ruler at three arbitrary ice core holes. The freeboard is negative when the snow thickness exceeded the hydrostatic equilibrium and pushes the ice below the sea level (Arrigo, 2014).

On each sampling day, two ice cores were collected for the physical parameters. A KOVACS ice corer (ø 9 cm) was used to extract the ice cores. The first ice core was used to determine the in-situ sea-ice temperature. The same hand-held thermometer as used to record the air temperature was placed in pre-drilled holes in the ice core, reaching halfway (~4.5 cm) into it. These measurements were made in the shade to avoid alteration of the measured temperature. The following intervals were recorded, starting from the bottom (sea-ice/ water interface) of the ice core towards the top (sea-ice/ snow or air interface): 2, 5 cm and every 5 cm intervals

for Ramfjorden and 1, 2, 3 cm, and every 10 cm intervals for Van Mijenfjorden. The second ice core was used to determine the bulk salinity, by measuring the electrical conductivity of the thawed ice-core samples (Eicken, 2009).

The processing of the ice cores was somewhat different during the field work in Ramfjorden and in Van Mijenfjorden according the difference in ice thickness. All ice cores were cut into sections using a saw and cutting always started at the bottom of the ice and continued towards the top. At RMF1 and RMF2, the following sections were cut: 0-3 cm, 3-10 cm, and every 10 cm intervals (10-20, 20-30, 30-Top), while at VMF1 and VMF2 the sections 0-3; 3-10; 10-20, and every 20 cm intervals (20-40, 40-60; 60-Top) were cut. The ice core sections were stored in sealed plastic bags and melted overnight at room temperature. The salinity was measured using a conductivity meter (Symphony SP90M5, Handheld Salinity Meter with Probe, VWR, USA).

The bulk salinity and the in-situ temperature of the ice cores were used to calculate the brine salinity and brine volume by using two different equations for greater accuracy of the derived values. Each equations were used depending if the in-situ sea-ice temperature was below or above – 2 °C.

For sea-ice temperature below – 2 °C, equations (1) and (2) following the calculations by Cox and Weeks (1983) were used:

$$Sb = \frac{1000}{\frac{1-54.11}{in\ situ\ Tice}} \qquad \text{(Eq. 1)}$$

with S_b being the brine salinity and in-situ T_{ice} being the temperature in the ice core in °C.

$$Vb = Sice * \frac{0.0532-4.919}{in\ situ\ Tice} \qquad \text{(Eq. 2)}$$

with V_b being the brine volume in %, S_{ice} representing the bulk salinity of the ice core sections.

For sea-ice temperature between – 2 °C and 0 °C, equations (3) and (4) following the calculations by Leppäranta and Manninen (1988) were used:

$$Sb = \alpha 0 + \alpha 1 * \mathrm{Tice} + \alpha 2 * (\mathrm{Tice})^2 + \alpha 3 * (\mathrm{Tice})^3 \qquad \text{(Eq. 3)}$$

with S_b being the brine salinity and T_{ice} being the temperature in the ice core in °C. The set of coefficients α0, α1, α2 and α3 can be found can in Leppäranta and Manninen (1988).

$$Vb = \frac{\rho\, S}{F1(T) - \rho\, S\, F2(T)} \quad \text{(Eq. 4)}$$

Here, V_b represents the brine volume (%), ρ the density of pure ice, S the bulk salinity, T the temperature in the ice core in °C, F1(T) and F2(T) the empirical polynomial functions of temperature based on phase relations in the ice. The set of coefficients can be found in Leppäranta and Manninen (1988).

2.2.3 Hydrographic measurements and observations

Water column

The hydrographic measurements of the water column were done by using a portable CTD (CastAway-CTD model in Ramfjorden and SAIV A/S CTD, model SD208 in Van Mijenfjorden). The CTDs were manually lowered at a speed of approximately 1 m s^{-1} from the water surface to few meters above the seabed, taking one measurement every second. The CTD collects data on conductivity (S m^{-1}) (which is converted to the salinity), temperature (°C), and depth (m). In addition, a fluorescence sensor (Chelsea Technologies Group, Ltd., UK) was mounted on the SAIV CTD, providing measurements of the fluorescence. The fluorometer data were calibrated by discrete water sample, the Chl *a* concentration (µg L^{-1}), by plotting the fluorescence against the Chl *a* concentration at the same sampled depth (1, 5, 15 and 30 m). From this plot, the slope coefficient (α = 0.87) of the linear trend line was used to multiplied the fluorescence data retrieved from the fluorometer, to obtain the fluorescence calibrated and estimated the Chl *a* concentration in the whole water column (Fig. A1).

The CTD data were retrieved and plotted with RStudio, Inc (version 1.1.463) and R (version 3.6.3) using the package *oce* (version 1.1.1). The density in Ramfjorden and Van Mijenfjorden was calculated and plotted using the function seawater density (swSigma) from the *oce* package in R using the UNESCO equation of state of seawater. In addition, the calibrated fluorescence (= Chl *a* concentration) was plotted for Van Mijenfjorden station.

To obtain the water temperature under the sea-ice for the period of the sediment trap deployment, a subsea temperature logger (Starmon mini, Star Oddi) was attached to the rope of the sediment trap array at 1 m. The logger measured the temperature every 10 min in Ramfjorden and every 5 min in Van Mijenfjorden.

Under-ice water velocity

To record the water velocity under-ice, an acoustic doppler current profiler (ADCP), a Teledyne RD Instruments 300 kHz WorkHorse Sentinel, was mounted in a frame and deployed through a hole in the sea-ice, approximately 10 m from the hole where the sediment trap array was deployed. Looking downward, the transducer head was approximately aligned with the underside of the ice. The ADCP measured every five minutes with 50 pings per ensemble and six seconds between pings. Raw measurements were transformed internally to velocity vectors in earth coordinates (east, north down) for 34 bins of 2 m depth. Blanking distance between the transducer head and the first depth bin was 1.8 m. During all deployments, the ADCP covered the entire water column.

The ADCP was programmed to start pinging automatically at a fixed time before deployment and was stopped after recovery upon data download. In Ramfjorden, deployment and recovery took place at the same time as the sediment trap deployments and recoveries, thus providing measurements over approximately 24 hours per sampling day. In Van Mijenfjorden, the ADCP was deployed before VMF1 and recovered after VMF2, and covered thus also the 24 h between VMF1 and VMF2.

Post-processing and plotting of the ADCP data were done by Angelika Renner using Matlab R2019b. This included removing data points before and after the ADCP was mounted in the ice, removing data that were affected by reflection from the sea floor or items in the water, and filtering data with insufficient data quality. Measurements were then converted to 30 minutes averages. The current speed U was calculated from the velocity components (north *u* and east *v*) according to this equation:

$$U = \sqrt{u^2 + v^2} \qquad \text{(Eq. 5)}$$

The current speed of the water (m s^{-1}) and its direction in vector plots are shown in plot Section 3.3.1.3. The two waters layers shown in Fig. 7 are computed according the fjords water masses

from the CTD data, with the surface layers from surface to 13 m and the deep layer from 25 m to the bottom.

Tide charts

The tide tables for both fjords were taken from the tides prediction from the Norwegian Mapping Authority (kartverket.no) which used the tide gauges present in the closest area. The tables are retrieved for the station Ramfjorden (69°33' N 19°04', Tromsø tide gauge) in March (Table A5) and for Van Mijenfjorden (78°55' 43.03"N, 11°56'15.57"E, Ny-Ålesund tide gauge) in April (Table A6).

2.3 Biological observations

2.3.1 Sea-ice

2.3.1.1 Chl *a* and Phaeo concentrations, Chl *a*/Phaeo ratio

Fieldwork

To investigate the autotrophic biomass in sea-ice, ice cores were collected in undisturbed snow in the proximity (< 15 m) of the holes in the sea-ice used to collect water samples and to deploy the sediment trap array. The respective numbers of full ice cores and ice core sections extracted (in order to provide enough material for the different parameters studied) for each parameter, are shown in the Appendix, Table A1. In Ramfjorden the ice cores extracted of each parameters were not pooled and melted together, while in Van Mijenfjorden the full and sections of ice cores were pooled in the same sealed plastics bags, see Table A1. The ice cores were extracted and sectioned as described in section 2.2.2. The sections of the ice cores were stored in sealed plastic bags in darkness (inside a cooler box) to avoid photodegradation of autotrophic biomass.

Laboratory analysis

Depending of the character of the ice, a volume of GF/F filtered seawater (FSW) per centimeter of ice thickness was added to the ice to prevent osmotic shock of the sea-ice algae (Garrison and Buck, 1986). The ice in Ramfjorden was fresher and did not present a high brine volume compared to the ice in Van Mijenfjorden. Therefore, 50 mL FSW cm^{-1} were added to the ice core sections from Ramfjorden and 100 mL cm^{-1} to those from Van Mijenfjorden. All ice core sample were melted for 48 to 72 h in darkness, at 4 °C to preserve the quality of the algal cells for further examination.

The melted ice core were filtered in triplicates onto GF/F glass microfiber filter (Whatmann, England, pore size 0.7 µm and ø 25mm) using a vacuum pump to determine the concentration of Chl *a* and Phaeo (filtration volume: 100-500 mL). The volume of the water filtered depended on the concentration of biomass in each ice core (obtained by the coloration on the filter), and the melted water available from the different ice core sections. The filtration was done at UiT for the Ramfjorden samples and in the laboratory in Svea for the Van Mijenfjorden samples. All filters were then kept frozen (- 20 °C) until further analysis in June 2019 at UiT.

The frozen GF/F filter samples with biomass from the ice cores were placed into Falcon tubes (15 mL) and the Chl *a* was extracted in 5 mL ethanol (96 %) during 24 h in a fridge (4 °C). The tubes were covered by aluminium foil to avoid exposure to sun light. One hour before measurements, the tubes were put into room temperature. Before analysis, the samples were well homogenized using a vortex mixer. Each filter sample was measured before and after acidification (2 drops, 5 % HCl) following the procedure described by Holm-Hansen and Riemann (1978). The measurements were conducted in a Turner Design Trilogy fluorometer (beforehand calibrated with Chl *a*, Sigma C6144). Some calibration problems were encountered during the measurements with the fluorometer. All Chl *a* and the Phaeophytin concentrations obtained from Eq. 6 and Eq. 7 were corrected by using a correction factor of 6.16 (pers. Comm. Miriam Marquardt and Rolf Gradinger, UiT). Nevertheless, the absolute Chl *a* and Phaeo concentrations are still potentially too low.

Calculation

The following equations were used to calculate the concentration (µg L^{-1}) of Chl *a* and Phaeo:

$$Chl\ a = Tau * Fd * (Rb - Ra) * \frac{Vm}{Vf} \quad \text{(Eq. 6)}$$

$$Phaeo = Tau * Fd * \big((2.839 * Ra) - Rb\big) * \frac{Vm}{Vf} \quad \text{(Eq. 7)}$$

Here, Tau and Fd are predetermined constants. Tau is the correction factor between the Chl *a* and Phaeo concentration and Fd the acid factor against the pure Chl *a* standard. Rb corresponds to the relative fluorescence reading before acidification, Ra is the relative fluorescence reading after the acidification. Vm corresponds to the volume of ethanol used for extraction (in mL), Vf, the volume of sample filtered (in mL), and the number 2.839 correspond to the acid calibration factor.

To convert the Chl *a* concentration (µg Chl *a* L^{-1}) obtained from the fluorometer over the area of each ice core section (in mg Chl *a* m^{-2}), the following equation was used:

$$Chl\ a\ _{(ice\ core)} = \frac{X\ *Df*Actual\ ice\ volume}{Ice\ core\ area} / 1000 \qquad \text{(Eq. 8)}$$

Here, Chl $a_{(\text{Ice core})}$ is the concentration in mg m^{-2}. X is the Chl *a* concentration obtained from the fluorometer in µg L^{-1}. Df is the dilution factor, which takes into account the FSW added to the ice core section (total volume of water melted / actual ice volume). The actual ice volume is in litre (L) and the ice core area in m².

The integrated Chl *a* (mg m^{-2}) for the whole ice core was additionally calculated by summing the Chl *a* concentration of each ice core section. The ratio Chl *a*/Phaeo (mg m^{-2}/ mg m^{-2}) was calculated as well for each ice core section.

2.3.1.2 Microalgae community composition

Preparation, examination and counting of the samples

The sea-ice algae community composition was investigated by transferring a volume of 100 mL of the melted ice core sections into 100 mL dark glass bottles. The water samples were preserved with 1 mL Lugol's solution per 100 mL of sample. The glass bottle were well mixed after adding the Lugol's solution and stored in the darkness at 4 °C until further processing. The samples from Van Mijenfjorden were unintentionally placed in the freezer during the transport from Longyearbyen to Tromsø, which slightly damaged some cells, but in lesser extent than expected. At VMF1, the glass bottle with water from the section 20-40 cm broke before analysis of the sample, therefore no algae composition could be obtained from this section. The cell counts of the species *Phaeocystis pouchetii* were discarded from the final results because their abundance was most likely underestimated by the used microscopy magnification.

Preparation, identification and counting of the sea-ice algae samples were performed following the Utermöhl (1958) method at UiT and the Institute of Oceanology of the Polish Academy of Sciences (IO PAN) with the help of Prof. Józef Wiktor. To not further damage the cells in the frozen sample, the samples from Van Mijenfjorden were put in the fridge for roughly 24 h to allow gentle defrosting. Samples from both stations were put into room temperature at least another 24 h to avoid formation of air bubbles which can distribute unevenly the cells in the

bottom-plate chamber. The sample were well mixed before transferring an aliquot into the Utermöhl sedimentation chambers with settling tubes (HYDRO-BIOS©, Kiel, Germany). Different volumes of settling tubes were used (50 mL/25 mL/10 mL/3 mL) according the algal abundance in the samples. The sedimentation chamber was placed on a horizontal surface, at room temperature, and protected from direct sun light. The settling time was set according the volume of the settling tubes (24 h for 50 mL, 18 h for 25 mL, 8 h for 10 mL, and 3 h for 3 ml). After the settling time, the settling tube was removed without disturbing the cells settled into the bottom-glass of the chamber. A glass square was placed carefully on the top of the chamber avoiding air bubble formation. The samples were kept in a closed plastic box with humid paper to prevent water sample evaporation. The cells identification and counting was performed in an inverted microscope no later than one week after preparation of the sample (at UiT: ZEISS Primovert equipped with phase contrasts and objectives 4, 10, 20, and 40x, IOPAN: Nikon Eclipse Ti-S equipped with differential and phase contrasts, picture acquisition system NIS-Elements (Imaging Software, Nikon) and objectives 4, 10, 20, 40, and 60x).

First the whole chamber bottom surface was examined under magnification of 40x and approved for the general distribution of the cells. If possible, at least 500 counting units of the dominant species were counted (maximum error for this group ± 8.9 % according to Edler and Elbrächter (2010)). Then, the whole chamber or parallel transects of the chambers were inspected under 100 or 200x magnification and cells >20 µm were counted. Abundant species were counted at a minimum of 50 cells (i.e., maximum error of ± 28 %). For sample with scarce abundance of protists (e.g., suspended biomass sample at 30 m depth for both fjords), the whole chamber surface was examined. The cells identification was done to the possible lowest taxonomic level and classified by group and size classification. The identification of the species and groups was done according the diverse identification guides used: Berard-Therriault et al. (1999); Halse and Syvertsen, (1996); Medlin and Hasle (1990); Medlin and Priddle (1991); Poulin and Cardinal (2011, 1982); Throndsen et al. (2007); Von Quillfeldt. (2001); Wiktor et al. (1995) and website “Nordic Microalgae” developed by the Swedish Meteorological and Hydrological Institute (SMHI, 2020).

Calculation

The absolute abundance of sea-ice algae was calculated by using the following equation:

$$Algae\ abundance = \frac{\frac{Ng * coeff}{Nf}}{Vs} * Df \quad \text{(Eq. 9)}$$

Here, algae abundance is in number of cells per litre of melted ice, Ng the number of cells per each group, the coeff corresponding to the coefficient of the magnification and microscope used calculated by: Field of chamber (mm^2)/ Field of view (mm^2), Nf the number of frames counted, Vs the volume sediment in the Utermöhl sedimentation chambers (L) and finally Df the dilution factor presented in the Eq. 8.

The algae plot were made with RStudio using ggplot2 package (version 3.3.0). The whole algae composition found at the different compartment (ice/ water column) and fjord is presented in the species list in Appendix (Table A1).

2.3.1.3 POC and PON concentrations, POC/PON and POC/Chl *a* ratios

Laboratory analysis

The melted sections of the ice cores were filtered in triplicates on pre-combusted Whatmann GF/F filters (pore size 0.7 μm) to determine the concentration of suspended particulate organic carbon (POC) and nitrogen (PON) (filtration volume: 200-900 mL, depending of the algal concentration on the filter). Larger organisms such as copepods were removed from all filters before packing the filters in aluminium foil and freezing them at -20 °C until later analyse in March 2020 at UiT.

The frozen GF/F filter samples were placed into glass tubes covered with aluminium foil to avoid any contamination and placed in the laboratory fridge (at 4 °C). The samples were dried at 60 °C for 24 h in an oven (Termaks AS), then placed in an acid fume bath (concentrated HCl) for 24 h to remove all inorganic carbon and finally placed another 24 h in the oven for drying (60 °C). The filters were packed into nickel capsules and stored into a desiccator until POC and PON analysis was processed in March 2020 in a CE-440 CHN Elemental Analyzer (Exeter Analytical, Inc.) through a series of combustive processes which measures POC and PON concentration. The combustion occurs at high temperature (975 °C) in pure oxygen, under static conditions, with lasting by dynamic burst of oxygen. The products of combustion passed through suitable reagents to remove all undesirable inorganic and organic substances such as sulfur, phosphorous and halogen gases and assured a complete oxidation. The gasses were mixed with copper to remove excess of oxygen and converted oxides of nitrogen to molecular nitrogen. Then, the gasses were homogenized into a mixing volume chamber at constant

temperature and pressure, and passed through a series of high-precision thermal conductivity detectors containing a pair of thermal conductivity cells each. Between the first pair of cells, an absorption trap measured the hydrogen by removing the water. The second pair of cells measured the carbon by removing the carbon dioxide, while in the last measurement the nitrogen content is defined against a helium reference. Due to a mechanical problem of the CHN Elemental Analyzer, the samples from all ice core sections at VMF1 were not analysed.

Calculation

Before and after each run of samples set (containing 48 samples), blank samples were run, along with standard samples, using acetanilide standard (C_8H_9NO), between each run of 8 samples, and these blanks were used in the calculation of the carbon and nitrogen weight per filter (Eq. 10, 11):

$$\mu g\ POC = \frac{CR-CZ-BC}{KC} - CFB \quad \text{(Eq. 10)}$$

$$\mu g\ PON = \frac{NR-NZ-BN}{KN} - NFB \quad \text{(Eq. 11)}$$

With µg POC and PON, resulting output in micrograms, CR/NR = signal value of the sample, CZ/NZ = the blank value of helium gas, BC/BN = blank value of POC and PON, KC/KN = standard reference for POC and PON, and finally CFB/NFB = Filter blank for POC and PON.

Finally, the POC and PON were calculated by dividing the weight of these elements by the volume filtered (Eq. 12):

$$POC\ (or\ PON) = \frac{\mu g\ C\ (or\ N)}{Vf} \quad \text{(Eq. 12)}$$

with POC in mg m^{-3} and Vf in L.

The integrated POC concentration of each ice core section was calculated by using the Eq. 8. However, instead of having X being the Chl *a* concentration, X was now the POC concentration obtained from the CHN Elemental analyzer (mg POC m^{-3}) and the integrated POC was given in mg POC m^{-2}. The integrated POC concentration of the whole ice core was calculated by summing the POC concentration of each ice core sections.

The POC/PON is here given as atomic ratio and calculated from the weight ratio by the following equation:

$$POC/PON = \frac{C}{12} \; / \; \frac{N}{14} \qquad \text{(Eq. 13)}$$

with C (=POC) and N (=PON) in mg m^{-3}.

The carbon-to-chlorophyll *a* ratio, (POC/Chl *a*; weight/weight) was calculated by dividing POC concentration (in mg m^{-2}) by the Chl *a* concentration (in mg m^{-2}).

2.3.2 Water column

2.3.2.1 Chl *a* and Phaeo concentrations, Chl *a*/Phaeo ratio

Fieldwork and laboratory

To investigate the suspended biomass, water samples were taken with a 5 L Niskin bottle (Ocean Test Equipment Inc., USA) manually lowered with a scaled rope through the ice hole before deploying of the sediment trap array or after its recovery. The water samples (3 L) were collected at four different depth (1, 5, 15, and 30 m). The water from the Niskin bottle was transferred to a 10 L canister, carefully pre-hand rinsed with the same water depth. The canister was immediately placed in a cooler box after collecting the samples, to prevent freezing and light disturbance to the photosynthetic pigments.

For analyses of the Chl *a* and Phaeo concentrations (µg L^{-1}), triplicate samples (filtration volume: 200-400 mL) were filtered following the same procedure as for the melted ice core samples (Section 2.3).

Calculation

The Chl *a* and Phaeo concentrations (µg L^{-1}) were calculated following the explanations in Section 2.3.1.1 and by using the Eq. 6 and Eq. 7.

The ratio Chl *a*/Phaeo (µg L^{-1}/ µg L^{-1}) was calculated as well for each depth.

The amount of integrated suspended material (in mg m^{-2}) in the first 30 m of the water column was calculated by using the following equation:

$$Integrated\ material = \sum_{i=1}^{n} \left(\frac{((sdi+1)-sdi)\ (Xi+(Xi+1))}{2} \right) \qquad \text{(Eq. 14)}$$

with the integrated material in mg m^{-2}, sd*i* is the sampled depth (with i, e.g., 1= 1 m) and X*i* is the chlorophyll *a* concentration in µg L^{-1} at the corresponding depth i.

2.3.2.2 Microalgae community composition

Preparation, examination and calculation of the samples

The preparation of the samples, the algae identification and counting were done as described in section 2.3.1.2. The algae abundance was calculated using the Eq. 9. without multiply by the dilution factor. The result are given in number of cells per litre of seawater.

2.3.2.3 POC and PON concentrations, POC/PON and POC/Chl *a* ratios

Preparation of the samples and calculations

To determine the POC and PON concentration in the water column, triplicated samples (volume filtered: 300-600 mL, depending on concentrations) were filtered, following the same procedure described section 2.3.1.3. The POC and PON concentration (mg POC m^{-3}) in the water column was calculated following equations Eq. 11 and Eq. 12. The integrated POC concentration (mg POC m^{-2}) in the water column was calculated using the Eq. 14. The POC/PON ratios were calculated by using the Eq. 13. The POC/Chl *a* ratios were calculated as described in the section 2.3.1.3. Note that at RMF2, probably a too low volume of water was filtered, resulting in the PON concentrations being close to the detection limit which likely resulted in wrong POC/PON ratios (Table A3).

2.3.3 Sinking biomass

2.3.3.1 Chl *a* and Phaeo flux, Chl *a*/Phaeo ratio

Fieldwork and laboratory analysis

The quantity and quality of vertically exported biomass was studied by deploying short-term sediment traps (KC Denmark AS) through a hole in the ice. The sediment trap array consisted of four paired cylinders mounted on a gimballed frame at 1, 5, 15 and 30 m. Each cylinder has a volume of 1.8 L, an inner diameter of 7.2 cm and a height of 45 cm. The sediment traps were deployed for roughly 24 hours (details on deployment time in Table 2), and because of the short time deployment no fixatives or poisons were added to the cylinders. However, FSW was added before deployment (with salinity similar to the water at the deepest trap) to avoid the loss of trapped particles by density difference. Right after recovery of the sediment trap, the water from the cylinder was gently transferred to a clean 10 L canister for each sampling depth and stored

the same way as the water sample collected from the Niskin bottle (Section 2.3.1.1). Subsamples of the water were filtered to determine the Chl *a* and Phaeo concentration (200 mL) following the same procedure as described in the section 2.3 for the ice core samples (Section 2.3.11).

Calculation

The following equation was used to calculate the vertical flux of Chl *a* and Phaeo (in mg m^{-2} d^{-1}):

$$Flux\ (mg\ m^{-2}d^{-1}) = \frac{(X\ /1000)\times Vt\ x\ (\frac{1}{0.036^2 x\ \pi})}{d} \quad \text{(Eq. 15)}$$

where X is the concentration of Chl *a* and Phaeo measured from the sediment traps (in µg L^{-1}), Vt is the total volume of the trap cylinder (1.8 L), multiplied by the area of the trap cylinder opening (in m^2) and d is the time (in days) of the sediment trap deployment.

The ratio Chl *a*/Phaeo (mg m^{-2} d^{-1}/ mg m^{-2} d^{-1}) was calculated as well for each depth.

2.3.3.2 Sinking of microalgae cells

Preparation and examination of the samples

From the water collected in the sediment trap cylinders, 100 mL were transferred into 100 mL dark glass bottle. Due to high abundance of microalgae, 2 mL of Lugol's solution/per 100 mL were added. The preparation of the sample, algae identification and counting were done as described in section 2.3.1.2.

Calculation

The export of the ice algae was calculated by using the Eq. 15. with replacing the factor (X/1000) by the algae abundance result calculated at the Eq. 9. The results are given in cells m^{-2} d^{-1}.

2.3.3.3 POC and PON concentrations, POC/PON and POC/Chl *a* ratios

Preparation of the samples and calculations

Subsamples of the water collected from the sediment trap cylinders were filtered for POC and PON concentration (filtration volume: 200-300 mL). The filters were analysed following the same procedure as for the ice core samples (section 2.3.1.3), and the subsequent calculation of the POC flux were done following the Eq. 15. The flux is given in mg POC m^{-2} d^{-1}. The

POC/PON ratios were calculated by using the Eq. 13. The POC/Chl *a* ratios were calculated as described in the section 2.3.1.3.

2.3.3.4 Particles

The qualitative composition of sinking particles was determined modifying one sediment trap cylinder per depth with a gel containing glass jar. These «gel traps» were prepared following the conceptual procedure of Lundsgaard (1999) and Ebersbach and Trull (2008) with the modifications described by Wiedmann et al. (2014). Glass jars (fitting the size of the sediment trap cylinder, 70 mm diameter) were filled with approximately 5 mm gel Tissue-TecVR (Sakura Finetek Europe B.V., Netherlands). The filled cup was frozen before deployment into the trap cylinder and covered with plastic to avoid contamination. In the field, one jar was added to one sediment trap cylinder at each sampling depth and covered with FSW to allow gentle defrosting of the water soluble gel, and deployed with the sediment trap array for approximately 24 h.

When recovering the sediment trap array, the over standing water in the trap cylinder with a gel containing glass jar was gently removed with a silicone hose (diameter: 3 mm) and a 3 mL plastic pipette. A small amount of over standing water on the gel was left to avoid any unintentional removal of particles. The gel jars were immediately frozen (- 20 °C) until further analysis at UiT.

The surface of the glass jar photography was done after defrosting the gel jar in a fridge (4 °C) one by one in September 2019. The remaining water layer covering the gel was gently removed with a 3 mL plastic pipette. Then, the surface of the gel was pictured using a stereo microscope (15x magnification, Zeiss Discovery. V20) with a digital camera, AxioCam ERc 5s (5 megapixels).

Unfortunately, some of the gel trap samples were loaded with too many particles due to a too long deployment time (~24 h) Therefore, no quantitative particles analysis was done, because the particles on top of each other would have resulted in a wrong size composition and abundance of particles. The gel trap pictures at the station VMF2, 1 m depth, are not presented due to the loss of the gel trap during the fieldwork.

3 Results

3.1 Physical and hydrographic data

3.1.1 Meteorology

During the sampling period in Ramfjorden the air temperature was stable (average -3 °C, Table A2), with measurements at RMF1 = - 3°C and RMF2 = - 5.4 °C. Weak precipitations were recorded the days prior the sampling field (7 mm, Table A2) with winds (~6 m s^{-1}) directed South/South-West (~210°) (Appendix, Table A2).

Before Van Mijenfjorden sampling period, the temperatures varied: with warmer period (16.04. – 20.04. = -2.1°C to 0.8 °C), combined with weak precipitation (0-6.5 mm, Table A2) and then colder period (21.04. - 24.04. = - 3.8 to -10.9 °C). During the sampling week temperature were as well above 0°C (0.5 – 0.8 °C) with weak precipitations noticed at VMF1 (4.3 mm, Table A2). The temperature measurements were VMF1 = -1.1 °C and VMF2 = -0.5 °C.

3.1.2 Snow and sea-ice

Table 3 Overview of the average snow depth, the ice thickness, and the freeboard (in cm) at the sampling stations.

Station (Label)	Mean snow depth (cm)	Mean sea ice thickness (cm)	Freeboard (cm)
RMF1	25.0	40.0	-0.2
RMF2	24.0	40.0	*nd*
VMF1	8.0	77.0	5.0
VMF2	4.5	79.0	5.5

nd no data

In Ramfjorden, the snow cover was comparably thick on both sampling days (24.5 cm on average) (Table 3). The ice thickness was also similar on both days and a negative freeboard was measured at RMF1 (no measurement taken at RMF2). At the sampling station in Van Mijenfjorden, the ice thickness was 78.0 cm average for both sampling days, but the snow depth differed between VMF1 and VMF2 (8 cm vs. 4.5 cm). The freeboard was positive on both VMF1 and VMF2 (Table 3).

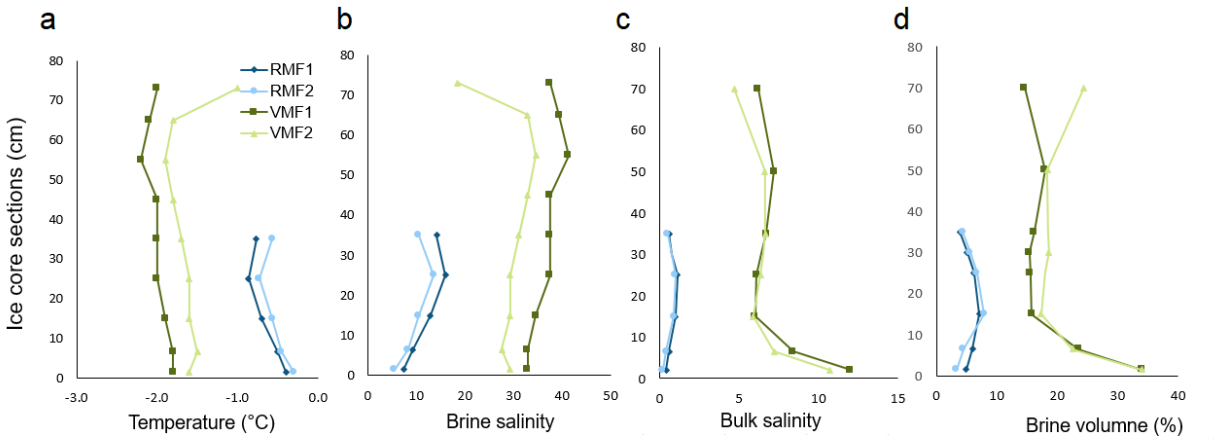

Figure 2. Physical parameters of the sea-ice with (a) temperature (°C), (b) brine salinity, (c) bulk salinity and (d) brine volume (%) for RMF1/RMF2 and VMF1/VMF2. Note the different y-axis scales for the ice core sections, with 0 corresponding to the bottom ice sections (= ice/water interface).

At RMF1, the ice core temperature was slightly colder in the top sections (20-40 cm: - 0.8 °C) than the bottom section (0-10 cm: - 0.4 °C) (Fig. 2a). In contrast, the brine salinity was higher in the top section (14) and lowest in the bottom section (7, Fig. 2b). The maximum bulk salinity at RMF1 was found at the section 20-30 cm (bulk salinity: 1, Fig. 2c). At the interfaces towards water and air, the bulk salinity was lowest (0.02 - 0.06 %, Fig. 2c). The brine volume, determined from bulk salinity and temperature, was also the lowest at the two interfaces at RMF1. The maximum brine volume was here found in the middle sections (20-30 cm) with volume corresponding of 7 % (Fig. 2d). At RMF2, the ice core temperature was slightly warmer than at RMF1 and had a lower brine salinity (Fig. 2a.2b). The bulk salinity was similar between RMF2 and RMF1, but the brine volume was slightly lower at the bottom ice sections 0-3 cm (Fig. 2c. 2d) at RMF2 than at RMF1 (5 % vs. 3.3 %).

At VMF1, the temperature of the ice core was stable (- 1.8 °C to – 2.2 °C). The brine salinity was also stable (33 - 41, Fig. 2a), but the bulk salinity was higher at the bottom section (12) than the top sections (5, Fig. 2b). The brine volume was highest at the bottom section (34 %) and decreased towards the sections in the middle of the ice core and reach 14 % at the top section. At VMF2, the temperature in the ice core was higher (+ 0.3 °C average) than at VMF1, especially at the top section (~ - 1.0 °C, Fig. 2a) and the brine salinity followed the same pattern (Fig. 2b). The bulk salinity was similar to what was observed at VMF1, though the salinity was slightly lower at the top sections (Fig. 2c). The brine volume was in general higher at VMF2 than at VMF1, especially at the top sections, where the brine volume was 24 % (Fig. 2d).

3.1.3 Water column

3.1.3.1 Vertical CTD profiles

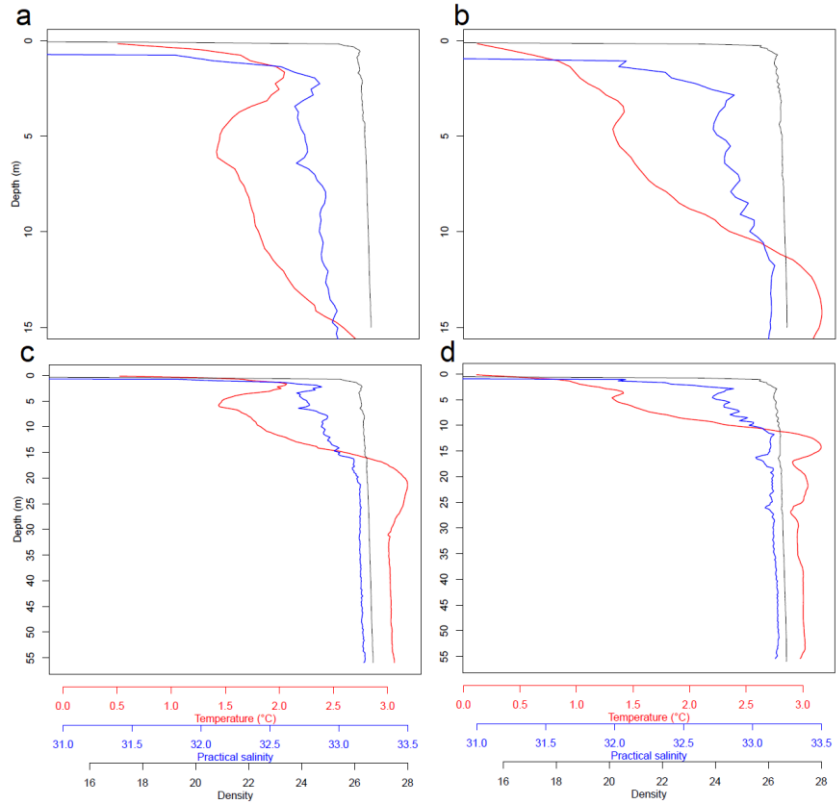

Figure 3. Vertical CTD profiles in Ramfjorden, with temperature (°C) (in red), salinity (blue) and density (black); with the top pannels (a) RMF1 and (b) RMF2 : measurements from 0 to 15 m and the bottom pannels: (c) RMF1 and (d) RMF2: measurments of the whole water column.

At RMF1 and RMF2, the water column was stratified with an upper colder layer (0-15 m: average temperature: 1.5 °C) and a deeper, warmer and saltier layer (20 m-bottom: average temperature: 3 °C, average salinity: 33.2) (Fig. 3). At RMF1, the temperature decreased in the first meters from ~2° C (at 2-3 m) to ~1.5 °C (at 5 m). It increased again to reach the maximum water temperature (3 °C) at 15-20 m and was constant to the bottom (Fig. 3a). At RMF2, the temperature increased contantly from approximately 2 °C under the sea-ice and reached 3 °C at 20 m. On both days, the salinity at RMF1 and RMF2 increased rapidly in the first meter under the ice (32 to 33.2) to stabilize at 15 m (Fig. 3a. 3b). The density increased rapidly between the surface to the first meters (at 1-2 m) to reach maximum density of 26.8 (Fig. 3a. 3b).

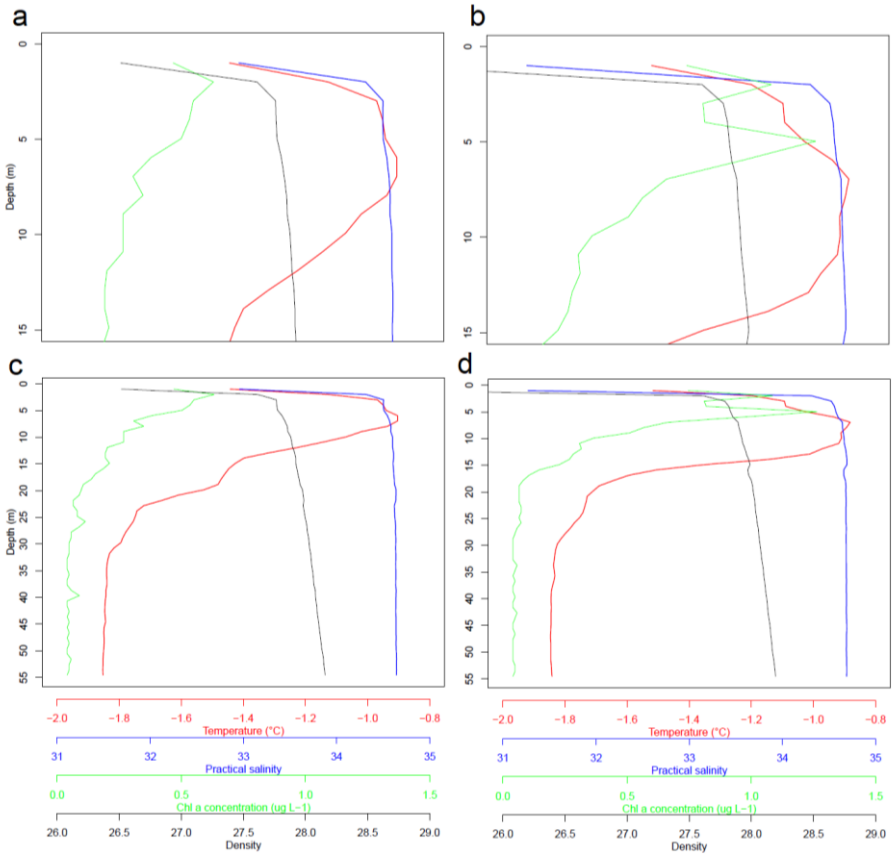

Figure 4. Vertical CTD profiles in Van Mijenfjorden, with temperature (°C) (red), salinity (blue), density (black) and Chl a (µg L-1) (green); with the top pannels (a) VMF1 and (b) VMF2 : measurements from 0 to 15 m and the bottom pannels: (c) VMF1 and (d) VMF2: measurments of the whole water column.

In Van Mijenfjorden, the water column at VMF1 and VMF2 was stratified into an upper warmer layer (0-15 m: average temperature: - 0.9 °C) and a deeper, colder and saltier layer (25 m to bottom: average temperature: - 1.8 °C, average salinity: 34.6) (Fig. 4). The increase of the water temperature under the sea-ice in Van Mijenfjorden was slightly different on both days. At VMF1 the water temperature reached – 0.9 °C at 3-4 m, while this happended at 7-8 m at VMF2 (Fig. 4). The under-ice salinity recorded at VMF1 and VMF2 was 32. It increased with depth to stabilized at 34.6 at 2-3 m, and remained fairly constant below (Fig. 4). The density increased rapidly between the surface and 2-3 m (to 27.8), and then increased constantly to the bottom (to reach 28.2, Fig. 4).

3.1.3.2 Under-ice temperature

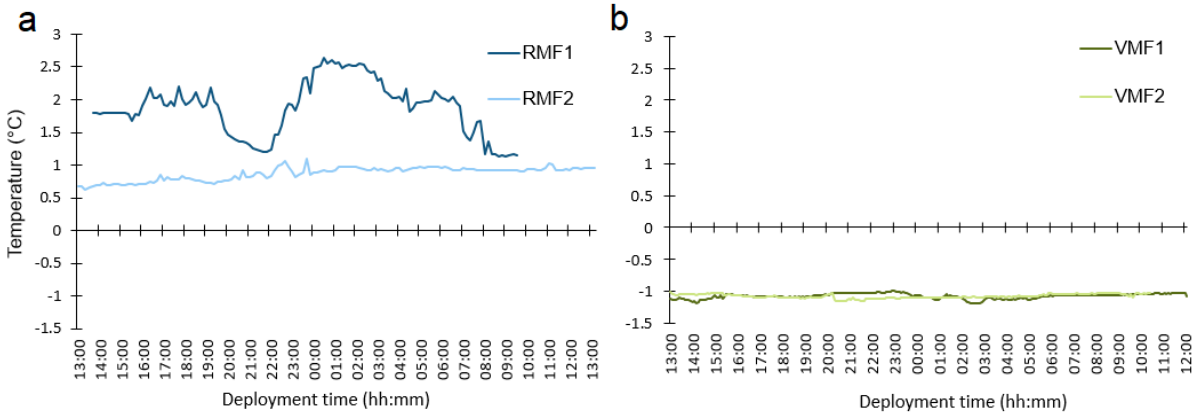

Figure 5. Time series of seawater temperature (°C) under the ice at 1 m depth. (a) RMF1 (dark blue)/ RMF2 (light blue) and (b) VMF1 (dark green)/ VMF2 (light green).

At RMF1, the temperature under the ice fluctuated with a range of 1.5 °C during the deployment period (Fig. 5a). Within 3 h the temperature increased from 1.2 °C at 22:00 to 2.6 °C at 00:50 (15.03.), before it decreased to 1.1 °C with minor fluctuations until the end of the recording period (9:00 the 16.03.). At RMF2, the temperature was more stable, increasing from 0.7 °C to 1 °C, during the recorded period (Fig. 5a). At VMF1 and VMF2 the seawater temperature was stable with weak fluctuations between -1.2 °C to -1 °C for the whole recorded period (Fig. 5b).

3.1.3.3 Under-ice velocity

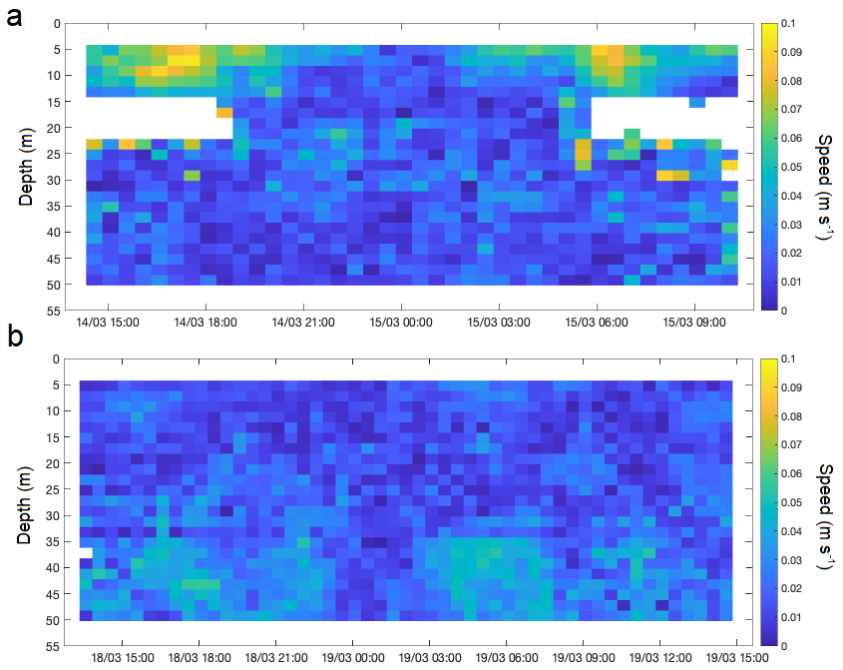

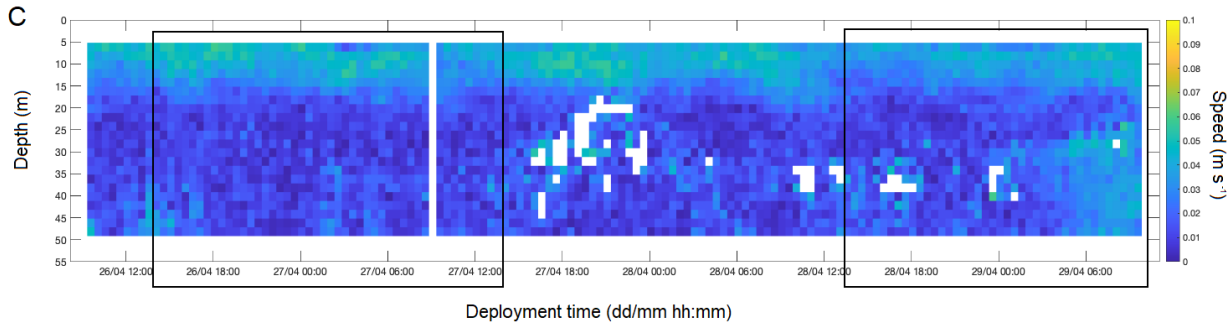

Figure 6. Current speed profile (m s-1) under the sea-ice. (a) RMF1, (b) RMF2 and (c) entire sampling period at Van Mijenfjorden (with sampling at VMF1 and VMF2 marked by black frames). Note the current speed data missing (e.g., beginning and end of RMF1) due to removal from the processign treatment.

At RMF1, a strong current speed was observed right under the sea-ice (at 5-10 m) from 14:00–20:00 (14.03.) and from 05:00-9:00 (15.03.), with speed of about 0.07-0.09 m s^{-1} (Fig. 6a). The currents were weaker the rest of the sampling period. The timing of the higher current velocity underneath the ice might be correlated with time prediction of high tides phase as seen in Appendix, Table A5. At RMF2 the current speed was generally weaker than at RMF1. The only period of a slightly higher current (with a speed of 0.04-0.06 m s^{-1}) was at the bottom layer (35-50 m), between 16:00 and 19:00 (18.03.) and between 4:00 and 8:00 (19.03.) (Fig. 6b). The timing of the slightly higher current agreed with the time prediction of the low tides phases (Table A5).

In Van Mijenfjorden, a strong current velocity (between 0.05 and 0.07 m s^{-1}) was recorded under the sea-ice (5 m to 15 m) at VMF1 (26.04.: 15:00-21:00, 27.04.: 00:00-8:00 (Fig. 6c). The current speed between 20 m and the bottom was low (0-0.01 m s^{-1}) during the sampling period but seemed to increase towards the end of the last deployment at VMF2 (Fig. 6c). No direct relation was observed between under ice current speed and timing of the tide forecast (neither high nor low tide phases) (Table A6).

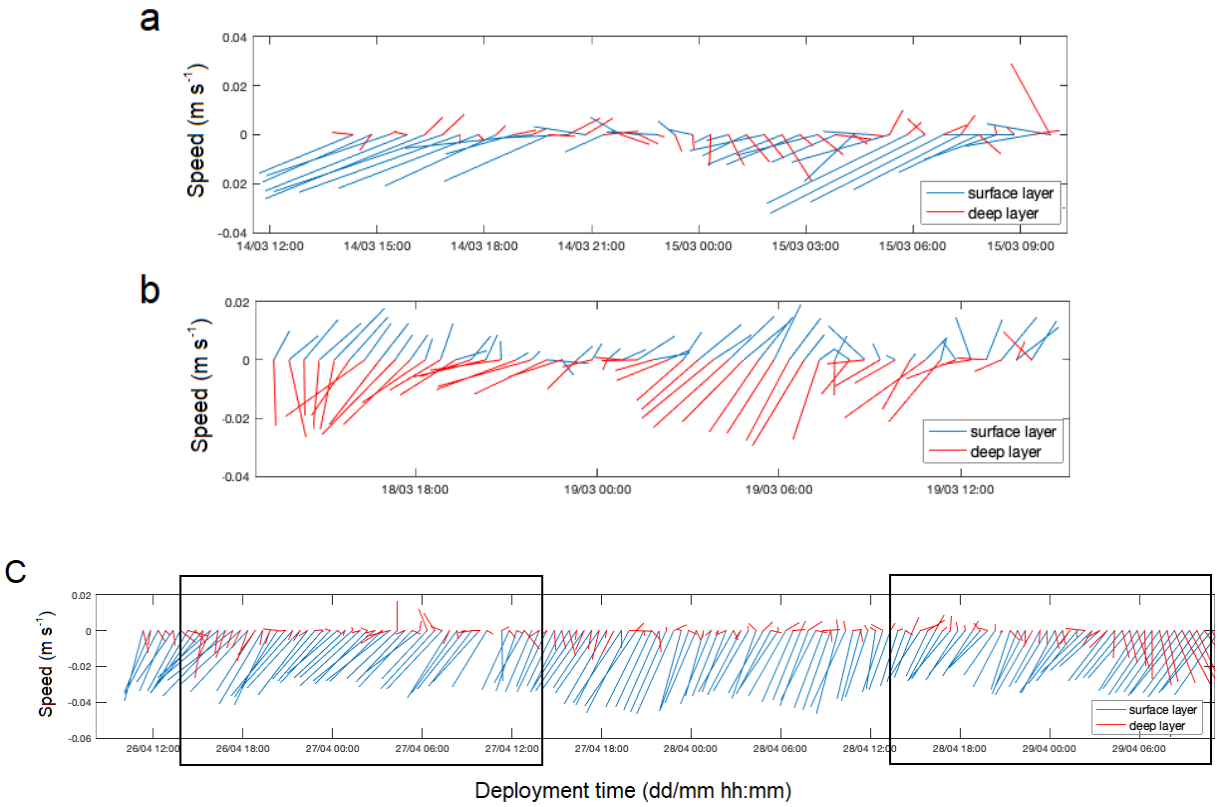

Figure 7. Currents direction under the sea-ice. Vectors are computed to 30 min average. The color of the vectors depicts the water layers: in blue the surface layer (from surface to 13 m) and in red the deep layer (from 25 m to the bottom). (a) RMF1, (b) RMF2 and (c) entire sampling period at Van Mijenfjorden (with VMF1 and VMF2 marked by black frames).

At RMF1, the direction of the surface currents were mostly directed towards south-west meaning the surface water layer was flowing into the fjord (Fig. 7a). The currents were slightly stronger (max speed 0.03 m s^{-1}) between 14:00 and 20:00 on the 14.03. and between 05:00 and 09:00 on the 15.03. The deeper layer did not show any clear trend and the velocity recorded was generally weaker (average speed: 0.01 m s^{-1}) than the surface current (Fig. 7a). At RMF2, the surface current was in the opposite direction compared to RMF1. The surface was flowing out of the fjord, while at depth, water was flowing into the fjord (Fig. 7b). The speed of the surface layer and deep layer were strong from 13:00 to 18:00 the 18.03. and from 01:00 to 07:00 the 19.03. (max speed surface current: 0.02 m s^{-1}, max. speed deep current: 0.03 m s^{-1}, Fig. 7b).

In Van Mijenfjorden, the speed of the surface current was higher (max speed: 0.04 m s^{-1}) than the current in the deeper layer (Fig. 7c). The surface current was directed southwest (=out of the fjord), while the water at depth moved with a low speed (average speed: 0.01-0.02 m s^{-1}) . At the end of VMF2, the speed of the current increased slightly (max speed: 0.04 m s^{-1}, Fig. 7c). The south east direction dominated for the current at depth during both VMF1 and VMF2.

3.2 Biological data

3.2.1 Ice cores

3.2.1.1 Chl *a* and Phaeo concentrations, Chl *a*/phaeo ratio

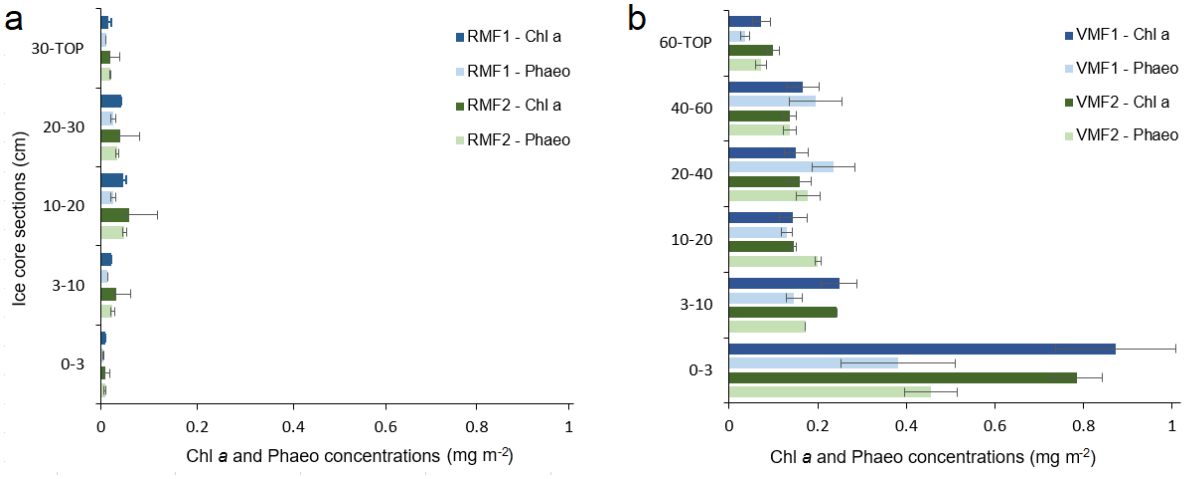

Figure 8. Integrated Chl a and Phaeo concentrations (mg m-2) in each ice core sections (cm); (a) RMF1 (blue)/ RMF2 (green) and (b) VMF1 (blue)/ VMF2 (green). Note the different scale on y-axis with the top section in Ramfjorden refers to 40 cm (average) and in Van Mijenfjordn to 78 cm (average).

The Chl *a* concentration in the ice cores from Ramfjorden was generally low (Fig. 8a). The highest concentration was found in the sections in the middle of the core (10-20 cm and 20-30 cm: 0.04 - 0.06 mg Chl *a* m^{-2}. No important difference in the Chl *a* concentration was noticed between the two sampling days, RMF1 and RMF2. The Phaeo concentration in the ice core sections followed the Chl *a* concentration but was slightly lower (e.g., for the sections 10-20 cm and 20-30 cm, between 0.03 and 0.05 mg Phaeo m^{-2}). The integrated Chl *a* concentration was low at both RMF1 and RMF2 and no considerable difference was seen (with 0.13 mg Chl *a* m^{-2} vs. 0.16 mg Chl *a* m^{-2}, Table A4).

In Van Mijenfjorden, the highest Chl *a* concentrations were observed in the bottom sections of the ice cores (Fig. 8b). Especially the section 0-3 cm had very high concentration (at VMF1: 0.9 and VMF2: 0.8 mg Chl *a* m^{-2}). The Chl *a* concentration decreased toward the top of the ice core with lowest concentration observed at the top section (60-TOP cm: 0.02 mg m^{-2} at VMF1, 0.01 mg m^{-2} at VMF2). No clear difference was observed between VMF1 and VMF2 with regard to the Chl *a* concentration in the ice core section, even though the concentration in the bottom section was somewhat higher at VMF2 than at VMF1. The distribution of the Phaeo concentration in the ice cores from Van Mijenfjorden was comparable to the pattern of the Chl

a concentration, however, in the section 0-3 cm, the Phaeo concentration was only half the Chl *a* concentration (in the lowerest ice core section: VMF1: 0.4 mg Phaeo m^{-2}, VMF2: 0.5 mg Phaeo m^{-2}). The integrated Chl *a* concentration of the whole ice core was not very different for both sampling days (VMF1 = 1.65 mg m^{-2} and VMF2 = 1.57 mg m^{-2}, Table A4).

3.2.1.2 Microalgal community composition

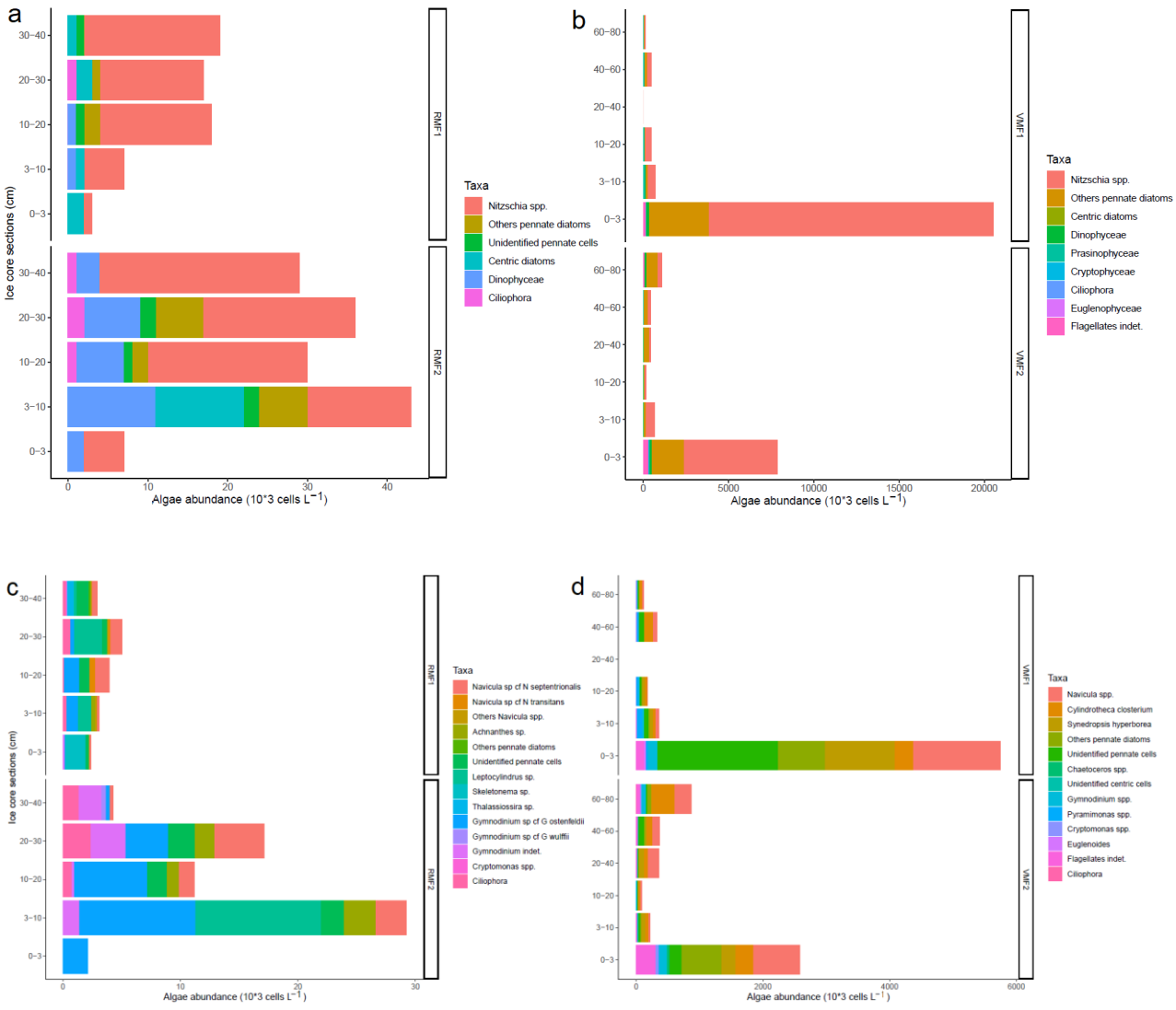

Figure 9. Microalgal abundance (cells L^{-1}) per ice core sections (cm). With the genus Nitzschia spp.: (a) RMF1/RMF2 and (b) VMF1/VMF2. Without the predominant Nitzschia spp., to give a more detailed composition of the other taxa: (c) RMF1/RMF2 and (d) VMF1/VMF2. Note the difference scale on x-axis and y-axis and additionally the sample of ice section 20-40 cm at VMF1 was lost (details in section 2.3.1.2).

At RMF1, the microalgae abundance was lowest at the lowermost sections of the ice core (0-3 cm: 4 x 10^3 cells L^{-1}, 3-10 cm: 7 x 10^3 cells L^{-1}, Fig. 9a), while at RMF2, the microalgae abundance was only low at the section 0-3 cm (7 x 10^3 cells L^{-1}). In contrast, higher abundances

were observed in the middle sections of the ice core on both sampling days (e.g., 10-20 cm section at RMF1: 20 x 10^3 cells L^{-1}, RMF2: 30 x 10^3 cells L^{-1}). The pennate diatom, *Nitzschia* spp. was the most dominant taxon for both sampling days. Dinophyceae was the second abundant taxon especially at RMF2, with mostly *Gymnodinium* sp. cf. *ostenfeldii* found in high abundance in the ice core section 3-10 cm (up to 10 x 10^3 cells L^{-1}). Other observed pennate diatoms were *Achnanthes* sp., *Navicula* sp. cf. *septentrionalis*, *Navicula* sp. cf. *transitans* and the centric diatoms *Leptocylindrus* spp., *Skeletonema* spp., *Thalassiosira* spp.. The microalgae diversity of all ice core section on both sampling days ranged between 3 and 15 taxa (Table A8). No considerable difference in diversity was found between the sampling days and the ice core sections, apart from the slightly lower diversity in the lowermost ice core sections. Interestingly, also the brackish species *Eunotia serra* and *Diploneis bombus* were found in the top section of the ice core at RMF1.

In Van Mijenfjorden, the algae abundance differed from Ramfjorden in terms of distribution in the ice core sections. Indeed, the highest cell abundance was found in the bottom section of the ice core (0-3 cm section at VMF1: 20 000 x 10^3 cells L^{-1}, at VMF2: 7 500 x 10^3 cells L^{-1}, Fig. 9b, with *Nitzschia* spp.). The abundance decreased toward the top sections (< 1000 x 10^3 cells L^{-1} at both sampling days). *Nitzschia* spp. was the most abundant taxon observed on both sampling days and in all ice core sections (highest cell abundance recorded: 16 700 x 10^3 cells L^{-1} at VMF1, section 0-3 cm, Fig. 9b). In addition to *Nitzschia* spp., others pennate diatoms dominated the microalgae composition with predominantly various *Navicula* species (Fig. 9d) (eight species, e.g., *Navicula directa, N pelagica, N vanhoeffenii*) followed by others pennate diatoms (e.g., *Fragilariopsis* sp. *Cylindrotheca closterium*, *Synedropsis hyperbora*, *Entomoneis* spp., *Pleurosigma*/*Gyrosigma*, Table A7). Some flagellates were also observed with the *Gymnodinium* spp. mostly with *Pyramimonas* spp. (Fig. 9d). The total microalgae diversity ranged between 12 and 28 taxa per ice core section and sampling day (Table A8), with highest diversity observed at the lowermost ice core sections. A minor difference was observed between VMF1 and VMF2, with lower overall microalgae abundance at the lowermost sections at VMF2 compared to VMF1 (e.g., at 0-3 cm section, abundance of *Nitzschia* spp., VMF1: 16 700 x 10^3 cells L^{-1}, VMF2: 5 000 x 10^3 cells L^{-1}, Fig. 9d). As well as the top ice section, the algae abundance was slightly higher at VMF2 than at VMF1 (60-80 cm section at VMF1: 200 x 10^3 cells L^{-1} and VMF2: 1000 x 10^3 cells L^{-1}, Fig. 9d).

3.2.1.3 POC concentration, POC/PON and POC/Chl *a* ratios

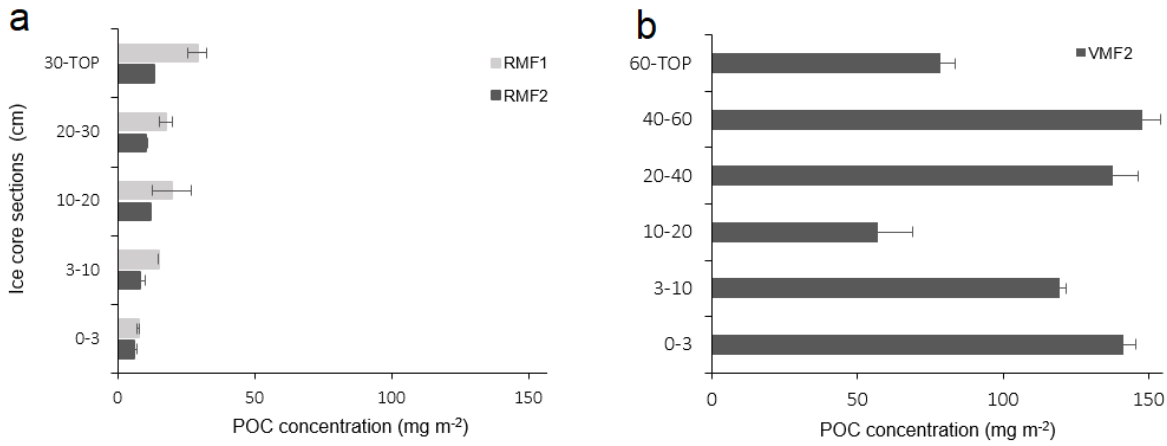

Figure 10. Integrated POC concentration (mg m^{-2}) in each ice core section (cm): (a) RMF1 (light grey)/ RMF2 (dark grey) and (b) VMF2 (dark grey). Note the different scale on y-axis and the concentrations at VMF1 are not presented (details in section 2.3.1.3).

The POC concentration in the ice was different between Ramfjorden and Van Mijenfjorden. In Ramfjorden, the POC concentration was highest at the top ice sections (e.g., 30-Top cm section, RMF1: 29 mg POC m^{-2}, RMF2: 13 mg POC m^{-2}) while the concentrations were lower at the ice-water interface (e.g., 0-3 cm section, RMF1: 8 mg POC m^{-2}, RMF2: 6 mg POC m^{-2}, Fig. 10a). The integrated POC concentration was low for both sampling day (RMF1: 89 mg POC m^{-2}, RMF2: 50 mg POC m^{-2}, Table A3). The POC/PON ratios in Ramfjorden were very high, especially at the top and bottom ice sections (0-3 cm section, RMF1: 19.8, RMF2: 12.8; 30-TOP cm section: RMF1: 19.8, RMF2: 21.2). In general the POC/PON ratios in the ice core sections were lower at RMF1 than at RMF2 (Table A3). The POC/Chl *a* ratios were higher at RMF1 than RMF2, with very high ratio observed at RMF1 (RMF1: POC/Chl *a* ratio: 423 - 1879, RMF2: 206 – 665, Table A3). On both sampling days the ratios were higher at the top and bottom ice sections than in the middle.

In Van Mijenfjorden, at VMF2 the POC concentrations were highest at the bottom section of the ice core (e.g., 0-3 cm section: 141 mg POC m^{-2}) and decreased toward the top of the ice, with lowest concentration found at the section 60-TOP cm (78 mg POC m^{-2}, Fig 10b). The POC concentration in Van Mijenfjorden was found low at the ice core section 10-20 cm (57 mg POC m^{-2}, Fig. 10b). The integrated POC concentration at VMF2 was 682 mg POC m^{-2} (Table A3). In Van Mijenfjorden the POC/PON ratio in the ice core sections was rather stable (POC/PON = 12.6 to 15, average 13.7 for all sections, Table A3). The POC/Chl *a* ratio were low at the

bottom sections (e.g., section 0–3 cm = POC/Chl *a* ratio of 180, Table A3) and did show little variation between the ice core sections. The POC/Chl *a* ratio was highest at the section 40-60 cm (POC/Chl *a* ratio: 1081, Table A3).

3.2.2 Water column

3.2.2.1 Chl *a* and Phaeo concentrations, Chl *a*/Phaeo ratio

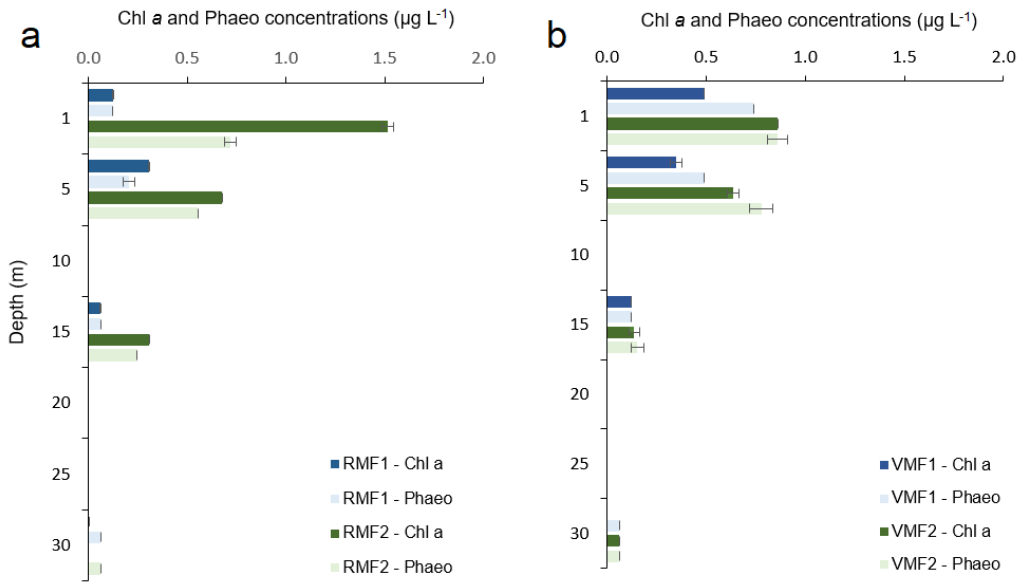

Figure 11. Chl a and Phaeo concentrations (µg L^{-1}) per depth (m): 1, 5, 15 and 30 m. (a) RMF1 (blue) / RMF2 (green) and (b) VMF1 (blue) / VMF2 (green).

At RMF1, the Chl *a* concentration observed was low, and the highest concentration was found at 5 m (0.3 µg Chl *a* L^{-1}, Fig. 11a). At RMF2, the Chl *a* concentration was higher than at RMF1 and the highest concentration was found at 1 m (1.5 µg Chl *a* L^{-1}, Fig. 11a). The Phaeo concentration at RMF1 was similar to the Chl *a* concentration. At RMF2, the Chl *a* concentration was higher than the Phaeo concentration, especially at 1 m (Fig. 11a). The integrated Chl *a* concentration in the water column (0-30 m) was different between the sampling days, with 3.2 mg m^{-2} at RMF1 and 11.6 mg m^{-2} at RMF2, respectively (Table A4).

In Van Mijenfjorden, the highest Chl *a* concentration on both sampling days was observed at 1 m (VMF1: 0.49 mg Chl *a* m^{-2}, VMF2: 0.86 mg Chl *a* m^{-2}, Fig. 11b). While the Chl *a* concentration at 1 m and 5 m was higher at VMF2 than at VMF1, the Chl *a* concentration at 15 m and 30 m was equal for both sampling days (Fig. 11b). The Phaeo concentration was higher than the Chl *a* concentration at VMF1 but fairly similar at VMF2 (Fig. 11b). The integrated Chl

a concentration (0-30 m) was higher at VMF2 than at VMF1 (8.4 mg Chl *a* m^{-2} vs. 5.0 mg Chl *a* m^{-2}, Table A4). From the CTD, the calibrated fluorescence showed that the Chl *a* concentration peaked at VMF1 at 2 m with a concentration of 0.5 µg L^{-1} (Fig. 4a. 4c). At VMF2, two peaks were observed, the first one was right under the sea-ice with Chl *a* concentration of 1.1 µg L^{-1} and a second peak at 5 m of 1.3 µg L^{-1} (Fig. 4b. 4d).

3.2.2.2 Microalgal community composition

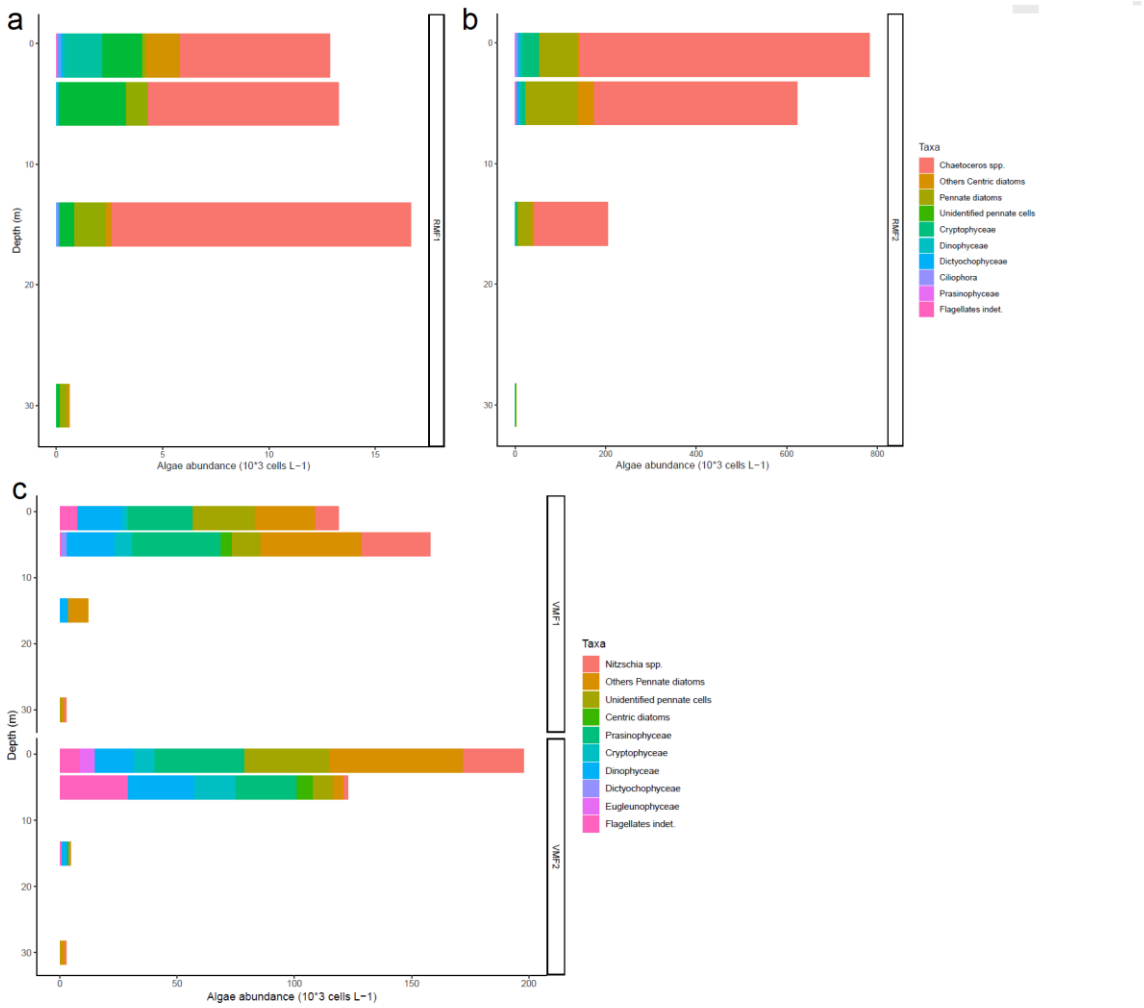

Figure 12. Microalgal abundance (cells L^{-1}) per depth (m): 1, 5, 15 and 30 m. (a) RMF1 (b) RMF2 and (c) VMF1/VMF2. Note the different scale on y-axis.

In Ramfjorden, the total microalgal abundance differed, with RMF2 having much more algae abundance than RMF1 (e.g., almost 50 times higher at 1 m, Fig. 12a.12b). The most abundant taxon observed was the centric diatom *Chaetoceros* spp., (abundance up to 800 x 10^3 cells L^{-1} at 1 m, RMF2). Often observed species were *C. gelidus*, *C. wighamii*, *C. furcelatus*, *C. dydimus*, *C. radicans*, *C. debilis*, *C. simplex*, and, *Attheya septentrionalis*. In addition, one cell of *C. minimus*, a brackish water species was found (at RMF2, 5 m). The other most often observed

centric diatoms taxa were *Thalassiossira* sp., and *Skeletonema* sp.. The most abundant species of the pennate diatoms were *Navicula transitans* and *Cylinrotheca closterium* (See appendix, Table A7 for more details). Other taxa observed were *Cryptomonas* sp., at 1 m and low abundance of *Nitzschia* spp.. The microalgae diversity in the water column at RMF1 and RMF2 was ranging between 6 and 18 taxa, with highest recorded at the upper water column at RMF2 (Table A8).

In Van Mijenfjorden, the microalgal cell abundance was similar between VMF1 and VMF2 and the highest number of cells was observed in the upper water column (at 1 and 5 m depth, ranged from 100 to 200 $x10^3$ cells L^{-1}, Fig. 12c). The algae abundance decreased with depth, with almost no algae at 15 m and 30 m (Fig. 12c). There was no major difference in the algae cell abundance between VMF1 and VMF2, except the highest abundance was at 5 m at VMF1, while it was at 1 m at VMF2 (Fig. 12c). The microalgae composition was diverse, but very similar on both days. The microalgal diversity ranged between 8 and 30 taxa, with the highest diversity at the upper layer (1 m) and lowest at depth (Table A8). Within the pennate diatoms, the most abundant taxa observed were *Cylindrotheca closterium* and *Synedropsis hyperborea* and in lower abundance *Navicula* spp. (See appendix, Table A7 for more details).The following most abundant taxa observed were the Prasinophyceae represented by *Pyramimonas* sp. and the Dinophyceae (mainly Gymnodiniales, e.g., *Heteroscapa rotundata*, *Gymnodinium wulffii*). In addition, Cryptophyceae (mostly represented by *Cryptomonas* spp.) and a few *Nitzschia* spp. were observed (Fig. 12c). The only small difference in terms of microalgae composition was the slightly higher abundance of flagellates in the upper water column of VMF2 (1 m and 5 m) than at VMF1 (Fig. 12c).

3.2.2.3 POC concentration, POC/PON and POC/Chl *a* ratios

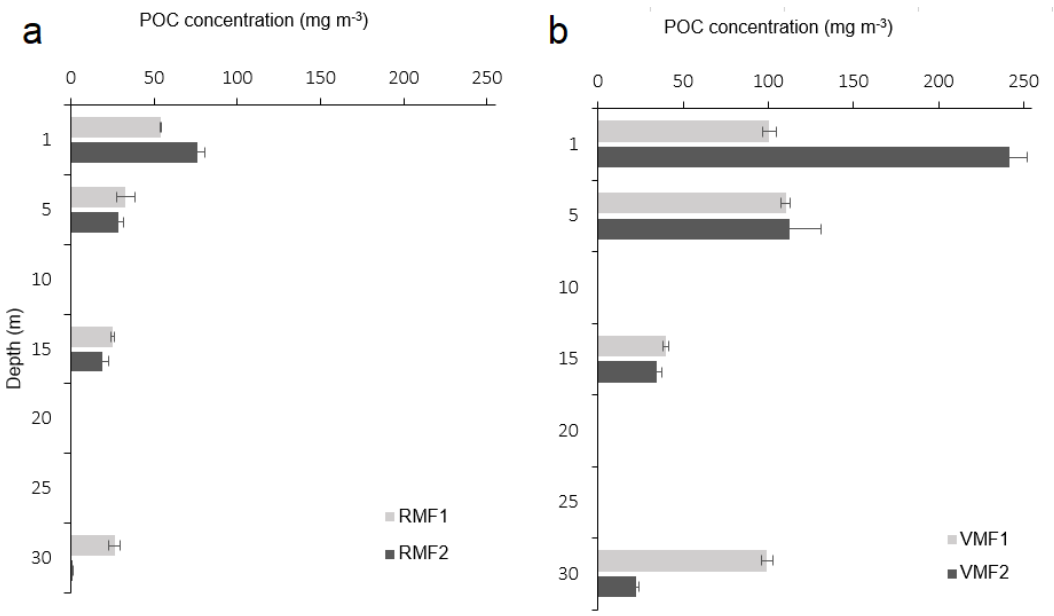

Figure 13. POC concentrations (mg m^{-3}) per depth (m): 1, 5, 15 and 30 m. (a) RMF1 (light grey)/ RMF2 (dark grey) and (b) VMF1 (light grey)/ VMF2 (dark grey). Note the concentrations at RMF2 are presented but might be underestimated (details in section 2.3.2.3).

In Ramfjorden, the POC concentrations were highest in the upper water column (RMF1, 1 m: 54 mg POC m^{-3}, RMF2, 1 m: 76 mg POC m^{-3}, Fig. 13a), and decreased then with depths. At RMF1, the POC/PON ratios in the upper water layer (1 - 5 m) were relatively low (5.9 - 5.3), but higher at greater depth (15 m: 12.3 and 30 m: 9.4, Table A3). The POC/Chl *a* ratios observed at RMF1 were highest at 1 m and 15 m (438 - 408), but lower at 5 m (POC/Chl *a* ratio of 107, Table A3).

At VMF2, the POC concentration was much higher than at VMF1 (VMF1: up to 242 mg POC m^{-3}, VMF2: up to 110 mg POC m^{-3}, Fig. 13b). At VMF2, the POC concentration constantly decreased with depth, but this could not be observed at VMF1. At VMF1, the POC concentrations were fairly similar at 1, 5 and 30 m (~100 mg POC m^{-3}), while it was lowest at 15 m (40 mg POC m^{-3}, Fig. 13b). The POC/PON ratios of the suspended biomass in the water column in Van Mijenfjorden did not show any clear trend and ranged between 7 and 10. However, the POC/PON ratios were slightly higher at 30 m on both sampling days (VMF1: POC/PON = 10.4, VMF2: POC/PON = 8.0, Table A3). The POC/Chl *a* ratios observed were also variable without any clear trend (on both days: 176 - 360, Table A3).

3.2.3 Vertical export of biomass

3.2.3.1 Chl *a* and Phaeo flux, Chl a/Phaeo ratio

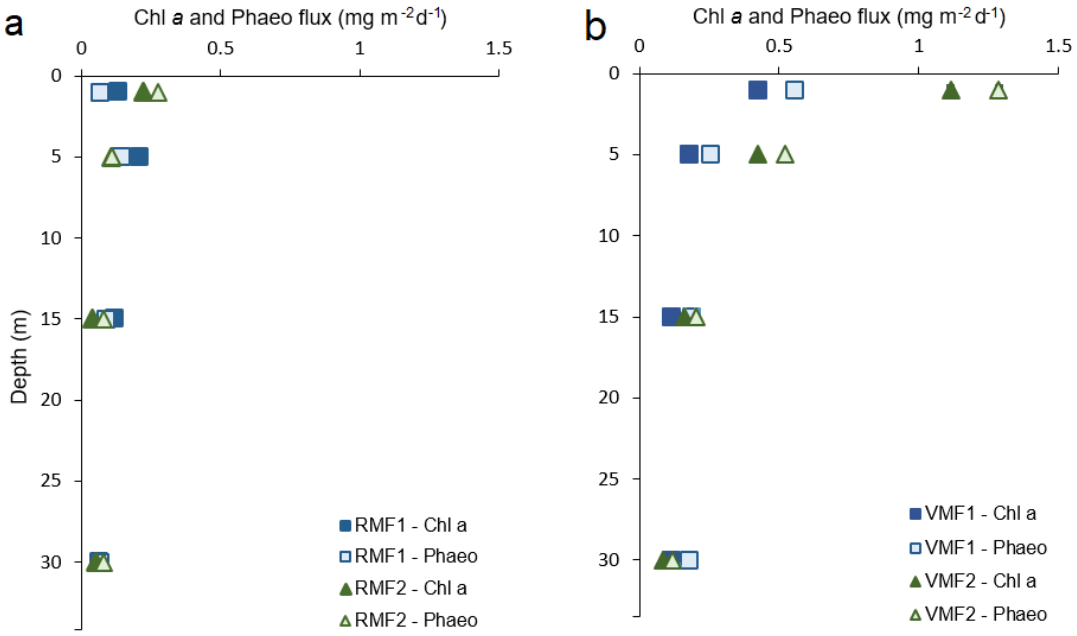

Figure 14. Downward flux of Chl a and Phaeo (mg m^{-2} d^{-1}) per depth (m): 1, 5, 15 and 30 m. (a) RMF1 (blue) / RMF2 (green) and (b) VMF1 (blue) / VMF2 (green).

For both fjords, the downward export of Chl *a* and Phaeo was higher close to the surface (1 m and 5 m) and lower at depth (15 m and 30 m, Fig. 14a). At RMF1, the Chl *a* flux at 1 m was slightly lower than at 5 m (0.13 vs. 0.21 mg Chl *a* m^{-2} d^{-1}). In Ramfjorden, the Phaeo flux followed the Chl *a* flux pattern, decreasing with depth (Fig. 14a). At RMF1, the Phaeo flux was slightly weaker than the Chl *a* flux, while the Phaeo flux at RMF2 was slightly higher at 1, 15 and 30 m depth than the Chl *a* flux (Fig. 14a). Therefore, the ratio Chl *a*/Phaeo was above 1 at RMF1, especially at 1 m (with ratio of 2) and decreased with depth (Table A3), while at RMF2, the Chl *a*/Phaeo ratio was below 1 (except at 5 m, Table A3).

At VMF2, the downward export of Chl *a* was higher at VMF2 than at VMF1, especially in the upper water column (VMF1, 1 m: = 0.42 mg Chl *a* m^{-2} d^{-1}, VMF2, 1 m: 1.1 mg Chl *a* m^{-2} d^{-1}, Fig. 14b). The Phaeo flux in Van Mijenfjorden was slightly higher than the Chl *a* flux at all depths and also decreasing with depth on both days (Fig. 14b). The Chl *a*/Phaeo ratios were therefore below 1 (ranged from 0.87 to 0.60, Table A3).

3.2.3.2 Export of microalgae

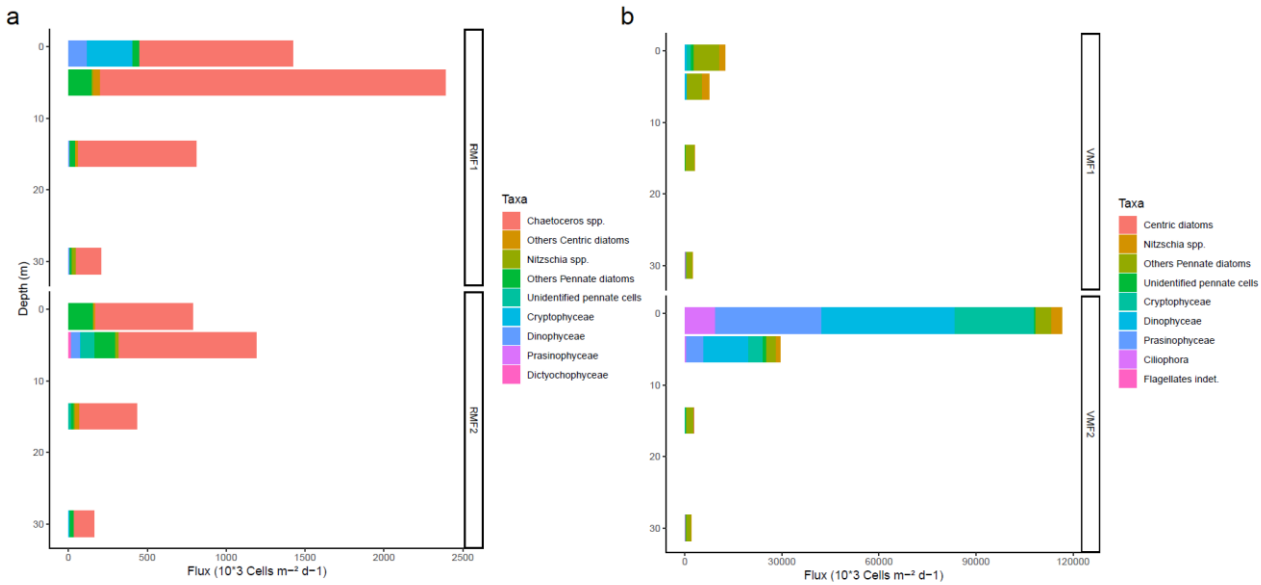

Figure 15. Export of microalgae (cells m^{-2} d^{-1}) per depth (m): 1, 5, 15 and 30 m. (a) RMF1/RMF2 and (b) VMF1/VMF2. Note the different scale on x-axis.

In Ramfjorden, the export of microalgae cells was slightly higher at RMF1 than at RMF2 (Fig. 15a). The highest cells export was observed at 5 m on both sampling days (RMF1, 5 m: 2 400 x 10^3 cells m^{-2} day^{-1}, RMF2, 5 m: 1 200 x 10^3 cells m^{-2} day^{-1}). *Chaetoceros* spp. was the most dominant taxon sinking out on both sampling days and at all depths (Fig. 15a). Pennate diatoms were the second most abundant algae group sinking out (mainly *Fragilariopsis* sp. and *Cylindrotheca closterium*). Other taxa sinking out were centric diatoms (e.g., *Skeletonema* sp. and *Thalassiosira* sp.), and Dinophyceae (mainly Gymnodiniales), pennate (*Nitzschia* spp.) and Cryptophyceae (mostly *Cryptomonas* spp.). The microalgae total diversity was ranging between 5 and 10 taxa with no clear pattern with depth. However, it was slightly higher at RMF2 than at RMF1 (Table A8).

In Van Mijenfjorden, a high number of microalgae was exported, especially in the shallow sampling depth, but decreased strongly with depth (Fig. 15b). At VMF1, the microalgae flux was stronger at 1 m (12 000 x10^3 cells m^{-2} d^{-1}) than at 5 m (7 500 x10^3 cells m^{-2} d^{-1}), and dominated by pennate diatoms (e.g., *Cylindrotheca closterium*, *Synedropsis hyperborea*, *Navicula* spp.) including some *Nitzschia* spp.. At VMF2 (Fig. 15b), the number of sinking cells was much higher than at VMF1 (total flux of algae cells at 1 m: 120 000 x 10^3 cells m^{-2} d^{-1}, 5 m: 30 000 x 10^3 cells m^{-2} d^{-1}, Fig. 15b), and dominated mostly by the taxa: Dinopyceae (e.g.,

Heterocapsa rotundata), Prasinophyceae (e.g., *Pyramimonas* sp.), and Cryptophyceae (e.g., *Teleaulax* sp. cf. *amphioxeia* and *Leucocryptos marina*, Fig. 15b). Also, high number of Ciliophora (Ciliate indet.) were observed at 1 m at VMF2. Within the pennate diatoms, *Nitzschia* spp. were sinking out especially at 1 m and 5 m, which higher export at VMF2 compared to VMF1 (e.g., for the highest flux recorded 1 m = 3400 x10^3 cells m^{-2} d^{-1}). The microalgae total diversity was ranging between 8 and 19 taxa. It decreased with depth and was slightly higher at VMF2 than VMF1 (Table A8).

3.2.3.3 POC flux, POC/PON and POC/Chl *a* ratios

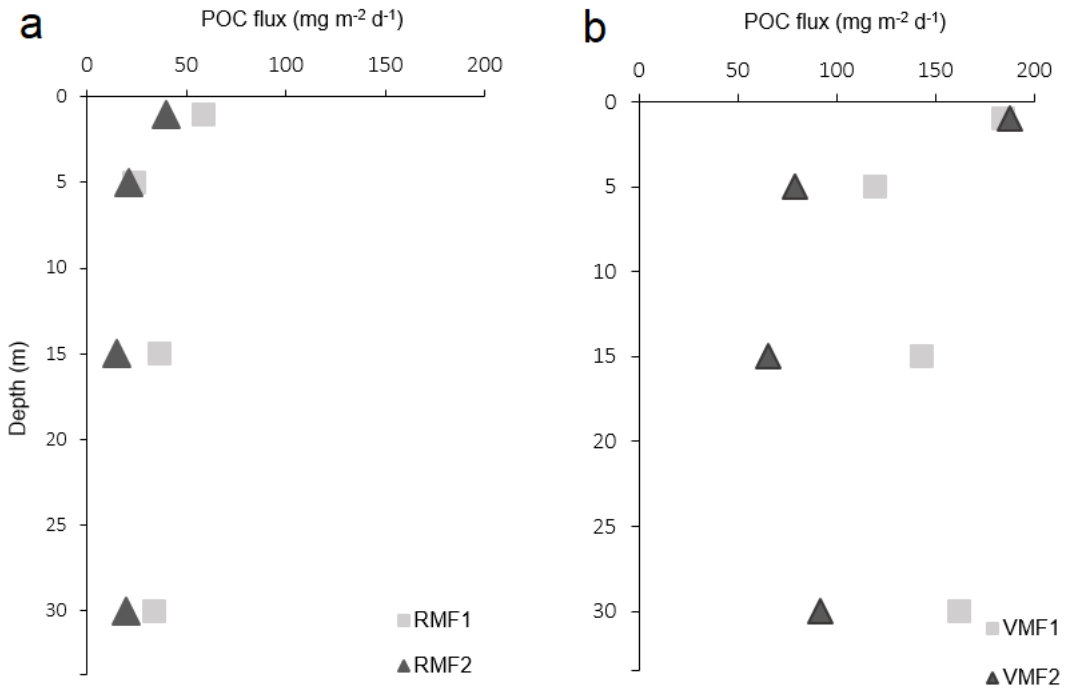

Figure 16. POC flux (mg m^{-2} d^{-1}) per depth (m): 1, 5, 15 and 30 m. (a) RMF1 (light grey)/ RMF2 (dark grey) and (b) VMF1 (light grey)/ VMF2 (dark grey).

In Ramfjorden, the observed POC flux was slightly higher at 1 m (RMF1: 59 mg POC m^{-2} d^{-1}, RMF2: 40 mg POC m^{-2} d^{-1}) than at 5 m (22-24 mg POC m^{-2} d^{-1} on RMF1 and RMF2, Fig. 16a). The flux was slightly increasing with depth at RMF1, but fairly constant with depth at RMF2 (Fig. 16a). The POC/PON ratios did not shown any clear trend with depth and were ranging between 7.8 and 21.2 on both sampling days (Table A3). The ratio was highest at RMF1, 1 m (12.4) and at RMF2, 5 m (21.7) and inversely, lowest at RMF1, 5m (7.9) and RMF2, 1 m (7.8) (Table A3). The POC/Chl *a* ratios did not show any major changes with depth or between

sampling days. The ratios were quite high on both days (ranging between 113 and 511, Table A3).

In Van Mijenfjorden, the POC flux was highest at the shallower depth (VMF1: 184 mg POC m^{-2} d^{-1}, VMF2: 188 mg POC m^{-2} d^{-1}, Fig. 16b). The POC flux did not considerably decrease with the deeper depths as expected (Fig. 16b). In contrast, at VMF1, the POC flux actually increased between 5 m and 30 m (from 120 mg m^{-2} d^{-1} to 162 mg m^{-2} d^{-1}, Fig. 16b). At VMF2, the flux was more constant with depth (average between 5 and 30 m: 79 mg POC m^{-2} d^{-1}). The POC/PON ratio at VMF1 was lowest at 1 m (with ratio of 12.4), and then increased with depth (5-30 m: 16.5 - 18.4) (Table A3). At VMF2, the POC/PON ratios were lower than at VMF1, especially at the surface (1 and 5 m: 5.8 - 6.8), but increased slightly at depth (ratio of ~10 at 15 m and 30 m). The POC/Chl *a* ratios observed were in general high, increased with depth, and they were very much higher at VMF1 than VMF2 (VMF1: 435 - 1435, VMF2: 169 – 1071, Table A3).

3.2.3.4 Particles characteristics

a

1 m

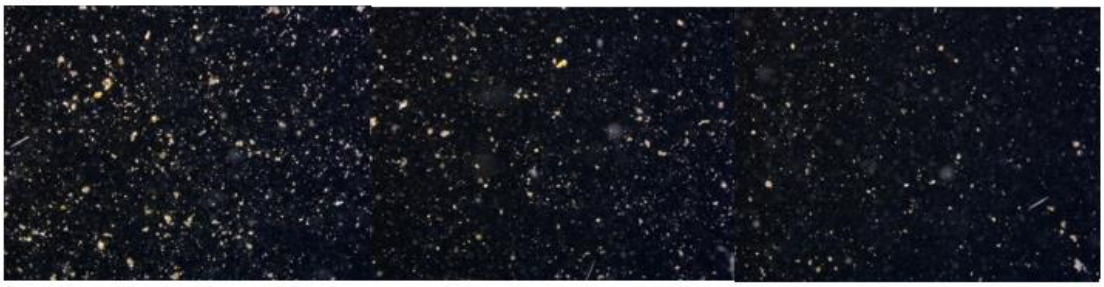

5 m

15 m

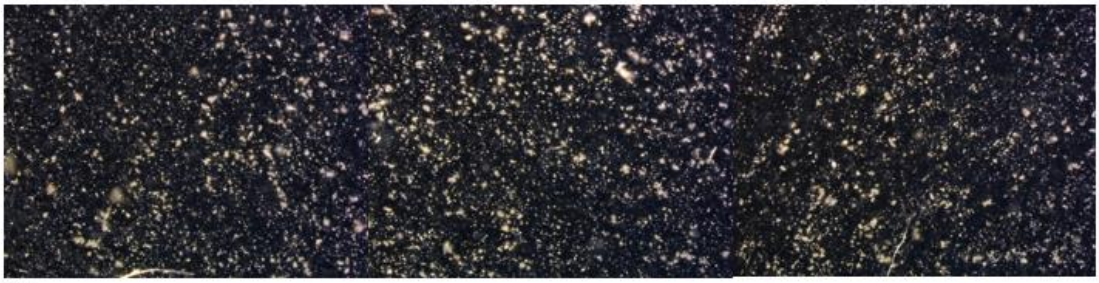

30 m

b

1 m

5 m

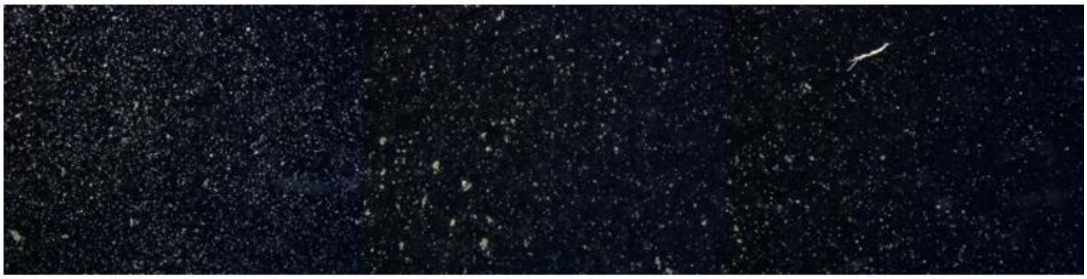

15 m

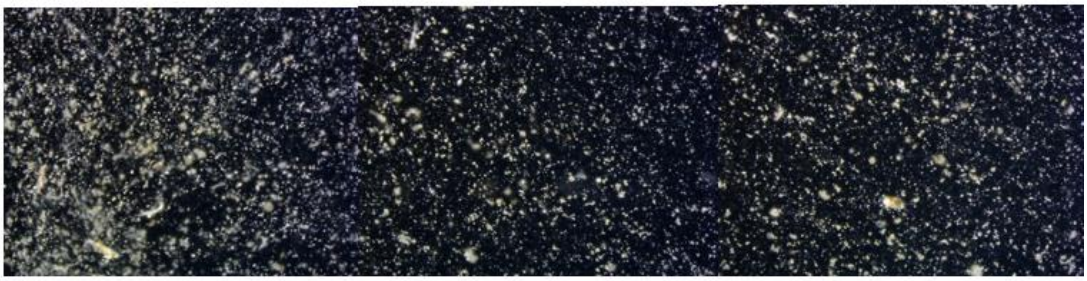

30 m

C

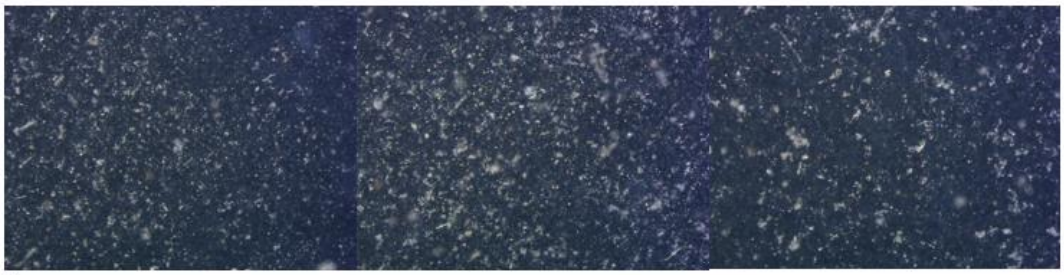

1 m

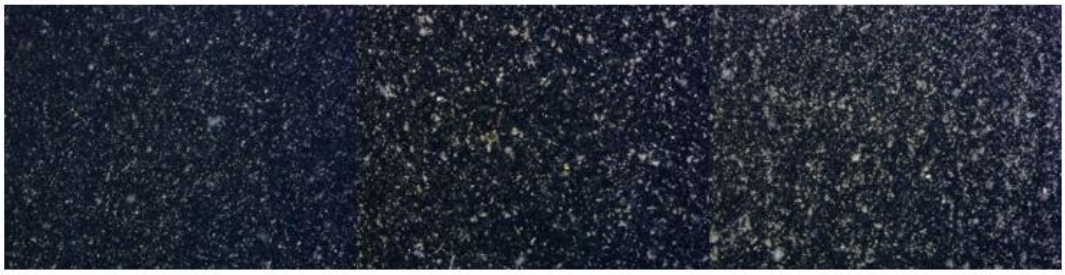

5 m

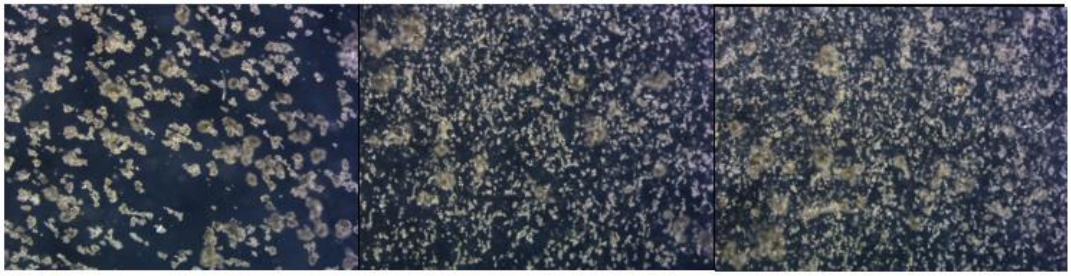

15 m

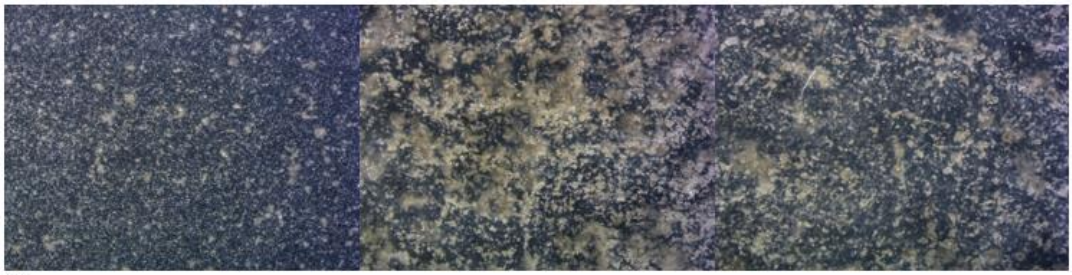

30 m

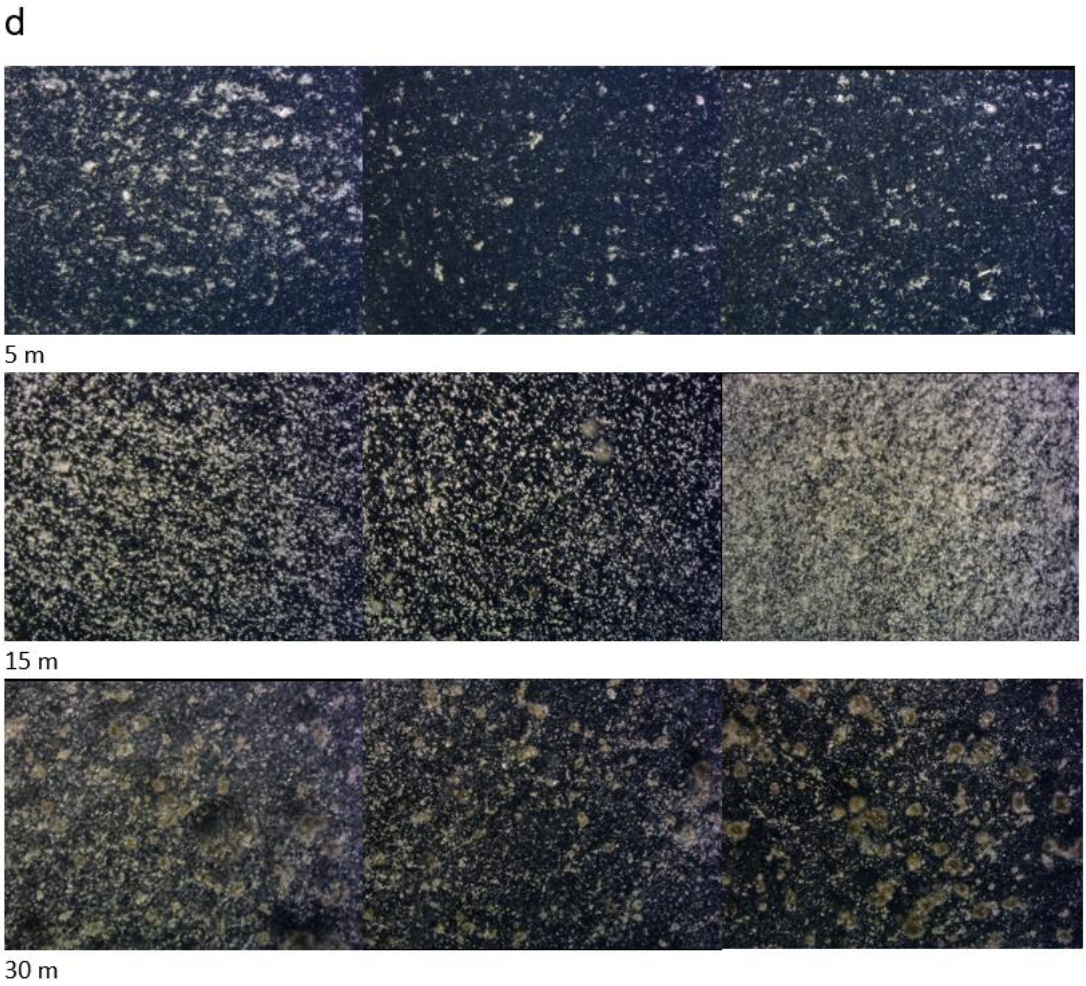

Figure 17. Pictures of the sinking particles (collected from the gels traps). (a) RMF1; (b) RMF2; (c) VMF1, and (d) VMF2, with examples from 1, 5, 15 and 30 m. Note the pictures at 1 m, VMF2 are not presented (details in sections 2.3.3.4).

In Ramfjorden, the size and abundance of particles flux from the gel trap pictures seemed to increase with the deeper depths. At 30 m, much higher number of particles was observed compared to the others shallower sampling depths (Fig. 17a.17b). At 1 m, the particles size and abundance seemed similar at RMF1 and RMF2, while at 5 m and 15 m, the particles seemed to be larger (aggregated) and more abundant at RMF1 (Fig. 17a).

In Van Mijenfjorden, much more particles were sinking out than in Ramfjorden (Fig. 17c.17d). The particles size and abundance seemed to increase at greater depths. At 15 m and especially at 30 m, a lot of aggregated particles were observed. Qualitatively, it is difficult to assess any considerable difference between the particles size and abundance between VMF1 and VMF2.

4 Discussion

4.1 Ramfjorden

4.1.1 Ice ecosystem

The land-fast sea-ice in Ramfjorden during March 2019 can be define as fresh-water ice because of its high temperature (on average -0.5 °C) and its low bulk salinity (on average: 1, Fig. 2c) (Leppäranta and Manninen, 1988). As river run-off in Ramfjorden has been high during February and March 2019 (Fig. A1), it can be assumed that brackish and freshwater masses were also present during the ice formation process between December 2018 and March 2019 prior to the RMF1 and RMF2 field work. The brine volume fraction of the sea-ice, which is a measure for the porosity of the ice, was below the 5 % threshold of brine channels connectivity (Golden et al., 1998) at the interfaces air/ ice and water/ ice on both sampling days (Fig. 2d). Therefore, any exchange between air or water and the sea-ice were limited and likely restricted the exchange of nutrient and brine expulsion (Arrigo, 2014; Golden et al., 1998, 2007).

The Chl *a* concentration observed in the ice sections was generally very low, but slightly higher in the middle of the ice (e.g., 20-30 cm, with 0.06 mg Chl *a* m^{-2}, Fig. 8a) than the others sections (0-3 cm: 0.009 mg Chl *a* m^{-2}, Fig. 8a). Compared to that, Olsen et al. (2017) observed a higher algal concentration in the top ice sections of first year ice (FYI) North of Svalbard. However, many other studies focus only on the lowermost sea-ice sections (0-10 cm), where the algal biomass accumulation is supposedly the highest (Leu et al., 2015; Syvertsen, 1991). Thus, it is hard to say if an enhanced Chl *a* concentration in the uppermost part of sea-ice, as found in Ramfjorden ice, is commonly found in other fjords. The integrated Chl *a* biomass (< 0.2 mg Chl *a* m^{-2}) found in the sea-ice in Ramfjorden (Table A4) was lower than the threshold of 1 mg Chl *a* m^{-2} in the ice bottom that has been used to define an ongoing sea-ice algae spring bloom (Leu et al., 2015). The Chl *a* concentration at RMF1 and RMF2 can therefore suggests a pre-bloom period. Typical sea-ice algae blooms have much higher Chl *a* standing stock as reported from land-fast ice in Billefjorden (Svalbard) with up to 14 mg Chl *a* m^{-2} (from February to June) and in the pack-ice, northwest of Svalbard, (March to May) where concentrations ranged from 0.3 to 9.8 mg Chl *a* m^{-2} (Leu et al., 2015).

The distribution of algae cells in the sea-ice followed the distribution of the Chl *a* concentration, with higher algal material observed at middle and top sections than at the lower most section (Fig. 9a). This matched the observation by Olsen et al. (2017). The algae abundance (ranged

between 5 x 10^3 cell L^{-1} and 40 x 10^3 cell L^{-1}, Fig. 9a) was similar with the algal abundance observed in June, North of Svalbard by Olsen et al. (2017), and slightly higher than the winter sea-ice algae assemblage observed on the Canadian Arctic shelves (4 x 10^3 cell L^{-1}, Niemi et al. (2011)). The ice algae diversity observed in Ramfjorden was however much lower (~15 taxa, Table A8) that the diversity usually observed during an ice algae spring bloom, where up to 134 taxa were observed (Niemi et al., 2011).

The community composition in Ramfjorden was mostly dominated by a single genus, the pennate diatom *Nitzschia* spp. (mostly *Nitzschia frigida/neofrigida*, Fig. 9a). This genus is characteristic for the Arctic sea-ice, and was also commonly observed in the top sections of FYI North of Svalbard (Leu et al., 2015; Olsen et al., 2017). *Nitzschia* spp. was observed in all ice sections in Ramfjorden (Fig. 9a). Usually, this species occurs mostly in the bottom sections or sub-ice assemblage as arborescent colonies (Leu et al., 2015; Smoła et al., 2018). In addition, various other taxa which are also commonly found in the Arctic sea-ice were observed, such as *Achnanthes* sp. (Arrigo, 2014), *Navicula* sp. cf. *septentrionalis* (Leu et al., 2010), and *Navicula transitans* (Smoła et al., 2018). Further, for centric diatoms have been found in the sea-ice in Ramfjorden, which have previously been observed in Arctic sea-ice such as, *Thalassiosira* sp. (Smoła et al., 2018), *Leptocylindrus* sp. in FYI in Canadian Arctic (Melnikov et al., 2002). Others suspended in the water column during spring, such as *Skeletonema* sp. in Kongsfjorden (Hegseth et al., 2019a), *Skeletonema* and *Leptocylindrus* in Balsfjorden (Eilertsen et al., 1981b) were observed in Ramfjorden. During both sampling days in Ramfjorden, the proportion of pennate was much higher than the proportion of centric (Fig. 9a). This represents a typical algal community composition during the beginning of the spring bloom (Von Quillfeldt, 2000). Higher abundance of flagellates and phagotrophic algae, such as *Gymnodinium* sp., and Ciliophora sp., previously found in ice (Arrigo, 2014; Smoła et al., 2018), were found in higher abundance at RMF2 than RMF1 (Fig. 9a.9c). That could mean the Ramfjorden land-fast ice community was developed between winter to beginning spring bloom with a community of both pelagic species and typical ones of sea-ice algae bloom.

The integrated POC concentration in the sea-ice cores was slightly higher at RMF1 than RMF2 (90 mg POC m^{-2} vs. 50 mg POC m^{-2}, Table A4), but the concentration was very low compared to many others study (Leu et al., 2015). Nevertheless, similar concentrations have been observed during spring in land-fast ice in Rijpfjorden (Svalbard) (54–450 mg POC m^{-2}, Leu et al., 2010) and in Canadian archipelago (1.5-46 mg POC m^{-2}, Smith et al., 1988). The POC

concentration was slightly higher in the uppermost ice sections (Fig. 10a), and as the Chl *a* and algae biomass had same pattern, it can be speculated that most of the POC was from algal material.

The POC/PON ratios in the sea-ice of Ramfjorden were very variable and generally high (8.8 - 21.2, Table A3), but matched with observations by Niemi and Michel (2015) in FYI of Arctic coastal ecosystems. Thick snow cover was observed in Ramfjorden (Table 3), which reduced highly the light transmittance. Therefore the reason for the high POC/PON ratio cannot be the light acclimation of sea-ice algae, as previously described by Gosselin et al. (1990). Indeed at high irradiance, microalgae have high photo-assimilation of carbon giving high ratio (Gosselin et al., 1990). Moreover, sea-ice algae with nitrogen deficiency may be one explanation for high POC/PON ratios (Demers et al., 1989), or simply a high amount of allochthonous organic carbon material, as detritus of marine/ terrestrial origin or non-photosynthetic organisms in the ice (Arrigo et al., 2003; Bianchi, 2006). These materials might have been brought to the fjord by river run off and incorporated during ice formation or by an event of river water flooding the ice. The latter seems likely in Ramfjorden, because during the microscopy examination of the algae samples, a lot of sediments were observed.

The high algae abundance at the uppermost sections of the Ramfjorden sea-ice, and slightly higher abundance at RMF2 than RMF1, may be explained by the freezing process. Prior to ice formation, a surface layer of freshwater, originating from river-run off, may have mix with the denser seawater below. The forming brackish water had a lower density, and can be assumed incorporated the brackish/ freshwater algae species community into the forming sea-ice. Brack water species (*Eunotia serra* and *Diploneis bombus*) found in the surface of the sea-ice in Ramfjorden support this hypothesis. Another possible explanation for the presence of these brackish water species can be the river flooding events over the fast ice, which entrains both algae and POC and may thus also explain the high POC/PON and POC/Chl *a* ratios obtained in the ice top sections in Ramfjorden (Table A3) (Rachold et al., 2004). Sea-ice algae usually thrive in high brine salinity conditions inside the ice (Arrigo, 2014), but in Ramfjorden the brine salinity was quite low (4 - 18, Fig. 2b). Hence, sea-ice algae have to cope here with low salinity, which may only be suitable for few species in the ice

A negative freeboard was observed (Table 3) which might resulted from thick snow cover (~ 25 cm, Table 3). The ice had favourable conditions for seawater flooding events into the ice

and ice-surface/ snow as with negative freeboard (Arrigo, 2014). Flooding events can contribute greatly to bring allochthonous material and infiltration communities in the ice (Arrigo, 2014; Sakshaug et al., 2009). *Phaeocystis pouchetii* have been observed in Ramfjorden sea-ice and in the underlying water, though the counts of cells of this species too small to be correctly counted in the microscope and are thus not included in the results. This prymnesiophyte has however previously been found as part of the infiltration community in the sea-ice in pack-ice, Southern Ocean (Kristiansen et al., 1998) and on Svalbard (Wiktor, personal communication, 2020), and thus this may also have happened in Ramfjorden. In Ramfjorden ice the POC/Chl *a* have been observed very variable (Table A3), which could either due to numerical dominance of potentially non-autotrophic species such as with Dinophyceae and Ciliophora at RMF2 (Fig. 9c) and as well observed by Kvernvik, (2019) and Niemi and Michel (2015). *Phaeocystis* sp. found in Ramfjorden, might also contributed to the high POC/Chl *a* alike possibly *Phaeocystis Antarctica* (Arrigo et al., 2003).

One reason for the low ice algal biomass in the bottom section of the ice may be due to the release of algae by episodic brine drainage, when brine channels interconnected during warming of the ice (Gradinger et al., 1991). A brine drainage event can cause fluctuation of the water temperature under the ice (Fig. 5a) and result in turbulent mixing, which can flush away the ice bottom layer of ice (skeletal layer) (Leu et al., 2015). Alternatively, rapid melting of the bottom of the sea-ice can affect the ability of ice algae to form or maintain at the underside of ice or even remove the cells (Leu et al., 2015; Olsen et al., 2017). With regard to Ramfjorden, the brine volume in the uppermost and lowermost part of the ice was under 5 %, the threshold of interconnectivity (Golden et al., 1998). Water flooding the brine channels or brine drainage were therefore likely restricted, at least during the sampling period, and thereby the seeding of brine by microalgae was limited (Stoecker et al., 1997). Furthermore, tidal currents under the ice (as explained Section 3.1.3.2) and eddies created by brine drainage can promote turbulent mixing which supply ice algae incorporation and growth by incorporation of inorganic nutrient into the ice (Leu et al., 2015; Syvertsen, 1991). As the brine volume recorded in Ramfjorden was very low, this can be assume to have played a minor role. The low abundance of microalgal cells may resulted by low incorporation of algae and cysts during ice formation (Syvertsen, 1991). It may as well result of low growth development at this early spring bloom stage, due to very low nutrient present, if behaving conservatively with the low bulk salinity observed in ice (Fig. 2c) (Søgaard et al., 2013), in combination with low light transmittance.

At RMF2, the algae cell abundance was almost twice as higher as at RMF1 (Fig. 9a), but the Chl *a* concentrations were quite similar. The most likely explanation is due to the methodology used, indeed only one ice core was collected to analyse the microalgal composition for each day in Ramfjorden (Table A1), which can result in abundance slightly different due to patchiness in algae distribution. As stated by Cimoli et al. (2017), spatial variation of ice algae biomass varies from scale of mm to km. The algae patchiness is drive by conditions in the brine channels during winter/spring (e.g., salinity, space available, grazing pressure) (Leu et al., 2015). The patchiness in algae distribution can also be explained by difference in snow surface and thickness (even a few variation in cm) which are negatively correlated with the microalgal biomass (Mundy et al., 2007). Snow falls recorded before the sampling period combined with wind tend to change snow surface (Table A2). Increasing light into ice lead to a rapid growth, as seen with characteristic arborescent colonies of *Nitzschia frigida* (Medlin and Hasle, 1990), as found in Ramfjorden ice and by Olsen et al. (2017) in the sea-ice North of Svalbard. An alternative explanation for the increase of algae abundance is the normal algae growth, even under thick snow cover as according Grossi et al. (1987): 0 – 25 cm of snow cover = 2.4 – 9.9 days to double algae population. The Chl *a* concentration observed in the ice were similar for both sampling days, and for this analysis duplicate and triplicate ice cores were extracted (Table A1). A better sampling methodology will be to collect at least three ice cores for the algae composition examination.

In summary, the sea-ice in Ramfjorden was comparable fresh and warm, had a low brine volume, and hence a weak interconnectivity of brine channels. The ice contained a low Chl *a* concentration, algae abundance, and POC concentration. The algae community composition was reflecting a combination of sympagic and pelagic species, and the high contribution of flagellates suggests that a transition between winter to beginning bloom situation was given in the sea-ice in Ramfjorden.

4.1.2 Water column

The hydrographic structures found in Ramfjorden in March presented late winter/early spring conditions with a colder and fresher layer (1.5 °C with salinity: 32 - 33.2) overlaying a weak thermocline (reaching 15 m depth), and a warmer layer underneath (3 °C) (Fig. 3a. 3c) (Cottier et al., 2010). This scenario represents a typical vertical temperature distribution in a North Norwegian fjord, also recorded in Balsfjorden during winter (Eilertsen et al., 1981b). The water in Ramfjorden was fresher than Atlantic Water masses (AW, salinity of ~34.5) found on the

shelf (Cottier et al., 2005). This was likely due to the limited inflow of coastal waters into Ramfjorden due to its inland location, and due to the relatively higher freshwater input from rivers and snow melt runoff (Eilertsen et al., 1981; Noji et al., 1993) (Fig. A1). Substantial precipitation was recorded from end of February to beginning of March which could have as well resulted in a high freshwater run-off into Ramfjorden (Table A2).

The surface water layer was directed into the fjord during RMF1 deployment (Fig. 7a). I assume that the surface layer of the entire inner fjord was moving into the fjord because of the width of the fjord being too small for the Coriolis effect to induce any circular water movement. Fjords typically present a surface water layer out-flowing over a denser saline water entering the fjord (Inall and Gillibrand, 2010). The wind were higher during the days before RMF1 and were directed south-southwest, pushing surface water towards the ice-edge, thus directing water into the fjord (Table A2). The higher current velocity underneath the ice at RMF1 (0.07-0.09 m s^{-1}) compared at RMF2, thus might have been a combination of wind effect and the high tides phase (Table A2 and A5). At RMF2 the currents speed was low (0.04-0.06 m s^{-1}, Fig. 6b) and corresponded with speed near the seafloor during winter in other fjord systems (Inall and Gillibrand, 2010). The surface layer was flowing into the fjord, and the deeper layer out the fjord fitting the principle of fjord circulation (Inall and Gillibrand, 2010).

The Chl *a* concentrations observed at RMF1 (0.1-0.3 µg Chl *a* L^{-1}, Fig. 11a.) were similar with the surface concentration observed during mid-November (0.2 µg Chl *a* L^{-1}) by Noji et al. (1993). At RMF2, the Chl *a* concentrations (0.7-1.5 µg Chl *a* L^{-1}, Fig. 11a.) were comparable to the Chl *a* concentrations observed in Balsfjorden between early April and late May (1.5 ug L^{-1}, Lutter et al., 1989) and in a Greenlandic fjord (1 µg Chl a L-1, Meire et al., 2016). However, the concentrations at RMF1 were lower than Chl *a* concentrations observed in Ramfjorden (2.9 µg Chl *a* L^{-1}, Bech, (1982)) and in Balsfjorden in late March (3.5 – 20 µg Chl *a* L^{-1}, Reigstad and Wassmann, (1996)). The integrated Chl *a* concentration in the water column was higher at RMF2 (11.6 mg Chl *a* m^{-2}) than at RMF1 (3.2 mg Chl *a* m^{-2}) (Table A4). Lutter et al. (1989) observed highest integrated Chl *a* concentration in Balsfjorden on the 29.04. (0-50 m: 205 mg Chl *a* m^{-2}) which is much higher of what observed in Ramfjorden. I speculate therefore that the Chl *a* biomass observed in Ramfjorden was in an early pelagic bloom phase, as the bloom (defined as > 0.5-1 µg Chl a L^{-1}) usually starts in Balsfjorden in the second half of March (Eilertsen et al., 1981b; Eilertsen and Frantzen, 2007; Hopkins et al., 1989; Lutter et al., 1989). The Phaeo concentrations were generally equal or lower than the Chl *a* concentrations at RMF1

and RMF2, especially lower at 1 m with Chl *a*/Phaeo ratio of 2.11 (at RMF2), indicating that freshly growing cells are abundant (Zajączkowski et al., 2010). This assumption was further supported by the high number of healthy-looking *Chaetoceros* sp. cells at this depth.

One potential explanation for the higher biomass observed at RMF2 than at RMF1 may be a horizontal advection from Balsfjorden as previously reported by Noji et al. (1993). The advection may have been a result of the prevailing S/SW wind, pushing surface water towards the ice-edge, thus into the fjord (Table A2). At RMF1 the incoming current into the fjord under the ice had average speed of 0.08 m s^{-1}, meaning water might have been transported over 1.7 km for a 6 h period. Therefore, an advection of water masses from Balsfjorden into Ramfjorden (total length: 14 km), assuming an accumulation of wind effect over several days, was most likely probable. The fluctuation of water temperature underneath the ice at RMF1 (Fig. 5a), plus the variation in water temperature through vertical profile with the slightly warmer water layer in upper water column at RMF1 than at RMF2 (RMF1: 2 °C at 2 m, RMF2: 2 °C at 8 m, Fig. 3a) might be combination of water advection from Balsfjorden. This may have increased the particles transport during RMF1. The high POC/PON ratio of 21.2 at 5 m at RMF2 likely support the idea of an allochthogenous carbon source by tidal current into Ramfjorden (Thornton and McManus, 1994), which might have brought as well as phytoplankton and nutrient, and enhanced the growth of autotrophic biomass (recorded at RMF2). No nutrients data in the water column were collected, therefore advection of nutrient is pure speculation. Similar processes have also been reported from other parts of the Arctic. Johnsen et al. (2018) found for example that the under-ice pelagic bloom observed in Chucki Sea was originated by species advected from free ice-covered waters sources. In Ramfjorden it is likely, that algae have been advected from ice-free Balsfjorden, where sun light might have trigger an earlier pelagic boom state.

Alternatively, algae growth during the days between RMF1 and RMF2 (total microalgae abundance at RMF1, 1 m: 12.5 x 10^3 cells L^{-1}, RMF2, 1 m: 800 x 10^3 cells L^{-1}) could also explain the higher algae abundance and Chl *a* concentration in the water column at RMF2 (Fig. 11a), because diatoms can have a high growth rate (Sakshaug et al., 2009). In Balsfjorden, in March, a total cells count of 100-300 x 10^3 cells L^{-1} was observed with a peak during mid to end of April (1000-6000 x 10^3 cells L^{-1}, Eilertsen et al. (1981); Eilertsen and Taasen, (1984)). The cell abundances at RMF1 were slightly lower than what found in Balsfjorden during March,

but the cells abundance observed at RMF2 corresponded of what recorded during spring bloom. Combined with a possible advection, it was most likely that algae were brought into Ramfjorden, and support the increase of algae growth at RMF2.

The species composition in Ramfjorden was mostly represented by centric and pennate diatoms (Fig. 12a.12b). The centric diatoms composition was dominated by far with the genus *Chaetoceros*, and its species are commonly observed during the spring bloom in sub-Arctic Balsfjorden (Eilertsen and Taasen, 1984). *Skeletonema* sp. and *Thalassiossira* sp. were also previously found in sub-Arctic Balsfjorden (Eilertsen et al., 1981). Others pennate diatoms, as *Fragilariopsis sp*., found in Balsfjorden during spring bloom (Hegseth et al., 2019), *Navicula transitans* found in Kongsfjorden (Hegseth et al., 2019) and *Cylinrotheca closterium*, were the most representative (Fig. 12a.12b). The Cryptophyte, *Cryptomonas* sp., was the third highest species found in upper depth in Ramfjorden, which was commonly found in Kongsfjorden (Hegseth et al., 2019).

The POC concentrations observed in Ramfjorden (26-54 mg POC m^{-3}, Fig. 13a) were lower than the ones observed in Noji et al. (1993) during winter months (70 - 270 mg POC m^{-3}). The POC concentrations were decreasing with depth (Fig. 13a). This may either indicate that the organic carbon was rapidly removed by grazers in the water column, while their grazing impact was negligible between 15 m and 30 m, where the POC concentrations did not decline. On the other hand, the resuspension of material from shallow areas in Ramfjorden and a subsequent horizontal advection may have resulted in a slight increase of POC concentrations at depth (Fig. 13a). The high POC/PON ratios observed at the bottom depth (9 - 12, Fig. 13a and Table A3) can be explained by more (refractory) detritus and terrestrial material, which may have been resuspended. The observations from the gel trap pictures seem to support this (Fig. 17a and 17b), because the particles were larger and more frequently found at 30 m. Moreover, the POC/PON ratios found in the present study fitted with POC/PON ratios of suspended material by Noji et al. (1993) (POC/PON = 8-25). Noji et al. (1993) concluded that the high POC/PON ratio was due to the advection of sediments from adjacent shallow area. The POC/PON ratios observed in the upper layer (5.3 - 5.9, at RMF1) were lower than the lowest ones previously recorded in Balsfjorden during the peak of the spring bloom (7-10) (Eilertsen and Taasen, 1984) and lower than typical range (6-9) of marine organic matter (Thornton and Macnus, 1994). That might result of higher fresh algal material produced/advected (from Balsfjorden) or due to a dysfunctional problem of the CHN Elemental Analyzer.

In Ramfjorden the Chl *a* concentration was much higher the second days of sampling than the first day, but it was in the range of previously observed concentrations in Ramfjorden during the spring bloom. As also the species composition was typical of spring bloom community composition in a North Norwegian fjord, and the cells abundance were comparable to earlier findings of a beginning bloom, it can be stated that Ramfjorden was during the present study in an early spring bloom phase.

4.1.3 Downward export

The Chl *a* flux observed in Ramfjorden at 1 to 30 m was low, and comparable with fluxes observed in Ramfjorden at similar depth (10 m and 30 m) during winter by Noji et al. (1993: 0.025 – 0.25 mg Chl *a* m^{-2} d^{-1}). Juul-Pedersen et al. (2008) also recorded similar Chl *a* fluxes under the sea-ice in a western Canadian Arctic fjord (Chl *a* flux at 1-30 m: 0.11 - 0.09 mg Chl *a* m^{-2} d^{-1}) prior early spring and Lutter et al. (1989) observed in Balsfjorden a Chl *a* flux exceeding 0.5 mg m^{-2} d^{-1} in mid-April. Therefore, the Chl *a* flux observed in Ramfjorden on both sampling days was typical for a pre-bloom situation, between winter and spring stage. The Chl *a* flux at RMF1 was slightly higher at 5 m and 15 m than the others depths, while at RMF2, the flux was higher at 1 m and was decreasing with depth (Fig. 14a). Noji et al. (1993) did not found any relation between depth and flux, while Juul-Pedersen et al. (2008) did. The Chl *a* flux observed in Ramfjorden was in any case higher in the upper water column than at depth (e.g., 30 m) and seemed to follow the characteristic pattern of low Chl *a* biomass sinking down under the sea-ice.

Similar as the Chl *a* flux, the export of algal cells was higher at RMF1 than at RMF2 at all depths (e.g., 1 m: 1500 x 10^3 cells m^{-2} d^{-1} vs. 800 x 10^3 cells m^{-2} d^{-1}). The export of algae was highest at 5 m for both days and decreased with depths (Fig. 15a). Olsen et al. (2017) observed a maximum algae cells flux (115-899 x 10^3 cells m^{-2} d^{-1}) at 1 m under an ice floe North of Svalbard during the end of May. Juul-Pedersen et al. (2008) observed an export of algal cells under the sea-ice (at 1 m) from March to May (3200 - 118 000 x 10^3 cells m^{-2} d^{-1}), which was much higher than what was observed in Ramfjorden. The export of algae cells in March in Ramfjorden was rather comparable to North of Svalbard than the Canadian Arctic flux during spring.

The most dominant genera sinking out were mainly pelagic species such as centric diatoms (dominated by *Chaetoceros* spp.) and lesser pennate diatoms (*Fragilariopsis* spp., *Navicula*

spp., *Cylindrotheca closterium*, Fig. 15a). In addition, few *Nitzschia* spp. cells were observed in the sediment traps, and these species are known to live both in the ice and the water column (Medlin and Hasle, 1990). In Ramfjorden, also Dinophyceae *(Gymnodiniales)* and Cryptophyceae *(Cryptomonas* sp.) were found to sink out (Fig. 15a). Lalande et al. (2016) reported sinking of these taxa also from ice-free Kongsfjorden in May, but in general the species composition of the microalgae sinking in Ramfjorden was similar to observations in Balsfjorden in April (Lutter et al. 1989). In addition Lalande et al. (2016) and Lutter et al. (1989) observed a lot of sinking *Phaeocystis pouchetii* cells. Some cells of this species were also found in the sediment traps in Ramfjorden, but as the cells were not counted (Section 2.3.1.2 for details), is not possible to assess its contribution to the export. In any case, the community composition of sinking algae cells in Ramfjorden was typical of spring bloom cell composition in (sub-)Arctic with high abundance of centric diatoms (Wassmann et al., 1999).

In Ramfjorden, the POC flux on both sampling days was a bit higher under the sea-ice (e.g., at 1 m: RMF1: 59 mg m^{-2} d^{-1}, RMF2: 40 mg m^{-2} d^{-1}) than the greater depth (5, 15, and 30 m) (Fig. 16a), and the POC flux at RMF1 was generally slightly higher than the flux at RMF2 (Fig. 16a). The POC flux observed here was in the same range as observed by Noji et al. (1993) in Ramfjorden during winter (10 – 70 m: 25 and 300 mg POC m^{-2} d^{-1}) and by Lutter et al. (1989) in ice-free Balsfjorden during March (10 - 50 m: on average 75 mg POC m^{-2} d^{-1}). Juul-Pedersen et al. (2008) observed a lower flux under the ice during the winter to spring period (1 - 25 m: 19 - 25 mg POC m^{-2} d^{-1}). Hence, the export of organic material in Ramfjorden presented typical value for winter to spring transition, with slightly higher export comparatively to western Canadian shelves (Juul-Pedersen et al., 2008), which might be due to more particles resuspended (by currents for instance) into the water column in this narrow fjord.

The POC/PON ratios were very variable on both sampling days with no clear pattern (POC/PON =7.8 - 21.7, Table A3). Noji et al., (1993) observed similarly high POC/PON ratios of sedimented material in the beginning of December and Lutter et al. (1989) observed as well high POC/PON ratios (10 – 170 m: POC/PON= 8-12) in Balsfjorden in March. In Northern Norway fjord, Malangen, high ratio was also found (up to 13 at 30 m, Keck and Wassmann (1996)) and likewise in Adventfjorden, Svalbard (ratio up to 20 at 5 m, Zajączkowski et al. (2010)). Additionally, empty frustules of potential brackish species at RMF2 (e.g., *Pinnularia* sp. at 30 m and *Chaetoceros minimus* at 5 m) were found and suggested terrestrial material may

have been contributed to the pool of POC in Ramfjorden. The high POC/PON ratios observed in Ramfjorden might be due therefore from resuspension of sediments (e.g., from river run-off), of detritus and sand grains, or high amount of terrestrial material contributing to the sinking particles as explained in these cited studies. The POC/Chl *a* ratios did not show a clear trend with depth, but high POC/Chl *a* ratios tended to be observed at 30 m (RMF1: POC/Chl *a* = 511, RMF2: POC/Chl *a* = 366).High POC/Chl *a* ratios have also been reported from Balsfjorden (POC/Chl *a* ratio: 900 - 1200) in February (Lutter et al., 1989) and up to 4900 in Malangen (Keck and Wassmann, 1996), where an extreme high POC flux was observed. That was probably due to a high contribution of non-algal material to the sinking POC as suggested previously by Juul-Pedersen et al. (2008). At 30 m, a high abundance of sediment particles and amorphous detritus was observed in the sediment trap on both sampling days in Ramfjorden (Fig. 17a.17b). It can be hypothesized that the relatively constant POC flux at depths was caused by the higher current velocity in the bottom layer (Fig. 6a.6b), which could have resuspended material from bottom sediment. This resupension has been described from other fjords as well (Passow, 1991; Zajączkowski et al., 2010).

Interestingly, the suspended biomass was higher at RMF2 than RMF1 (Chl *a* and POC concentration and algae abundance), but the sinking biomass did not change. That may suggest that organisms in the pelagic realm did not contribute strongly to the flux. It seemed that the biomass did not sink out or do not sink fast downward. The gels trap pictures showed that a high number of zooplankton got stuck on the sticky gels, especially at the shallower depths. It may therefore be assumed that their grazing impact contributed to a retention of the algae in the upper water column (Bach et al., 2019), and explain why the suspended biomass was increasing between RMF1 and RMF2, but not the biomass flux. The grazing impact could further explain the slightly higher Phaeo flux compared to Chl *a* flux at RMF2, meaning that more herbivorous faecal material was present on the second day of sampling. Similar processes have been found in the Canadian Arctic (Juul-Pedersen et al., 2008). The pictures of the gels traps revealed that smaller (or less aggregated) and fewer particles were present at RMF2 than at RMF1, especially at 5 and 15 m (Fig. 17a.17b), which potentially also had an impact on the particles' sinking speed and the downward export of material. The POC flux was also observed slightly lower at RMF2 than RMF1 (Fig. 16a).

To summarize, the sinking biomass in Ramfjorden was low and matched with previous observations during the pre-bloom period in the winter-spring transition. The flux was not very

different between the two sampling days in terms of Chl *a* flux, export of microalgae and export of particulate organic carbon. The microalgae composition sinking out were similar between days. Finally, the exported biomass seemed to be decoupled from the suspended biomass.

4.2 Van Mijenfjorden

4.2.1 Ice ecosystem

Van Mijenfjorden (77°) is located further north than Ramfjorden (69°), on the west coast of Svalbard, and it experiences an extended seasonal ice-cover period because of the longer winter at high latitudes. Van Mijenfjorden can be regarded as Arctic fjord, even though the average winter air temperature in west Spitsbergen is relatively warm (– 15 °C) compared to others Arctic fjords (Høyland, 2009; Skarðhamar and Svendsen, 2010). During the present field work, Van Mijenfjorden experienced thick ice cover (80 cm on average, Table 3). Similar observations have been made in the several previous winters (Høyland, 2009). The land-fast sea-ice in Van Mijenfjorden during April 2019 was not as cold as it could be at the interface ice/air, but rather warm air temperatures were recorded (e.g., 60-Top cm section: VMF1 = -2 °C, VMF2 = -1 °C, Fig. 2a). The land-fast ice was not covered by thick snow depth during the sampling period (VMF1: 8 cm, VMF2: 4.5 cm on average, Table 3) compared to what has been observed during April by Høyland (2009). The brine salinity in the sea-ice was in the range of previous findings (average of 30, Fig. 2c) and related to the underlying seawater salinity (Arrigo, 2014). The land-fast ice in Van Mijenfjorden had typical characteristics of first year ice, i.e., common bulk salinity of 5-8 (Høyland, 2009) and it reminds the typical "C-shape" salinity profile of FYI (Malmgren, 1927) (Fig. 2c). The brine volume was higher at VMF2 comparatively than at VMF1 at the top ice core section (25 % vs. 15 %), which was likely a result of a rapid desalinisation (Lake and Lewis, 1970). This can be assumed because the overall bulk salinity at VMF2 was lower than at VMF1, and a higher connectivity of brine channels was found (Golden et al., 1998).

The integrated Chl *a* concentration in the whole ice core was slightly higher at VMF1 than VMF2 (1.65 mg Chl *a* m^{-2} vs. 1.57 mg Chl *a* m^{-2}, Table A4). At both stations, the highest Chl *a* concentrations were found in the lowermost sections (0-3 and 3-10 cm) and lowest concentrations at the interface ice/air (Fig. 8b). This pattern corresponded to previous findings in Arctic sea-ice (Arrigo, 2014; Kvernvik, 2019; Leu et al., 2015). The integrated Chl *a* concentration of these lowermost sections were slightly higher than the concentrations

previously reported from the bottom ice section alone (i.e., 1 mg Chl *a* m^{-2} in the ice bottom, Leu et al. 2015). However, the concentrations were low compared to the bottom ice Chl *a* concentrations (~ 300 mg Chl *a* L^{-1}) reported in Van Mijenfjorden in April and May by Kvernvik (2019). Indeed, the concentration obtained (~ 0.04 mg Chl *a* L^{-1} at VMF1 and VMF2, not integrated over the ice core area section) were much lower than concentrations reported by Kvernvik (2019). Moreover, compared to studies conducted in Billefjorden and North of Svalbard, the Chl *a* concentration in the ice cores were low (up to 14 mg Chl *a* m^{-2}, from February to June, by Leu et al. (2015)) and in Rijpfjorden (end of April: up to 48 mg Chl *a* m^{-2} at the lowermost ice core section, by Leu et al. (2010)). The Chl *a* concentration were also low compared to observations from the starting bloom (mid-April to end April) on the ice-covered Canadian shelves (5 - 10 mg Chl *a* m^{-2}, Juul-Pedersen et al. (2008)). Finally, the concentrations at VMF1 and VMF2 were also lower than observations by students of the UNIS course during the parallel field campaign in spring 2019 (integrated Chl *a* concentration of 4.5 mg Chl *a* m^{-2}, Persson et al., 2019). As the UNIS course was using another fluorometer, than the present study, an underestimated of the Chl *a* concentration in the ice was likely due to the technical problem with the fluorometer at UiT (as explained in section 2.3.1.1). Despite the low sea-ice Chl *a* concentration found here, it is - based on the concentrations obtained by Persson et al. (2019) – assumed that an early peak bloom period prevailed in Van Mijenfjorden during the present study.

The sea-ice algae abundance followed the same distribution pattern as the Chl *a* concentration in the sea-ice, i.e., highest algae abundance in the bottom sections. Pennate diatoms, and especially *Nitzschia* spp., dominated the micro-algal assemblage (with a maximum diversity observed in ice of ~28 taxa, Table A8). Kvernvik (2019) also observed that *Nitzschia* spp. was in high abundance in Van Mijenfjorden and Olsen et al. (2017) found *Nitzschia* spp. dominating the species composition in the bottom FYI North of Svalbard during May. *Nitzschia* spp. had high abundance in Van Mijenfjorden (VMF1: 16.7 x 10^6 cells L^{-1}, VMF2: 5.5 x 10^6 cells L^{-1}, Fig. 9b), which was a bit higher than the cell numbers found by Olsen et al., (2017) (*Nitzschia* spp.: 0.15 x 10^6 cells L^{-1}) but lower than the large colony with densities up to 2.5 x 10^9 cells L^{-1} by Sakshaug et al. (2009). The genus *Nitzschia* spp. observed in Van Mijenfjorden might be composed mainly by *N.frigida/neofrigida* but also other *Nitzschia* species such as *N. promare* were found, which are important species in FYI (Sakshaug et al., 2009). The algae abundance, excluding *Nitzschia* spp., was < 1 x 10^5 cells L^{-1}, which is similar to the range found by

Okolodkov (1997) in the lowermost 10 cm of ice, North of Svalbard during June-July. Ratkova and Wassmann (2005) observed also similar algae abundances in the lowermost part of land-fast ice in White Sea during March. Many of the species observed in Van Mijenfjorden have also previously been found in this fjord (e.g., *Navicula* spp., (Kvernvik, 2019)), in other Svalbard fjords, such as Rijpforden (Leu et al., 2015) and Kongsfjorden (Hegseth et al., 2019), or in Arctic land-fast ice (Ratkova and Wassmann, 2005) and Arctic sea-ice (Arrigo, 2014; Smoła et al., 2018). Therefore, the species composition, dominated by pennate diatoms, observed in Van Mijenfjorden represented a typical Arctic sea-ice microalgae community during spring bloom.

The POC concentration in the sea-ice at VMF2 (no data available at VMF1, see section 2.3.1.3) followed the same trend as the Chl *a* concentration and distribution of algae cells with the highest concentration at the bottom ice section and the lowest in the top section (Fig. 10b). The total integrated POC concentration was high, with concentration of 682 mg POC m^{-2} (Table A4), and of this ~40 % of the POC were located in the bottommost 10 cm. Similar observations have been made in FYI East of Svalbard in mid-July (543-620 mg POC m^{-2}, Tamelander et al. (2009)) and North of Svalbard in the end of May (537-1071 mg POC m^{-2}, Fernández-Méndez et al. (2018)). This shows that the land-fast ice at other coasts of Svalbard contained similar carbon concentrations as Van Mijenfjorden during the spring bloom and summer. The POC/PON ratios in the ice core sections was on average 13.7 (Table A3), which is higher than the Redfield ratio, but typically observed in Arctic sea-ice (Niemi and Michel, 2015). Leu et al. (2010) also observed similar POC/PON ratios in the ice bottom section, in Rijpfjorden in April and also the species composition there was dominated by diatoms (e.g., *Nitzschia* spp.). The low Chl *a* and high POC concentrations comparatively to others Arctic studies during spring might show that the POC was not originating entirely from algal material. The POC/Chl *a* ratio was rather high at the uppermost ice sections (e.g., 40-60 cm section: POC/Chl *a* = 1081, 60-TOP: POC/Chl *a* = 786, Table A3). These high ratios could origin from entrained terrestrial carbon, from plankton species (non-photosynthetic) contributing to the POC biomass or algae with high carbon content. This non-algal content in top ice sections might origin from infiltration community but no negative freeboard or cracks were observed to promote this event during the sampling week. However, some *Chaetoceros* spp. were observed in the lowermost ice section (0-3 cm, at VMF2) and also in the water column (5 m, at VMF2), which occur usually only in young ice due to infiltration community (Smoła et al., 2018). This finding

highlight the possibility of a previous formation of infiltration community of algae and possibly non-algal material into the (uppermost) ice, which could explain the high POC content observed.

During the present field study, the weather was variable with increasing air temperatures between the two sampling days (Section 3.1.1 and Table A2). Some weak precipitation occurred at VMF1 and before the field sampling (Table A2), potentially causing a rain-on-snow event (Sturm and Massom, 2016). Most likely, this resulted in physical changes within the ice (e.g., ice melting and crack appearing, Fernández-Méndez et al., 2018). Combined with snow drift, the snow cover in Van Mijenfjorden was very patchy (personal obs) and thinner at VMF2 than VMF1 (4.5 cm vs. 8 cm, Table 3). The thinner snow cover, combined with positive air temperature (Table A2) might have changed the physical ice characteristics and resulted in the higher brine volume observed at VMF2 than at VMF1 (Fig. 2d). It might have caused a brine drainage that in turn flushed the ice algae into the water column (Gradinger et al., 1991). That could explain the lower algae abundance observed in the lowermost ice section (0-3 cm) at VMF2 compared at VMF1. The brine volume was slightly higher at the ice section 10-20 cm, combined with relatively low microalgae abundance, Chl *a* and POC biomass at VMF2 than at VMF1 (Fig. 8b, 9b.9d, 10b). Some material could have been flushed from the top of the ice, and especially from this sections due to higher brine volume, and transported downward into the water column. The low POC concentration at the uppermost ice section compared to the rest of the ice profile, might be also caused by brine drainage. Higher current velocity under the ice (surface to 15 m) was recorded in Van Mijenfjorden, especially at VMF1 than at VMF2, compared to bottom current velocity (Fig. 6c). Rózańska et al. (2009) observed that algae on the underside of the ice were washed away within a week (short time scale as our study) possibly due to strong spring tide current. Therefore, the water movement may potentially contribute of washed away microalgae at the underside of the ice prior to VMF2. In addition, melting underneath the ice may have caused a mixing under the ice and disturbed the attached algae in the lowermost part of the ice. The temperature underneath the ice was stable (~1.1 °C) during VMF1 and VMF2 (Fig. 5b), but at VMF2 a cold water layer (-0.9 °C) underneath the ice was reaching deeper (7-8 m) than at VMF1 (3-4 m) (Fig. 4b.4d) which could result of colder water mixing downward. The grazing by meiofauna could also explain the lower biomass observed at the lowermost ice section at VMF2 compared to VMF1. A high concentration of meiofauna (e.g., nematodes, rotifers and ciliates) was observed in bottom ice sections (Persson

et al., 2019). They may have contributed to the POC biomass, especially at the bottom section (Fig. 10b), and their sloppy feeding on algae have potentially produced feeding particles which increase the POC concentration in the ice bottom section (Smith et al., 1997). Finally, the difference in biomass in the lowermost ice section between VMF1 and VMF2 could be explained by irradiance reaching the lowermost ice section which will lead to difference in microalgae distribution and as well for Chl *a* (Smith et al., 1997).

The snow depth reduction at VMF2 compared to VMF1 may explain the disparity between algal abundance in ice top sections between the two stations. Due to the more favourable conditions of more irradiance (as a result of less snow cover), higher temperature, lower brine salinity, more space available (Fig. 2d), algal growth was likely higher in the top layer than below and this may explain the slightly higher algae abundance at VMF2 than at VMF1 (Fig. 9d). Indeed, vertical migration of microalgae (daily cm-scale movement) under favourable environmental conditions have been observed (Aumack et al., 2014). The high POC/Chl *a* ratios in uppermost part of the ice could origin as well from, microalgae light acclimated, due to the higher irradiance reaching the top ice section (Gosselin et al., 1990; Michel et al., 1996).

The difference in algae abundance at the bottom ice section or at the top ice section between VMF1 and VMF2 could also result from the patchiness in algae distribution as explained in Ramfjorden, Section 4.1.1. Slightly higher number of ice cores and sections were collected at VMF1 than at VMF2, which could influence the results obtained in algae abundance and Chl *a* concentrations between the two sampling days (Table A1).

Overall the sea-ice in Van Mijenfjorden presented typical characteristics of Arctic first year ice regarding the ice thickness, ice temperature, brine salinity, and brine volume. It is assumed that a beginning spring bloom took place during the field sampling because a typical combination of the Chl *a* concentrations especially at the lowermost ice section, microalgae cell abundances (with typical Arctic sympagic algae) and POC concentrations was observed.

4.2.2 Water column

In Van Mijenfjorden, a top layer of less dense water (0-15 m: - 0.9 °C with salinity of 32) and a deeper denser layer (25 m-bottom: -1.8 °C with salinity of 34.6) were found (Fig. 4d). According to their temperature and salinity characteristics, the top lighter water layer corresponded to Arctic Water (ArW) masses and the deeper layer corresponded to Winter-Cooled Water (WCW) with higher salinity due to brine released and sank out during ice

formation (Cottier et al., 2005, 2010) (Fig. 4d). The current direction in Van Mijenfjorden followed a general pattern with the upper layer out-flowing and the deep layer flowing into the fjord (Inall and Gillibrand, 2010). Currents in the deep water layer were less pronounced (0.01 - 0.03 m s^{-1}) than the surface currents (0.05 - 0.07 m s^{-1}, Fig. 6c). This range in speed, especially in the deeper water layer, was similar to the low current speed previously observed by Kowalik et al. (2015) in Van Mijenfjorden (0.02 m s^{-1}). Only a weak relationship between the under ice water velocity and tide forecast could be found at VMF1 and VMF2, probably due to the restricted inflow of water into Van Mijenfjorden through the narrow passages around Akseløya Island (Table A6).

The Chl *a* concentrations in the water column were slightly higher at VMF2 than VMF1 (1 m: 1.0 µg L^{-1} vs. 0.5 µg L^{-1}, Fig. 11b), but overall the concentrations were lower than typically observed during Arctic spring blooms (e.g., North of Svalbard: ~0.5 µg L^{-1} - 7.5 µg L^{-1} during peak bloom in June, by Assmy et al. (2017), and in Van Mijenfjorden: ~16 mg L^{-1} during bloom in April-May, by Kvernvik (2019)). The Phaeo concentration observed was higher than the Chl *a* concentration at VMF1 (for 1 m and 5 m especially, Fig. 11b) which could be related to more sloppy grazing and Chl *a* degradation by zooplankton.

The vertical distribution of the microalgae abundance in Van Mijenfjorden followed the Chl *a* concentration and a higher cell abundance was found at the shallower depth (1 m and 5 m: 125 and 200 x 10^3 cells L^{-1}) compared to deeper depths (at 15 m and 30 m: 1-3 x 10^3 cells L^{-1}, Fig. 12c). The highest abundance observed was at VMF2, 1 m (200 x 10^3 cells L^{-1}), which is similar to the findings in mid-May in ice-free Kongsfjorden during a no-bloom situation (Hegseth et al., 2019). In contrary, the cell abundance at VMF1 and VMF2 was very low compared to a bloom setting in Kongsfjorden (up to 17 × 10^6 cells L^{-1}, Eilertsen et al. (1989)). The algae abundance in ice-covered Van Mijenfjroden was not different of other ice-free fjords on West Spitsbergen during this early spring bloom period. The abundance might probably increase during the ice retreat at the future ongoing spring bloom.

The pelagic microalgal community composition was dominated by the pennate diatoms (Fig. 12c), with for example *Cylindrotheca closterium*, commonly found in Arctic shelf seas (Poulin et al., 2011), and also *Synedropsis hyperborea* (Wiktor, unpublished). *Nitzschia* spp. was present in the upper water layer for both sampling days, but at very low density. The same was true for the chlorophyte *Pyramimonas* sp., which was also found in ice-free Kongsfjorden in

April at similar abundance (Hegseth et al., 2019). Finally, the taxon *Gymnodinium* spp., mainly represented by *Heteroscapa rotundata* and *Gymnodinium wulffii*, were the most abundant group, and are commonly observed in pelagic Arctic systems, for example in August in Van Mijenfjorden (Kvernvik, 2019) and in in Kongsfjorden in July (Hegseth et al., 2019).

The POC concentrations in the water column ranged between 22 – 241 mg POC m^{-3} during the present study (Fig. 13b). The integrated POC concentration in the water column at VMF1 and VMF2 (1.8 - 2.2 g POC m^{-2}, Table A3) fits well with pre-bloom concentration observed under the sea-ice North of Svalbard during mid-May (average 2 g POC m^{-2}, Assmy et al., 2017). However, the suspended POC concentrations here were much lower than findings during a under-ice bloom in June (9-22 g POC m^{-2}, Assmy et al. (2017)). The highest POC concentrations recorded in Van Mijenfjorden was lower than previous recordings during spring in others ice-free Svalbard fjords (Wiedmann et al., 2016; Zajączkowski et al., 2010). Therefore the POC concentration in Van Mijenfjorden shown low POC accumulation of biomass in the fjord during spring which is potentially related to the ice-cover limiting the phytoplankton growth.

The POC/Chl *a* ratios observed in the water column of Van Mijenfjorden were high (176 – 360), with no clear pattern observed with depth (Table A3) as previously reported by Kvernvik (2019), which can result of high contribution of organic material to the suspended material (Kvernvik, 2019). High POC concentration at deeper depth might come from resuspension of material which can be explained as well by the highest POC/PON ratio observed (VMF1, 30 m: POC/PON ratio of 10.4, Table A3). Some slightly higher bottom currents at the beginning at VMF1 compared to the rest of the sampling period were observed (Fig. 6c) which can induced resuspension of sedimented material. Resuspension of sediments and organic particles have been observed in others Arctic fjords from the ocean floor and shore (Keck and Wassmann, 1996; Noji et al., 1993; Wiedmann et al., 2016; Zajączkowski et al., 2010).

Overall, it can be suggested that the decrease of snow depth (as seen Table 3), might have allowed higher light penetration through the ice and into the water column. This likely explains the slightly higher Chl *a* concentration and algae abundance at VMF2 compared to VMF1 especially in upper water column. The high POC concentration observed at VMF2, 1 m, compared to VMF1, might be explained by the organic matter produced from increasing

photosynthesis at the upper layer or by the possibly sinking down of sea-ice algae from the underside of the ice at VMF1, as explained in section 4.2.1.

To summarize, Van Mijenfjorden sea-ice ecosystem, might have been in a beginning bloom stage during the present study, because the pelagic Chl *a* and POC concentrations were similar with others Arctic fjords studies during this bloom phase. The observed microalgae assemblage in Van Mijenfjorden consisted of typical species found in the European Arctic and in coastal Arctic regions.

4.2.3 Downward export

In Van Mijenfjorden, the Chl *a* flux was higher at the upper layer (1 m: 1.1 mg m^{-2} d^{-1} Fig. 14a) and then decreased with depth. The same has been observed in a seasonally ice-covered fjord in Greenland (Juul-Pedersen et al., 2008), but there the Chl *a* flux between February to late May was lower (1 m: 0.02 - 0.23 mg Chl *a* m^{-2} d^{-1}) under the sea-ice. A change in the Chl *a* flux was found between the two sampling days (VMF1: 0.4 mg Chl *a* m^{-2} d^{-1}, VMF2: 1.1 mg Chl *a* m^{-2} d^{-1}), suggesting that more algae were sinking down during the second day. Juul-Pedersen et al. (2008) observed a maximum Chl *a* flux during the melting period, end of May (at 15 - 25 m: 0.97 - 2 mg Chl *a* m^{-2} d^{-1}) which was in a similar range as found here in Van Mijenfjorden directly under the sea-ice. The Phaeo flux also decreasing with depth (Fig. 14b), with the Chl *a*/Phaeo ratio < 1, meaning more fresh than degraded material was sinking out in Van Mijenfjorden (Fig. 14b and Table A3).

As the Chl *a* flux, the export of microalgae cells declined with depth. The highest total algae export was observed right under the sea-ice on the second sampling day (VMF2, 1 m: 120 000 x10^3 cells m^{-2} d^{-1}), while the microalgae export at VMF1 was one order of magnitude lower (Fig. 15b). Some *Nitzschia* spp. cells were found in the sediment trap at 1 and 5 m depth (mainly at VMF1, Fig. 15b), while this species co-dominated with *Navicula* spp. under the sea-ice of the fjord in Greenland (March to May, at 1 m: 3 200 - 118 000 x 10^3 cells m^{-2} d^{-1}, Juul-Pedersen et al., (2008)). This was considerably higher compared to what was observed in Van Mijenfjorden (e.g., 3.4 x10^3 *Nitzschia* spp. cells m^{-2} d^{-1} at 1 m, VMF2, Fig. 15b).

At VMF2, the algae composition sinking out was different than VMF1. A higher abundance of flagellates was exported especially at 1 m and 5 m (Fig. 15b). The increase of flagellates was not observed in the suspended material (Fig. 12c) and thus it is likely that the difference in the

community composition in the sediment trap was due to the melting event of the ice between VMF1 and VMF2. Indeed, as stated in the Section 4.2.1 for Van Mijenfjorden, melting of the ice may have triggered the export of the flagellates from the sea-ice which have been growing in few days (between VMF1 and VMF2) in combination with favourable conditions in the upper water column (e.g., with snow cover reduced = higher light transmittance). In addition, while sampling, human factor as stepping around the station might have also removed snow and let higher irradiance through ice and trigger growth of the species trapped into the traps.

The high flux of these flagellates species was only observed at the upper layer and not in the deeper sediments traps. According to Kamykowski et al. (1992), the sinking velocity of dinoflagellates, including *Gymnodinium* sp., follow the cell-size relationship reported for the diatoms by Smayda (1971), meaning healthy cells sink faster than senescent. The low POC/PON ratios observed in the sediment trap at the upper layer at VMF2 (Table A3) could reflect the contribution of the fresh algal material from the flagellates to the sinking export. *Gymnodinium* spp. may have a low sinking rate (e.g., ≤ 1 m per day, Kamykowski et al., (1992)), which might explain why these algae were found highly in the sediment trap in the upper water layer.

The POC flux was highest under the ice (1 m: 180 mg POC m^{-2} d^{-1} for both days, Fig. 16b) and, at greater depth higher at VMF1 (30 m: 150 mg POC m^{-2} d^{-1}) than at VMF2. Combined with high POC/PON ratio (VMF1 = ~17 average at all depths, Table A3), this may suggest an export of degraded material from the sea-ice, or POC with non-algal origin or resuspended degraded material from the side of the fjord was sinking out during early spring. The latter has also been observed by Juul-Pedersen et al. (2008) on Greenland with much lower POC flux under the ice (1 - 25 m = ~ 23 mg POC m^{-2} d^{-1} from winter to spring). The qualitative assessment of the gel trap pictures showed that a lot more particles were sinking at 15 m and 30 m compared to the upper layer (1 and 5 m) on both sampling days (Fig. 17c.17d). This may support the explanation of sinking resuspended material. However, the potential resuspension of material at both days could not be directly linked to any increase of current speed at the bottom depth (Fig. 6c), but the low speed average (0.02 m s^{-1}, Fig. 6c.7c) could have resuspended and bring particles into this inner station in Van Mijenfjorden.

The higher flux at VMF2 of Chl *a*, Phaeo and algal cells, did not show an higher POC flux at VMF2, as expected, comparatively than at VMF1 (Fig. 16b). The POC flux was fairly constant at lower depth (5 - 30 m: ~75 mg POC m^{-2} d^{-1}, Fig. 16b) combined with very low POC/PON

ratios (5 – 10, Table A3), meaning fresh algal material was exported at greeter depth. As suggested for the Northern Norwegian fjord Malangen, the organic flux seemed here to be decoupled from the Chl *a* flux (Keck and Wassmann, 1996). The underlying reason for that, in turn, may have been a possible rapid removal of the material sinking down, by from the slightly higher currents recorded underneath the ice (Fig. 6c). Another explanation for relatively low POC flux at VMF2 than at VMF1 could be the algal biomass content very low POC content (relatively to the Chl *a*) which did not increase the POC sinking down.
Furthermore, heterotrophic species can decouple the POC/PON and the POC/Chl *a* ratios (Kvernvik, 2019). Indeed, some flagellates observed at VMF1 and VMF2 might be heterotroph and/or mixotroph consumers more than autotroph. For instance, the taxa *Gymnodinium spp*., *Leucocryptos marina* and *Pyramimonas* spp. might have heterotroph tendency depends on environmental conditions (Wiktor, personal communication 2020) and as combined with Ciliophora cells observed (Fig. 15b).

In Van Mijenfjorden both sympagic and pelagic have been found in the exported material, but a strong relation between the sympagic and exported material was observed. For example, *Pyramimonas* spp. and *Gymnodinium* spp. (*G. arcticum, G. wulfii, G. ostenfeldii*) were found in high abundance at the bottom ice sections 0 -10 cm (VMF1), and also in the sediment traps under the ice (1 m and 5 m). However, at VMF2, *Pyramimonas* sp., (idem for *Gymnodinium* sp.) was found in lower quantity in the ice (VMF1: 20 x 10^3 cells L^{-1}, VMF2 = 9 x 10^3 cells L^{-1}), but in high abundance in the sediment traps (1 m and 5 m, Fig. 12c). This support the idea of a melting event have been occurred during VMF1 and VMF2. Kauko et al. (2018) concluded that the dinoflagellates (including *Gymnodinium* spp.) within the young ice (YI) during early spring period may have originated from the surrounding water column. Potentially, an inverse mechanisms, where the dinoflagellates from FYI seed the pelagic system by sinking from the ice, was found here.

To summarise, the biomass exported in Van Mijenfjorden was representative of spring bloom in terms of Chl *a* (with slightly higher sinking than observed in Canadian shelves) and algae (in the range of Canadian shelves export). The POC flux was high and might be representative of material resuspension. The algae community composition sinking out was highly composed of sympagic species. The biomass sinking down in Van Mijenfjorden differed highly between the two days, which might be the results of physicals factors combination impacting ice ecosystem.

4.3 Fjords comparison

Ramfjorden in northern Norway is a narrow sub-Arctic fjord which is distantly influenced by Norwegian Coastal Waters, because it is isolated fjord from the coast due to its inland location. Further, the water exchange with the open sea is limited by two shallow sills (both ~8 m) and strongly influenced by freshwater run-off. Van Mijenfjorden, in contrast, is a high Arctic system, which is exposed to high-Arctic climate and the West Spitsbergen Current, which is influenced by Atlantic Water (Skarðhamar and Svendsen, 2010). Van Mijenfjorden, is much wider and longer than Ramfjorden, but as well sheltered due to its almost closed entrance and also impacted by freshwater run-off impacted (river and glacial run-off) (Skarðhamar and Svendsen, 2010).

Thus, due to the fjords location and their topography, distinct differences between the two sea-ice ecosystems were observed. The sea-ice in Ramfjorden may be characterized as "freshwater ice" because of its very low bulk salinity and relatively high ice temperature. Van Mijenfjorden, in contrast, was covered by a typical Arctic sea-ice with regard to its physics (e.g., bulk salinity and temperature) and observed algae composition. In Ramfjorden, the brine volume and the permeability of the sea-ice was much lower than in Van Mijenfjorden, leading to a very different habitat available for sea-ice algae. In addition, the ice was much thinner in Ramfjorden than in Van Mijenfjorden (~40 cm vs. ~80 cm). This habitat difference seemed to have a major impact on the algae abundance and diversity and as well linked with concentration of Chl *a* and POC, which were all lower in Ramfjorden. It impacts also the algae distribution in the ice, with in Ramfjorden ice, algae cells found in higher abundance in the middle/top sections of the ice, which is unusual of Arctic FYI. Though, Ramfjorden had typical species composition of beginning of spring bloom with mix between pennate diatoms and flagellates. Within the pennate, typical sympagic species found also in other Arctic region were present (e.g., *Nitzschia* spp., *Navicula* spp., *Achnantes* sp.). In addition, some local pelagic centric diatoms (e.i., *Leptocylindrus* sp. and *Skeletonema* sp.) and even brackish water species (e.g., *Eunotia serra*) were found in Ramfjorden. The latter indicated a strong high fresh-water influence on the sea-ice while forming. Compared to Ramfjorden, Van Mijenfjorden was a typical Arctic FYI ecosystems and a diverse sympagic species composition and high cell numbers were found especially at the lowermost ice section. As in other Arctic ecosystems, pennate diatoms were the most abundant algae group (e.g., *Nitzschia* spp. and *Navicula* spp., *Fragilariopsis* sp. *Cylindrotheca closterium*, *Synedropsis hyperbora*).

Due to the different field sampling period, the two fjords systems presented here were in a slightly different phase of the spring bloom, with Ramfjorden being in a pre-bloom/early–bloom and Van Mijenfjorden being in a more advanced stage of an early bloom. Thus, the two ice ecosystems are not entirely comparable, but the present data suggest that due to the latitudinal gradient, the seasonal ice ecosystem in a sub-Arctic fjord might be more influenced by fresh-water run-off, especially if it is a narrow fjord surrounded by steep mountains. This seems to result in a poorer sea-ice community with regard to biomass and species diversity compared to a true Arctic fjord, where sea-ice with a high porosity allows a more abundant and diversity of ice algae. Nevertheless, sea-ice ecosystems in sub-Arctic fjords may represent an important first source of carbon to higher tropic levels in the pelagic and benthic realm.

The water column in Ramfjorden, though sampled earlier in the season than Van Mijenfjorden, was characterized by warmer water masses (1.5 – 3 °C) than Van Mijenfjorden - 0.9 to - 1.9 °C). Both fjords however had a thermocline at approximately 15 – 20 m. In terms of salinity, Ramfjorden was slightly fresher than Van Mijenfjorden (33.2 and 34.6, respectively). The currents in both fjords were of low speed during the sampling period, and tended to be higher under the sea-ice and close to the bottom depth at both stations. The latter may be the reason, why resuspension of sedimented material likely occurred at the bottom in both fjords. The pelagic system, however, differed somewhat in Ramfjorden and Van Mijenfjorden. The phytoplankton diversity was lowest in Ramfjorden and was largely dominated by the centric diatoms (e.g., *Chaetoceros* spp. and *Thalassiossira* sp.), few pennate diatoms (e.g., *Navicula transitans*, *Cylinrotheca closterium*, few *Nitzschia* spp.), and some brackish water species (e.g., *Chaetoceros minimus*). Van Mijenfjorden, mainly pennate diatoms (e.g., *Nitzschia* spp., *Cylindrotheca closterium* and *Synedropsis hyperborea*, *Navicula* spp.) were found in the water column. The microalgae abundance was highest right under the ice in both fjords, with slightly higher algae abundance and Chl *a* biomass noticed at the deeper depth (e.g., 5 and 15 m) in Ramfjorden relatively to Van Mijenfjorden. Van Mijenfjorden showed more carbon content than Ramfjorden, and for both fjords the concentration was as well higher right under the sea-ice.

In Ramfjorden the algae composition was different between the sea-ice and water column. Indeed, the pennate diatoms prevailed the low algal biomass in the ice while the centric diatoms dominated the pelagic ecosystem. Few shared species in very low abundance were observed between the two assemblages but overall the community composition was very different, and

it is assumed that the sympagic-pelagic coupling in Ramfjorden was rather poor. It seems that the hydrodynamic forcing (e.i., the higher currents under the ice, the fluctuating temperature) did not stimulate an exchange between both realms. Instead, the pelagic realms in Ramfjorden seemed to be influenced by the water masses in outer ice-free Ramfjorden and neighbouring Balsfjorden. Meteorological forcing event (e.g., higher wind speed pushing water into Ramfjorden) were observed, and it may have resulted in the higher Chl *a* and POC concentrations as well as cell numbers at RMF2 compared to RMF1. This speculation is further supported by the community composition found, dominated by centric diatoms in upper layers, which has been suggested to be typical for a high latitude spring bloom in the area (Wassmann et al., 1999).

In Van Mijenfjorden, in contrast, a strong connection between the sea-ice and pelagic realm was observed and this matches previous observation from FYI in the Arctic (Leventer, 2008). A high number of shared algal species was here found between the sea-ice and the pelagic system (e.g., pennate diatoms), suggesting that sympagic algae were drained into the pelagic system. This was likely also caused by meteorological forcing, as the higher air temperature changing the ice physics, which has potentially impacted the sea-ice community by decrease of biomass in the bottom of the sea-ice during the sampling period. In addition, Van Mijenfjorden is a much protected fjord and only linked to the open sea by the shallow and narrow entrance at Akseløya Island, which restrict highly water masses exchange.

To summarize, seasonally ice-covered sub-Arctic fjords of minor dimension may thus have sea-ice ecosystems and pelagic ecosystems more influenced by the surrounded water masses (freshwater and side fjord water mass), than large, high Arctic fjords with an extensive ice cover. In summary, this means that the sea-ice ecosystems in sub-Arctic and Arctic fjords may be substantially different and that the sympagic-pelagic coupling may be much weaker, in fjords with a system comparable to the one of Ramfjorden and tight in the high Arctic Van Mijenfjorden.

In terms of sympagic-pelagic-export coupling, in Ramfjorden, it was generally characterized by a low export of biomass, and the quality and quantity of the flux did not considerably differ between days. As the algae community composition found in the sediment trap shared more species with the pelagic assemblage (both dominated by *Chaetoceros* spp.), it is assumed that sinking biomass rather originated from the pelagic realm than the ice ecosystem. A delayed between the suspended biomass and sinking biomass is shown in Ramfjorden, indeed the suspended biomass was increasing (from RMF1 to RMF2, for Chl *a*, export of algae and POC)

but the sinking biomass was not. That revealed that the pelagic content do not contribute highly to the flux and that the sympagic-pelagic-export coupling was weak at the sampling time. In contrast, in Van Mijenforden, was characterized by a higher export of biomass and the quality and quantity of the flux differed between days. Numerous algal species have been found both in the sea-ice, the water column and the sediment traps. Indeed, the sinking biomass was rather originated from the sea-ice, with the high increase of sinking flux (from VMF1 to VMF2, for Chl *a* and export of algae) than the pelagic realm, with rather stable suspended biomass (Chl *a,* algae and POC concentrations) between days. That revealed a tight sympagic-pelagic-export coupling at the sampling period.

In summary, there were differences in the sympagic-pelagic coupling and export between the two systems. The sinking export in Ramfjorden was mainly influenced by pelagic material and in Van Mijenfjorden mainly by biomass originated from sympagic realm. The exported biomass depends as well, highly on the timing of the sympagic/pelagic bloom stages (Leu et al., 2015), but most likely the difference in the two systems was due to a freshwater influence; strong on a sub-Arctic system, Ramfjorden, and weak on a high-Arctic system, Van Mijenfjorden.

5 Conclusion

In conclusion, this sampling study has revealed that there are some short-time scale changes in the autotrophic biomass in the sea-ice in Van Mijenfjorden (e.g., a small decrease in microalgae abundance in the lowermost ice section) and in the water column in Ramfjorden (e.g., an increase in the suspended biomass). In addition, it could be shown that physical drivers influenced the quantity and composition of the vertical flux in each fjord. In Ramfjorden, higher current speed and possible horizontal advection likely enhanced the biomass export, while in Van Mijenfjorden, an increase in air temperature, snow removal, and changes in the ice physics increased the export. The ecosystems in the two investigated fjords during early spring were thus different with regard to the quality and quantity of the biomass in the sea-ice, in the pelagic system and in their export. This was likely due to their latitudinal difference and the contrasting influence of freshwater run-off on the sea-ice. Therefore, the present study confirms previous findings that “no two fjords are truly alike” (Inall and Gillibrand, 2010).

6 References

Arrigo, K.R., 2014. Sea Ice Ecosystems. Ann. Rev. Mar. Sci. 6, 439–467.

Arrigo, K.R., Robinson, D.H., Dunbar, R.B., Leventer, A.R., Lizotte, M.P., 2003. Physical control of chlorophyll a, POC, and TPN distributions in the pack ice of the Ross Sea, Antarctica. J. Geophys. Res. C Ocean. 108, 14–1.

Assmy, P., Fernández-Méndez, M., Duarte, P., Meyer, A., Randelhoff, A., Mundy, C.J., Olsen, L.M., Kauko, H.M., Bailey, A., Chierici, M., Cohen, L., Doulgeris, A.P., Ehn, J.K., Fransson, A., Gerland, S., Hop, H., Hudson, S.R., Hughes, N., Itkin, P., Johnsen, G., King, J.A., Koch, B.P., Koenig, Z., Kwasniewski, S., Laney, S.R., Nicolaus, M., Pavlov, A.K., Polashenski, C.M., Provost, C., Rösel, A., Sandbu, M., Spreen, G., Smedsrud, L.H., Sundfjord, A., Taskjelle, T., Tatarek, A., Wiktor, J., Wagner, P.M., Wold, A., Steen, H., Granskog, M.A., 2017. Leads in Arctic pack ice enable early phytoplankton blooms below snow-covered sea ice. Sci. Rep. 7, 1–9.

Aumack, C.F., Juhl, A.R., Krembs, C., 2014. Diatom vertical migration within land-fast Arctic sea ice. J. Mar. Syst. 139, 496–504.

Bach, L.T., Stange, P., Taucher, J., Achterberg, E.P., Horn, H., Esposito, M., Riebesell, U., 2019. The In fl uence of Plankton Community Structure on Sinking Velocity and Remineralization Rate of Marine Aggregates Global Biogeochemical Cycles 33, 971–994.

Bech, P.A., 1982. Planteplankton og primaerproduksjon i Ramfjorden og Tromsdysundet 1980. University of Tromso, Norway.

Berard-Therriault, L., Poulin, M., Bosse, L., 1999. Guide d'Identification du Phytoplankton Marin de L'Estuaire et du Golfe du Saint-Laurent. NRC Res. Press.

Berge, J., Daase, M., Renaud, P.E., Ambrose, W.G., Darnis, G., Last, K.S., Leu, E., Cohen, J.H., Johnsen, G., Moline, M.A., Cottier, F., Varpe, O., Shunatova, N., Bałazy, P., Morata, N., Massabuau, J.C., Falk-Petersen, S., Kosobokova, K., Hoppe, C.J.M., Węsławski, J.M., Kukliński, P., Legeżyńska, J., Nikishina, D., Cusa, M., Kędra, M., Włodarska-Kowalczuk, M., Vogedes, D., Camus, L., Tran, D., Michaud, E., Gabrielsen, T.M., Granovitch, A., Gonchar, A., Krapp, R., Callesen, T.A., 2015. Unexpected levels of biological activity during the polar night offer new perspectives on a warming arctic. Curr. Biol. 25, 2555–2561.

Bianchi, T.S., 2006. Biochemistry of Estuaries. In: Press, O.U. (Ed.), . Cary, NC, USA.

Bluhm, B., Hop, H., Melnikov, I., Poulin., M., Vihtakari, M., Collins, R.E., Gradinger, R., Juul-Pedersen, T., Quillfeldt, C. von, 2017. Sea Ice Biota. In: State of the Arctic Marine Biodiversity Report. Conservation of Arctic Flora and Fauna International Secretariat, Akureyri, Iceland.

Bowditch, N., 2002. Tides and Tidal Current. In: The American Practical Navigator. p. 896.

Cimoli, E., Lucieer, A., Meiners, K.M., Lund-Hansen, L.C., Kennedy, F., Martin, A., McMinn, A., Lucieer, V., 2017. Towards improved estimates of sea-ice algal biomass: Experimental assessment of hyperspectral imaging cameras for under-ice studies. Ann. Glaciol. 58, 68–77.

Cottier, F., Tverberg, V., Inall, M., Svendsen, H., Nilsen, F., Griffiths, C., 2005. Water mass modification in an Arctic fjord through cross-shelf exchange: The seasonal hydrography of Kongsfjorden, Svalbard. J. Geophys. Res. Ocean. 110, C1200, 1–18.

Cottier, F.R., Nilsen, F., Skogseth, R., Tverberg, V., Skarðhamar, J., Svendsen, H., 2010. Arctic fjords: A review of the oceanographic environment and dominant physical processes. Geol. Soc. Spec. Publ. 344, 35–50.

Demers, S., Legendre, L., Maestrini, S.Y., Rochet, M., Grant Ingram, R., 1989. Nitrogenous nutrition of sea-ice microalgae. Polar Biol. 9, 377–383.

Domack, E.W., Mcclemen, 1996. Accumulation of Glacial Marine Sediments in Fjords of the Antarctic Peninsula and Their Use As Late Holocene Paleoenvironmental Indicators. Antarct. Res. Ser. 70, 135–154.

Ebersbach, F., Trull, T.W., 2008. Sinking particle properties from polyacrylamide gels during the KErguelen Ocean and Plateau compared Study (KEOPS): Zooplankton control of carbon export in an area of persistent natural iron inputs in the Southern Ocean. Limnol. Oceanogr. 53, 212–224.

Edler, L., Elbrächter, M., 2010. The Utermöhl method for quantitative phytoplankton analysis. Microsc. Mol. methods Quant. Phytoplankt. Anal.

Eicken, H., 2009. Ice Sampling and Basic Sea Ice Core Analysis. Sea ice F. Res. Tech. 117–140.

Eilertsen, H.C., 1993. Spring blooms and stratification. Nature 363, 23–24.

Eilertsen, H.C., Falk-Petersen, S., Hopkins, C.C.E., Tande, K., 1981a. Ecological investigations on the plankton community of Balsfjorden, Northern Norway: Program for the project, study area, topography, and physical environment. Sarsia 66, 25–34.

Eilertsen, H.C., Frantzen, S., 2007. Phytoplankton from two sub-Arctic fjords in northern Norway 2002-2004: I. Seasonal variation in chlorophyll a and bloom dynamics. Mar. Biol. Res. 3, 319–332.

Eilertsen, H.C., Schei, B., Taasen, J.P., 1981b. Investigations on the plankton community of Balsfjorden , Northern Norway. Sarsia 66, 37–41.

Eilertsen, H.C., Skarðhamar, J., 2006. Temperatures of north Norwegian fjords and coastal waters: Variability, significance of local processes and air-sea heat exchange. Estuar. Coast. Shelf Sci. 67, 530–538.

Eilertsen, H.C., Taasen, J.P., 1984. Investigations on the plankton community of Balsfjorden , Northern Norway . The phytoplankton 1976 – 1978 . Environmental factors , dynamics of growth , and primary production. Sarsia, 691, 1-15 37–41.

Eilertsen, H.C., Taasen, J.P., Wesiawski, J.M., 1989. Phytoplankton studies in the fjords of West Spitzbergen : physical environment and production in spring and summer. J. Plankton Res. 11, 1245–1260.

Fernández-Méndez, M., Olsen, L.M., Kauko, H.M., Meyer, A., Rösel, A., Merkouriadi, I., Mundy, C.J., Ehn, J.K., Johansson, A.M., Wagner, P.M., Ervik, Å., Sorrell, B.K., Duarte, P., Wold, A., Hop, H., Assmy, P., 2018. Algal hot spots in a changing Arctic Ocean: Sea-ice ridges and the snow-ice interface. Front. Mar. Sci. 5.

Garrison, D.L., Buck, K.R., 1986. Organism losses during ice melting: A serious bias in sea ice community studies. Polar Biol. 6, 237–239.

Gerland, S., Hall, R., 2006. Variability of fast-ice thickness in Spitsbergen fjords. Ann. Glaciol. 44, 231–239.

Golden, K., Ackley, S., Lytle, V.I., 1998. The Percolation Phase Transition in Sea Ice. Science 282, 2238–2241.

Golden, K.M., Eicken, H., Heaton, A.L., Miner, J., Pringle, D.J., Zhu, J., 2007. Thermal evolution of permeability and microstructure in sea ice. Geophys. Res. Lett. 34, 1–6.

Gosselin, M., Legendre, L., Therriault, J.-C., Demers, S., 1990. Light and nutrient limitation of sea-ice microalgae (Hudson Bay, Canadian Arctic) 26, 220–232.

Gradinger, R., Spindler, M., Henschel, D., 1991. Development of Arctic sea-ice organisms under graded snow cover. Polar Res. 10, 295–308.

Granskog, M.A., Kaartokallio, H., Kuosa, H., Vainio, J., 2016. Ice in subarctic seas. In: Sea Ice: Third Edition. pp. 531–577.

Grossi, S.M., Kottmeier, S.T., Moe, R.L., Taylor, G.T., Sullivan, C.W., 1987. Sea ice microbial communities. VI. Growth and primary production in bottom ice under graded snow cover.

Mar. Ecol. Prog. Ser. 35, 153–164.
Halse, G.R., Syvertsen, E.E., 1996. Marine Diatoms. In: Academic Press, S.D. (Ed.), Identifying Marine Diatoms and Dinoflagellates.
Hambrey, M., 1994. Glaciomarine processes and sediments. In: UBC Press (Ed.), Glacial Environments. pp. 188–219.
Hancke, K., Lund-Hansen, L.C., Lamare, M.L., Højlund Pedersen, S., King, M.D., Andersen, P., Sorrell, B.K., 2018. Extreme Low Light Requirement for Algae Growth Underneath Sea Ice: A Case Study From Station Nord, NE Greenland. J. Geophys. Res. Ocean. 123, 985–1000.
Hegseth, E.N., Assmy, P., Wiktor, J.M., Wiktor, J., Kristiansen, S., Leu, E., Tverberg, V., Gabrielsen, T.M., Skogseth, R., Cottier, F., 2019. Phytoplankton Seasonal Dynamics in Kongsfjorden, Svalbard and the Adjacent Shelf. In: H. Hop, C.W. (Ed.), The Ecosystem of Kongsfjorden, Svalbard. pp. 173–227.
Hodal, H., Falk-Petersen, S., Hop, H., Kristiansen, S., Reigstad, M., 2012. Spring bloom dynamics in Kongsfjorden , Svalbard : nutrients , phytoplankton , protozoans and primary production. Polar Biol. 35, 191–203.
Holm-Hansen, O., Riemann, B., 1978. Chlorophyll a Determination: Improvements in Methodology. Oikos 30, 438.
Hopkins, C.C.E., Grotnes, P.E., Eliassen, J.E., 1989. Organization of a fjord community at 70° north: The pelagic food web in Balsfjord, northern Norway. Rapp. P.-v. Réun. Cons. int. Explor. Mer 188, 146–153.
Horner, R., Ackley, S.F., Dieckmann, G.S., Gulliksen, B., Hoshiai, T., Legendre, L., Melnikov, I.A., Reeburgh, W.S., Spindler, M., Sullivan, C.W., 1992. Ecology of sea ice biota - 1. Habitat, terminology, and methodology. Polar Biol. 12, 429–444.
Howe, J.A., Austin, W.E.N., Forwick, M., Paetzel, M., Harland, R.E.X., Cage, A.G., 2010. Fjord systems and archives : a review Scottish Association for Marine Science , Scottish Marine Institute , Oban , Argyll , Department of Geography and Geoscience , St Andrews University , Irvine Building , Department of Environmental and Geographical Sci. Geol. Soc. London 344, 5–15.
Høyland, K. V., 2009. Ice thickness, growth and salinity in Van Mijenfjorden, Svalbard, Norway. Polar Res. 28, 339–352.
Inall, M.E., Gillibrand, P.A., 2010. The physics of mid-latitude fjords: A review. Geol. Soc. Spec. Publ. 344, 17–33.
Johnsen, G., Norli, M., Moline, M., Robbins, I., von Quillfeldt, C., Sørensen, K., Cottier, F., Berge, J., 2018. The advective origin of an under-ice spring bloom in the Arctic Ocean using multiple observational platforms. Polar Biol. 41, 1197–1216.
Juul-Pedersen, T., Michel, C., Gosselin, M., Seuthe, L., 2008. Seasonal changes in the sinking export of particulate material under first-year sea ice on the Mackenzie Shelf (western Canadian Arctic). Mar. Ecol. Prog. Ser. 353, 13–25.
Kamykowski, D., Reed, R.E., Kirkpatrick, and G.J., 1992. Comparison of sinking velocity, swimming velocity, rotation and path characteristics among six marine dinoflagellate species D. Mar. Biol. 328, 319–328.
Kauko, H.M., Olsen, L.M., Duarte, P., Peeken, I., Granskog, M.A., Johnsen, G., Fernández-Méndez, M., Pavlov, A.K., Mundy, C.J., Assmy, P., 2018. Algal colonization of young arctic sea ice in spring. Front. Mar. Sci. 5.
Keck, A., Wassmann, P., 1996. Temporal and spatial patterns of sedimentation in the subarctic fjord malangen, Northern Norway. Sarsia 80, 259–276.
Kowalik, Z., 2005. Tides. In: Routledge (Ed.), . M. Nuttall, pp. 2027–2029.
Kowalik, Z., Marchenko, A., Brazhnikov, D., Marchenko, N., 2015. Tidal currents in the

western Svalbard Fjords. Oceanologia 57, 318–327.
Kristiansen, S., Farbrot, T., Kuosa, H., Myklestad, S., Quillfeldt, C.H.V., 1998. Nitrogen uptake in the infiltration community, an ice algal community in Antarctic pack-ice. Polar Biol. 19, 307–315.
Kvernvik, A.C., 2019. Ecophysiological Responses of Sea Ice Algae and Phytoplankton to a Changing Arctic. The Arctic University of Norway.
Kwok, R., 2018. Arctic sea ice thickness, volume, and multiyear ice coverage: Losses and coupled variability (1958-2018). Environ. Res. Lett. 13, 105005.
Lake, R.A., Lewis, E.L., 1970. Salt rejection by sea ice during growth. J Geophys Res 75, 583–597.
Lalande, C., Moriceau, B., Leynaert, A., Morata, N., 2016. Spatial and temporal variability in export fluxes of biogenic matter in Kongsfjorden. Polar Biol. 39, 1725–1738.
Laurenceau-Cornec, E.C., Trull, T.W., Davies, D.M., De La Rocha, C.L., Blain, S., 2015. Phytoplankton morphology controls on marine snow sinking velocity. Mar. Ecol. Prog. Ser. 520, 35–56.
Legendre, L., Michaud, J., 1999. Chlorophyll a to estimate the particulate organic carbon available as food to large zooplankton in the euphotic zone of oceans. J. Plankton Res. 21, 2067–2083.
Legendre, L., Ackley, S., Dieckmann, G., Gulliksen, B., Horner, R., Hoshiai, T., Melnikov, I., Reeburgh, W., Spindler, M., Sullivan, C., 1992. Ecology of sea ice biota. Polar Biol. 12, 429–444.
Leppäranta, M., Manninen, T., 1988. The brine and gas content of sea ice with attention to low salinities and high temperatures. Finnish Inst. Mar. Res. Intern. Rep. 2, 1–14.
Leu, E., Mundy, C.J., Assmy, P., Campbell, K., Gabrielsen, T.M., Gosselin, M., Juul-Pedersen, T., Gradinger, R., 2015. Arctic spring awakening - Steering principles behind the phenology of vernal ice algal blooms. Prog. Oceanogr. 139, 151–170.
Leu, E., Søreide, J.E., Hessen, D.O., Falk-Petersen, S., Berge, J., 2011. Consequences of changing sea-ice cover for primary and secondary producers in the European Arctic shelf seas: Timing, quantity, and quality. Prog. Oceanogr. 90, 18–32.
Leu, E., Wiktor, J., Søreide, J.E., Berge, J., Falk-Petersen, S., 2010. Increased irradiance reduces food quality of sea ice algae. Mar. Ecol. Prog. Ser. 411, 49–60.
Leventer, A., 2008. Particulate Flux from Sea Ice in Polar Waters. In: Thomas, D.N., Dieckmann, G. (Eds.), Sea Ice. ed. Blackwell, pp. 303–332.
Li, W.K.W., McLaughlin, F.A., Lovejoy, C., Carmack, E.C., 2009. Smallest algae thrive as the arctic ocean freshens. Science (80-.). 326, 539.
Lundsgaard, C., 1999. Sources of settling material : aggregation and zooplankton mediated fluxes in the Gulf of Riga. J. Mar. Syst. 23, 197–210.
Luneva, M.V., Aksenov, Y., J. D. Harle, and J.T.H., 2015. The effects of tides on the water mass mixing and sea ice in the Arctic Ocean. J. Geophys. Res. Ocean. 120, 6669–6699.
Lutter, S., Taasen, P., Hopkins, E., Smetacek, V., 1989. Phytoplankton Dynamics and Sedimentation Processes During Spring and Summer in Balsfjord, Northern Norway. Polar Biolo 10, 113–124.
Malmgren, F., 1927. On the properties of sea-ice. Nor. North Polar Exped. “Maud” 1918–1925 1, 1–67.
Medlin, L.K., Hasle, G.R., 1990. Some Nitzschia and related diatom species from fast ice samples in the Arctic and Antarctic. Polar Biol. 10, 451–479.
Medlin, L.K., Priddle, J., 1991. Polar marine diatoms (1990)., British An. ed, Antarctic Science. Natural Environment Research Council.
Meire, L., Mortensen, J., Rysgaard, S., Bendtsen, J., Boone, W., Meire, P., Meysman, F.J.R.,

2016. Spring bloom dynamics in a subarctic fjord influenced by tidewater outlet glaciers (Godthåbsfjord, SW Greenland). J. Geophys. Res. C Ocean. 121, 1581–1592.
Melnikov, I.A., Kolosova, E.G., Welch, H.E., Zhitina, L.S., 2002. Sea ice biological communities and nutrient dynamics in the Canada Basin of the Arctic Ocean. Deep. Res. Part I Oceanogr. Res. Pap. 49, 1623–1649.
Meteorologisk institutt (MET), 2020. Eklima [WWW Document]. Weather data. URL http://eklima.met.no/wsKlima/start/start_en.html (accessed 4.1.19).
Michel, C., Legendre, L., Ingram, R.G., Gosselin, M., Levasseur, M., 1996. Carbon budget of sea-ice algae in spring: Evidence of a significant transfer to zooplankton grazers. J. Geophys. Res. 101, 345–360.
Miklasz, K.A., Denny, M.W., 2010. Diatom sinking speeds : Improved predictions and insight from a modified Stokes ' law. Limnol. Oceanogr. 55, 2513–2525.
Mundy, C.J., Ehn, J.K., Barber, D.G., Michel, C., 2007. Influence of snow cover and algae on the spectral dependence of transmitted irradiance through Arctic landfast first-year sea ice. J. Geophys. Res. Ocean. 112, 1–10.
Niemi, A., Michel, C., 2015. Temporal and spatial variability in sea-ice carbon:nitrogen ratios on canadian arctic shelvestemporal and spatial variability in sea-ice carbon: Nitrogen ratios. Elementa 3, 1–12.
Niemi, A., Michel, C., Hille, K., Poulin, M., 2011. Protist assemblages in winter sea ice: Setting the stage for the spring ice algal bloom. Polar Biol. 34, 1803–1817.
Noji, T.T., Noji, C.I., Barthelee, K., 1993. Pelagic -benthic coupling during the onset of winter in a northern Norwegian fjord . Carbon flow and fate of suspended particulate matter. Mar. Ecol. Prog. Ser. 93, 89–99.
NVE, 2020. Norwegian Water Resources and Energy Directorate [WWW Document]. URL http://nve.no (accessed 9.20.03).
Okolodkov, Y., 1997. Sea-ice algae. Scientific Cruise Report of the Arctic Expedition ARK-XI1112 of RV "Polarstern" in 1997.
Olsen, L.M., Laney, S.R., Duarte, P., Kauko, H.M., Fernández-Méndez, M., Mundy, C.J., Rösel, A., Meyer, A., Itkin, P., Cohen, L., Peeken, I., Tatarek, A., Różańska-Pluta, M., Wiktor, J., Taskjelle, T., Pavlov, A.K., Hudson, S.R., Granskog, M.A., Hop, H., Assmy, P., 2017. The seeding of ice algal blooms in Arctic pack ice: The multiyear ice seed repository hypothesis. J. Geophys. Res. Biogeosciences 122, 1529–1548.
Osuch, M., Wawrzyniak, T., 2017. Inter- and intra-annual changes in air temperature and precipitation in western Spitsbergen. Int. J. Climatol. 37, 3082–3097.
Passow, U., 1991. Species-specific sedimentation and sinking velocities of diatoms. Mar. Biol. 455, 449–455.
Perovich, D.K., 1990. Theoretical estimates of light reflection and transmission by spatially complex and temporally varying sea ice covers. J. Geophys. Res. 95, 9557.
Persson, E., Shepherd, H., Fredheim, K., Haas, L.-M., Kasbauer, R., 2019. Technical report on Sea Ice Biology. Longyearbyen, Svalbard.
Poulin, M., Cardinal, A., 1982. Sea ice diatoms from Manitounuk Sound, southeastern Hudson Bay (Quebec, Canada). I. Family Naviculaceae. Can. J. Bot. 60, 1263–1278.
Poulin, M., Cardinal, A., 2011. Sea ice diatoms from Manitounuk Sound, southeastern Hudson Bay (Quebec, Canada). I. Family Naviculaceae. Can. J. Bot. 60, 1263–1278.
Poulin, M., Daugbjerg, N., Gradinger, R., 2011. The pan-Arctic biodiversity of marine pelagic and sea-ice unicellular eukaryotes : a first-attempt assessment. Mar. biodiv 41, 13–28.
Rachold, V., Eicken, H., Gordeev, V. V., Grigoriev, M.N., Hubberten, H.-W., Lisitzin, A.P., Shevchenko, V.P., Schirrmeister, L., 2004. Modern Terrigenous Organic Carbon Input to the Arctic Ocean. In: The Organic Carbon Cycle in the Arctic Ocean.

Ratkova, T.N., Wassmann, P., 2005. Sea ice algae in the White and Barents seas: Composition and origin. Polar Res. 24, 95–110.
Redfield, A., Ketchum, B., Richards, F., 1963. The influence of organisms on the composition of sea-water. In: MN, H. (Ed.), The Sea. John Wiley, New York, pp. 26–77.
Reigstad, M., Wassmann, P., 1996. Importance of advection for pelagic-benthic coupling in north Norwegian fjords. Sarsia 80:4, 245–257.
Riebesell, U., Schloss, I.R., Smetacek, V., 1991. Aggregation of algae released from melting sea ice : implications for seeding and sedimentation. Polar Biol. 11, 239–248.
Riedel, A., Michel, C., Gosselin, M., LeBlanc, B., 2008. Winter-spring dynamics in sea-ice carbon cycling in the coastal Arctic Ocean. J. Mar. Syst. 74, 918–932.
Rózańska, M., Gosselin, M., Poulin, M., Wiktor, J.M., Michel, C., 2009. Influence of environmental factors on the development of bottom ice protist communities during the winter-spring transition. Mar. Ecol. Prog. Ser. 386, 43–59.
Sakshaug, E., Johnsen, G., Kristiansen, S., Von, C., Rey, F., Slagstad, D., Thingstad, F., 2009. Ecosystem Barents Sea. In: Ecosystem Barents Sea. p. 587.
Screen, J.A., 2014. Arctic amplification decreases temperature variance in northern mid- to high-latitudes. Nat. Clim. Chang. 4, 577–582.
Screen, J.A., Simmonds, I., 2010. The central role of diminishing sea ice in recent Arctic temperature amplification. Nature 464, 1334–1337.
Shestov, A., Wrangborg, D., Marchenko, A., 2015. Hydrology of Braganzavågen under ice-covered conditions. In: Port and Ocean Engineering under Arctic Conditions.
Skarðhamar, J., Svendsen, H., 2010. Short-term hydrographic variability in a stratified Arctic fjord Short-term hydrographic variability in a stratified Arctic fjord. Geol. Soc. Spec. Publ. 344, 51–60.
Smayda, T.J., 1971. Normal and accelerated sinking of phytoplankton in the sea. Mar. Geol. 11, 105–122.
SMHI, 2020. Nordic Microalgae (developped by the Swedish Meterological and Hydrological Institute) [WWW Document]. URL http://nordicmicroalgae.org/ (accessed 3.24.20).
Smith, R., Anning, J., Clement, P., Cota, G., 1988. Abundance and production of ice algae n Resolute Passage, Canadian Arctic. Mar. Ecol. Prog. Ser. 48, 251–263.
Smith, R.E.H., Gosselin, M., Kudoh, S., Robineau, B., Taguchi, S., 1997. DOC and its relationship to algae in bottom ice communities. J. Mar. Syst. 11, 71–80.
Smith, R.W., Bianchi, T.S., Allison, M., Savage, C., Galy, V., 2015. High rates of organic carbon burial in fjord sediments globally. Nat. Geosci.
Smoła, Z.T., Kubiszyn, A.M., Różańska, M., Tatarek, A., Wiktor, J.M., 2018. Protists of arctic sea ice. GeoPlanet Earth Planet. Sci. 133–146.
Søgaard, D.H., Thomas, D.N., Rysgaard, S., Glud, R.N., Norman, L., Kaartokallio, H., Juul-Pedersen, T., Geilfus, N.X., 2013. The relative contributions of biological and abiotic processes to carbon dynamics in subarctic sea ice. Polar Biol. 36, 1761–1777.
Søreide, J.E., Carroll, M.L., Hop, H., Ambrose, W.G., Hegseth, E.N., Falk-Petersen, S., 2013. Sympagic-pelagic-benthic coupling in Arctic and Atlantic waters around Svalbard revealed by stable isotopic and fatty acid tracers. Mar. Biol. Res. 9, 831–850.
Søreide, J.E., Leu, E.V.A., Berge, J., Graeve, M., Falk-Petersen, S., 2010. Timing of blooms, algal food quality and Calanus glacialis reproduction and growth in a changing Arctic. Glob. Chang. Biol. 16, 3154–3163.
Stoecker, D., Gustafson, D., Merrell, J., Black, M., Baier, C., 1997. Excystment and growth of chrysophytes and dinoflagellates at low temperatures and high salinities in Antarctic Sea-ice. J. Phycol. 33, 585–595.
Sturm, M., Massom, R.A., 2016. Snow in the sea ice system: Friend or foe? In: Thomas, D.N.

(Ed.), Sea Ice: Third Edition.
Syvertsen, E.E., 1991. Ice algae in the Barents Sea: types of assemblages, origin, fate and role in the ice-edge phytoplankton bloom. Polar Res. 10, 277–288.
Syvitski, J.P.M., Burrell, D.C., Skei, J.M., 1987. Fjords: Processes and Products. Springer-Verlag, N.Y.
Tamelander, T., Reigstad, M., Hop, H., Ratkova, T., 2009. Ice algal assemblages and vertical export of organic matter from sea ice in the Barents Sea and Nansen Basin (Arctic Ocean). Polar Biol. 32, 1261–1273.
Thomas, D., 2012. Sea ice. In: Elanor M. Bell (Ed.), Life at Extremes: Environments, Organisms and Strategies for Survival. CABI, Wallingford, Oxfordshire, United Kingdom, pp. 62–80.
Thornton, S.F., McManus, J., 1994. Application of Organic Carbon and Nitrogen Stable Isotope and CN Ratios as Source Indicators in Estuarine Systems Evidence from the Tay Estuary. Estuar. Coast. Shelf Sci. 38, 219–233.
Throndsen, J., R, H.G., Tangen, K., 2007. Phytoplankton of Norwegian Coastal Waters. Almater Forlag, Oslo.
Turner, J.T., 2002. Zooplankton fecal pellets, marine snow and sinking phytoplankton blooms. Aquat. Microb. Ecol. 27, 57–102.
Utermöhl, H., 1958. Zur Vervollkommnung der quantitativen Phytoplankton-Methodik. SIL Commun. 1953-1996.
Vader, A., Marquardt, M., Meshram, A.R., Gabrielsen, T.M., 2014. Key Arctic phototrophs are widespread in the polar night. Polar Biol. 38, 13–21.
Von Quillfeldt, C.H., 2000. Common diatom species in Arctic spring blooms: Their distribution and abundance. Bot. Mar. 43, 499–516.
Von Quillfeldt, C.H., 2001. Identification of some easily confused common diatom species in arctic spring blooms. Bot. Mar. 44, 375–389.
Wassmann, P., Andreassen, I., Reigstad, M., Slagstad, D., 1996. Pelagic-benthic coupling in the Nordic Seas: The role of episodic events. Mar. Ecol. 17, 447–471.
Wassmann, P., Olli, K., Riser, C.W., Svensen, C., 2003. Ecosystem Function, Biodiversity and Vertical Flux Regulation in the Twilight Zone. In: Marine Science Frontiers for Europe. pp. 279–287.
Wassmann, P., Ratkova, T., Andreassen, I., Vernet, M., Pedersen, G., Rey, F., 1999. Spring bloom development in the marginal ice zone and the central Barents Sea. Mar. Ecol. 20, 321–346.
Wassmann, P., Reigstad, M., 2011. Future Arctic Ocean seasonal ice zones and implications for pelagic-benthic coupling. Oceanography 24, 220–231.
Wiedmann, I., Reigstad, M., Marquardt, M., Vader, A., Gabrielsen, T.M., 2016. Seasonality of vertical flux and sinking particle characteristics in an ice-free high arctic fjord-Different from subarctic fjords? J. Mar. Syst. 154, 192–205.
Wiedmann, I., Reigstad, M., Sundfjord, A., Basedow, S., 2014. Potential drivers of sinking particle's size spectra and vertical flux of particulate organic carbon (POC): Turbulence, phytoplankton, and zooplankton. J. Geophys. Res. Ocean. 119, 6121–6139.
Wiktor, J.M., Okolodkov, J.B., Vinogradova, K.L., 1995. Atlas of the Marine Flora of Southern Spitsbergen. Institute of Oceanology of the Polish Academy of Sciences.
Yentsch, C.S., 1965. Distribution of chlorophyll and phaeophytin in the open ocean. Deep. Res. 12, 653–666.
Zajączkowski, M., Nygård, H., Hegseth, E.N., Berge, J., 2010. Vertical flux of particulate matter in an Arctic fjord: The case of lack of the sea-ice cover in Adventfjorden 2006-2007. Polar Biol. 33, 223–239.

7 Appendix

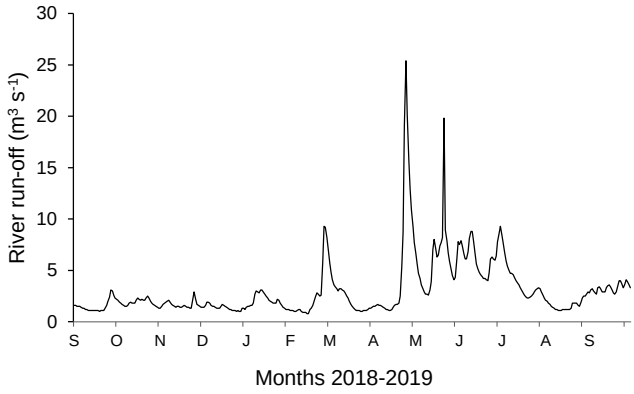

Figure A 1. River run-off (in m3 s^{-1}) into Ramfjorden between September 2019 and 2020. Retrieved from http://nve.no in March 2020.

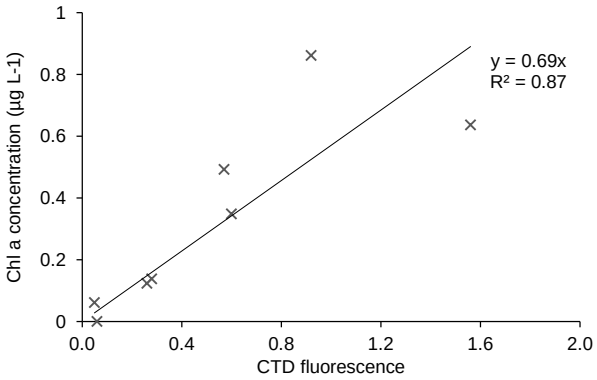

Figure A 2. Linear trendline of Chl a concentration (µg L^{-1}) water sample agaisnt the fluorometer data for the same specific sampled depth (1, 5, 15 and 30 m) at VMF. The linear trendline (equation with the slope coefficient α and R2 presented in inset) was forced through the origin, to prevent the negative values when calibrated the fluorescence data.

Table A 1 Respective numbers of full/sections ice cores extracted for each parameters at each sampling day.

Parameters / Station	Chl *a*/Phaeo	POC/PON	Microalgae community	Physics (salinity + temperature)
RMF1	2	3	1	2
RMF2	3	3	1	2
VMF1	3 + 1 (section 3-10 cm) + 2 (section 0-3 cm)			2
VMF2	3			2

Table A 2. Weather variables during March in Tromsø (Station Langnes and Breivikeidet) and April 2019 in Svalbard, Station Sveagruva I and Longyearbyen, Lufthavn). Data retrieved from Eklima. The variables presented are daily average of : air temperature (°C), pre precipitation (mm), snow depth (cm), wind speed (m s^{-1}) and wind direction (degrees). The grey shaded boxes represent the field sampling days (RMF1, RMF2, VMF1 and VMF2).

	Station : Tromsø, Langnes					Station : Breivikeidet
Day of March	Mean temperature (°C)	Precipitation (mm)	Snow depth (cm)	Wind speed (m/s)	Direction (degrees)	Snow depth (cm)
1	-3.9	2.5	17	6.3	103	95
2	-7.3	0.5	15	3.0	119	nd
3	-7.0	nd	14	7.5	202	nd
4	-7.7	10	35	5.1	183	109
5	-7.4	3	30	7.3	197	108
6	-4.5	15	40	4.4	244	120
7	-6.3	8	43	3.3	192	nd
8	-9.9	nd	43	1.8	96	nd
9	-5.0	0.1	37	5.6	26	115
10	-6.5	nd	37	3.2	34	113
11	-7.3	nd	33	5.6	211	nd
12	-3.4	6	43	6.4	212	121
13	-5.8	8	59	2.9	113	124
14	-2.9	1	55	3.1	147	121
15	-3.2	0	53	1.4	160	119
16	-2.5	3	53	5.3	216	126
17	-2.5	3.6	50	5.6	140	125
18	-5.2	0	50	1.4	151	122
19	-2.5	nd	50	6.1	183	nd
20	2.2	0	50	8.3	194	119
21	2.0	1	50	5.9	228	119
22	1.3	8	45	9.4	236	128
23	3.6	3.2	37	8.5	187	122
24	0.8	0.3	35	2.9	205	116
25	-1.9	7.3	35	3.5	143	121
26	-2.2	12.5	49	3.2	192	139
27	0.9	5	50	9.2	212	140
28	2.2	11.5	42	8.9	201	nd
29	0.9	11.5	40	10.0	235	126
30	-0.4	6.4	41	7.9	197	141
31	-1.0	13.5	54	3.1	223	160

nd no data

	Station : Sveagruva I		Station : Longyearbyen, Lufthavn
Day of April	Mean temperature (°C)	Precipitation (mm)	Snow depth (cm)
1	-18.6	0	15
2	-14.2	nd	15
3	-14.2	0.1	14
4	-16.7	0.2	18
5	-4.5	2.4	14
6	-6.4	0	14
7	-15.2	nd	14
8	-20.8	nd	14
9	-8.7	0	14
10	0.1	1.7	15
11	-7.6	1.3	17
12	-7.1	nd	13
13	-3.1	0.3	13
14	-0.2	0	14
15	-0.6	1	13
16	2.6	1	11
17	2.8	0	8
18	3.8	4	5
19	3.5	1.6	3
20	1.0	6.5	3
21	-8.5	2.6	3
22	-10.9	nd	3
23	-7.9	nd	3
24	-3.8	nd	3
25	0.1	2.1	6
26	-2.1	4.3	12
27	-1.5	0.2	8
28	0.5	0.7	11
29	0.8	nd	8
30	-6.3	0.3	10

Table A 3. Chl a/Phaeo, C/N (=POC/PON) and POC/Chl a ratios for the ice core, suspended biomass and sedimented biomass at the different stations (RMF1, RMF2, VMF1 and VMF2) for the different ice sections (e.g., 0-3 an 3-10 cm) and depth (e.g., 1 and 5m).

		RMF1			RMF2			VMF1			VMF2		
	Sections (cm)	Chl a/Phaeo	C/N	POC/Chl a	Chl a/Phaeo	C/N	POC/Chl a	Chl a/Phaeo	C/N	POC/Chl a	Chl a/Phaeo	C/N	POC/Chl a
Ice core	60-TOP							2.00	*nd*	*nd*	1.38	13.6	786
	30-TOP/40-60	1.68	15.1	1879	1.00	21.2	665	0.85	*nd*	*nd*	1.00	15.4	1081
	20-30/20-40	1.50	10.0	423	1.20	10.3	255	0.64	*nd*	*nd*	0.89	12.6	864
	10-20	1.80	8.8	436	1.21	12.9	206	1.11	*nd*	*nd*	0.73	13.8	391
	3-10	1.60	9.6	715	1.30	13.1	261	1.70	*nd*	*nd*	1.41	14.4	492
	0-3	1.51	19.8	985	1.13	12.8	649	2.28	*nd*	*nd*	1.72	12.6	180
		RMF1			RMF2			VMF1			VMF2		
	Depth (m)	Chl a/Phaeo	C/N	POC/Chl a	Chl a/Phaeo	C/N	POC/Chl a	Chl a/Phaeo	C/N	POC/Chl a	Chl a/Phaeo	C/N	POC/Chl a
Suspended biomass	1	1.00	5.9	438	2.11	4.8[a]	50[a]	0.67	7.8	204	1.00	9.1	281
	5	1.50	5.3	107	1.22	3.6[a]	42[a]	0.71	7.1	316	0.82	7.1	176
	15	1.00	12.3	408	1.25	2.9[a]	62[a]	1.00	8.3	322	0.90	7.1	251
	30	0.00	9.4	*nd*	0.01	1.1[a]	*nd*	0.00	10.4	*nd*	1.00	8.0	360
		RMF1			RMF2			VMF1			VMF2		
	Depth (m)	Chl a/Phaeo	C/N	POC/Chl a	Chl a/Phaeo	C/N	POC/Chl a	Chl a/Phaeo	C/N	POC/Chl a	Chl a/Phaeo	C/N	POC/Chl a
Sedimented biomass	1	2.00	12.4	447	0.81	7.8	180	0.76	12.4	435	0.87	6.8	168
	5	1.46	7.9	113	1.00	21.2	200	0.70	16.5	666	0.82	5.8	185
	15	1.38	11.6	305	0.50	8.7	371	0.60	18.4	1264	0.79	10.2	405
	30	1.00	8.1	511	0.67	10.5	366	0.63	17.5	1434	0.73	9.9	1071

nd no data (samples not analyzed or due to wrong concentrations obtained from the Chl *a* fluorometer, under detection level)

[a] data shown are wrong due to too low POC/PON concentrations obtained from the CE440 CHN Elemental Analyzer

Table A 4. Integrated Chl a and POC concentrations (mg m-2) in the whole ices cores and in the water column (0 – 30 m) at the field sampling days (RMF1, RMF2, VMF1 and VMF2).

	Compartment	RMF1	RMF2	VMF1	VMF2
Integrated mg Chl *a* m^{-2}	Sea-ice	0.13	0.16	1.65	1.57
	Water column	3.2	11.6	5.0	8.4
Integrated mg POC m^{-2}	Sea-ice	89	50[a]	*nd*	682
	Water column	848	*nd*	2213	1870

nd no data

[a] data shown are wrong due to too low POC/PON concentrations obtained from the CE440 CHN Elemental Analyzer

Table A 5. Tides table chart modified from Kartverket. Used to to compare current time with Ramfjorden station, March 2019. Station Ramfjorden (69°33' N 19°04' E). Table retrieved from https://www.kartverket.no/

Kartverket

Ramfjorden

69°33' N 19°04' E

Observations, predictions, weather effect and forecast.

March 2019					March 2019									
	Time	Obs	Pre	Wea	For		Time	Obs	Pre	Wea	For		Time	Obs	Pre	Wea	For
1 Fr	0329		114			19 Tu	1204		273								
	0949		220				1823		35								
	1616		109				0037		276								
	2224		214			20 We	0643		42								
2 Sa	0441		109				1254		292								
	1054		229				1911		16								
	1719		98			21 Th	0125		290								
	2324		223				0729		29								
3 Su	0536		98				1340		305								
	1145		241				1955		6								
	1806		84			22 Fr	0209		296								
4 Mo	0011		235				0812		23								
	0620		86				1424		309								
	1227		253				2038		6								
	1845		72			23 Sa	0251		295								
5 Tu	0051		246				0854		25								
	0657		75				1506		304								
	1304		263				2120		15								
	1920		62			24 Su	0332		287								
6 We	0126		255				0936		33								
	0730		67				1548		291								
	1337		270				2201		31								
	1951		54			25 Mo	0412		273								
7 Th	0159		261				1018		47								
	0800		61				1630		272								
	1409		275				2243		52								
	2021		49			26 Tu	0453		256								
8 Fr	0230		265				1102		64								
	0831		58				1714		250								
	1440		277				2326		74								
	2051		47			27 We	0538		238								
9 Sa	0301		266				1151		83								
	0902		57				1804		227								
	1511		276			28 Th	0016		95								
	2123		49				0632		222								
10 Su	0332		264				1253		99								
	0935		61				1910		208								
	1543		271			29 Fr	0120		111								
	2156		54				0745		210								
11 Mo	0404		259				1415		108								
	1010		67				2036		200								
	1617		263			30 Sa	0248		118								
	2232		62				0910		209								
12 Tu	0440		251				1543		106								
	1049		76				2156		203								
	1654		252			31 Su	0510		112								
	2312		72				1121		217								
13 We	0520		242				1749		95								
	1133		87				2358		213								
	1738		239														
	2359		84														
14 Th	0609		231														
	1228		97														
	1835		227		-> 15:00	- 20:00 = higher current under ice											
15 Fr	0058		94														
	0715		223		-> 5:00	- 8:00 = higher current under ice											
	1338		103														
	1951		219														
16 Sa	0214		100														
	0838		222														
	1503		99														
	2121		222														
17 Su	0339		95														
	1001		233														
	1624		83														
	2240		237														
18 Mo	0454		80														
	1108		252														
	1729		59		-> 16:00	- 19:00 = mild current bottom layer											
	2343		257														
	0553		60		-> 4:00	- 8:00 = mild current bottom layer											

Table A 6. Tides table chart modified from Kartverket. Used to compare with Van Mijenfjorden station, April 2019. Station Ny-Ålesund (78°13' N 15°39' E). Table retrieved from https://www.kartverket.no/.

Kartverket

NY-ÅLESUND

78°13' N 15°39' E

Observations, predictions, weather effect and forecast.

April 2019					April 2019									
Time	Obs	Pre	Wea	For	Time	Obs	Pre	Wea	For	Time	Obs	Pre	Wea	For
1 Mo	0552	66			19 Fr	1400	185							
	1209	144				2015	7							
	1837	52				0229	178							
2 Tu	0044	136			20 Sa	0831	15							
	0641	56				1443	187							
	1254	153				2055	6							
	1915	43			21 Su	0308	181							
3 We	0123	146				0913	14							
	0720	47				1524	184							
	1331	161				2134	9							
	1949	35			22 Mo	0348	179							
4 Th	0158	154				0954	17							
	0755	39				1606	176							
	1404	167				2214	17							
	2019	28			23 Tu	0428	173							
5 Fr	0228	161				1036	25							
	0827	34				1648	164							
	1435	171				2253	28							
	2046	24			24 We	0509	165							
6 Sa	0257	165				1120	35							
	0856	30				1731	150							
	1504	173				2334	40							
	2113	21			25 Th	0552	155							
7 Su	0325	168				1207	47							
	0926	28				1819	136							
	1534	173			26 Fr	0019	54							
	2142	21				0641	144							
8 Mo	0354	169				1303	59							
	0958	29				1916	123		-> 15:00 - 21:00 = higher current under ice					
	1606	170			27 Sa	0112	66							
	2214	23				0743	135		-> 00:00 : 10:00 = higher current under ice					
9 Tu	0427	168				1419	66							
	1033	31				2035	115							
	1642	165			28 Su	0228	74							
	2250	28				0907	130							
10 We	0504	164				1558	66							
	1113	37				2210	115							
	1723	156			29 Mo	0404	74							
	2331	35				1030	133		-> 5:00 - 11:00 = higher current under ice and from ~30 m to bottom					
11 Th	0546	157				1710	60							
	1158	44				2321	123							
	1810	146			30 Tu	0516	68							
	0017	46				1130	140							
12 Fr	0635	149				1801	51							
	1252	53			1 We	0012	133							
	1907	135												
13 Sa	0113	56												
	0736	142												
	1401	59												
	2020	127												
14 Su	0226	64												
	0856	138												
	1530	59												
	2154	127												
15 Mo	0356	64												
	1025	144												
	1702	50												
	2321	136												
16 Tu	0517	55												
	1136	155												
	1805	36												
17 We	0020	149												
	0617	43												
	1230	168												
	1852	23												
18 Th	0106	162												
	0705	30												
	1317	179												
	1935	13												
19 Fr	0148	172												
	0749	21												

Table A 7 Microalgae species list observed in the ice and in the water column in Ramfjorden and Van Mijenfjorden.

Group /Class	Species name	RMF - Ice core	RMF - Water column	VMF - Ice core	VMF - Water column
Chaetocerotaceae	*Chaetoceros spp.*		x	x	x
Bacillariophyceae	*Cocconeis sp.*	x			
Bacillariophyceae	*cyclotella choctawhatcheana*	x			
Bacillariophyceae	*Cylindrotheca closterium*	x	x	x	x
Bacillariophyceae	*Diploneis bombus*	x		x	
Bacillariophyceae	*Diploneis littoralis*			x	
Bacillariophyceae	*Entomoneis Kjellmani*			x	x
Bacillariophyceae	*Entomoneis sp cf E paludosa*			x	x
Bacillariophyceae	*Entomoneis sp.*			x	x
Bacillariophyceae	*Eucampia sp.*		x		
Bacillariophyceae	*Eunotia serra*	x			
Bacillariophyceae	*Fragilariopsis sp cf F oceanica*		x	x	
Bacillariophyceae	*Fragilariopsis sp cf F cylindrus*		x	x	
Bacillariophyceae	*Fragilariopsis sp.*		x	x	x
Bacillariophyceae	*Gyrosigma sp cf G sutxbergii*		x	x	x
Bacillariophyceae	*Haslea crucigeroides*			x	x
Bacillariophyceae	*Haslea sp.*			x	x
Bacillariophyceae	*Navicula spp.*	x	x	x	x
Bacillariophyceae	*Navicula cf algida*		x		
Bacillariophyceae	*Navicula sp cf N pelagica*			x	
Bacillariophyceae	*Navicula sp cf N algida*		x	x	x
Bacillariophyceae	*Navicula sp cf N directa*			x	x
Bacillariophyceae	*Navicula sp cf N glaciei*			x	
Bacillariophyceae	*Navicula sp cf N kariana*			x	x
Bacillariophyceae	*Navicula sp cf N novadecipiens*				x
Bacillariophyceae	*Navicula sp cf N recurvata*				x
Bacillariophyceae	*Navicula sp cf N septentrionalis*	x	x		x
Bacillariophyceae	*Navicula sp cf N spicula*			x	x
Bacillariophyceae	*Navicula sp cf N transitans*	x	x	x	x
Bacillariophyceae	*Navicula sp cf N valida*			x	x
Bacillariophyceae	*Navicula sp cf N vanhoeffenii*			x	x
Bacillariophyceae	*Nitzschia sp cf N levissima*	x			
Bacillariophyceae	*Nitzschia sp cf N promare*			x	x
Bacillariophyceae	*Nitzschia sp cf N scabra*		x		
Bacillariophyceae	*Nitzschia frigida/neofrigida*	x	x	x	x
Bacillariophyceae	*Pinnularia sp.*		x		
Bacillariophyceae	*Pleurosigma/Gyrosigma sp.*		x	x	x
Bacillariophyceae	*Stenoneis sp.*			x	x
Bacillariophyceae	*Synedropsis hyperborea*		x	x	x
Bacillariophycidae	*Achnanthes sp.*	x			
Ciliophora	*Lohmanniella oviformis*	x	x		
Ciliophora	*Strombidium indet.*	x			x
Ciliophora	*Tintinnina sp.*	x			
Coscinodiscophyceae	*Leptocylindrus sp.*	x			
Coscinodiscophyceae	*Skeletonema sp.*	x	x		
Coscinodiscophyceae	*Thalassiossira sp.*	x	x		x
Coscinodiscophyceae	*Unidentified centric cells*	x	x	x	x

Table continued from previous column.

Cryptophyceae	*Teleaulax sp cf T amphioxeia*				x
Dictyochophyceae	*Apedinella radians*		x		
Dictyochophyceae	*Dictyocha speculum*		x		x
Dinophyceae	*Alexandrium sp cf A tamarense*		x		x
Dinophyceae	*Gonyaulax sp cf G polygramma*			x	
Dinophyceae	*Gymnodinium sp cf G arcticum*			x	x
Dinophyceae	*Gymnodinium sp cf G irregulare*				x
Dinophyceae	*Gymnodinium sp cf G ostenfeldii*	x		x	x
Dinophyceae	*Gymnodinium sp cf G wulfii*	x		x	x
Dinophyceae	*Gyrodinium sp cf G fusiforme*		x	x	x
Dinophyceae	*Gyrodinium sp cf G lachryma*		x	x	x
Dinophyceae	*Gyrosigma sp cf G sutxbergii*		x		
Dinophyceae	*Heterocapsa rotundata*		x	x	x
Dinophyceae	*Karlodinium sp cf K micrum*				x
Dinophyceae	*Katodinium glaucum*				x
Dinophyceae	*Lessardia elongata*		x		
Dinophyceae	*Protoperidinium bipes*		x	x	x
Dinophyceae	*Protoperidinium sp.*		x	x	x
Eugleunophyceae	*Eutreptiella sp.*				x
Peranemaceae	*Anisonema sp.*			x	
Prymnesiophyceae	*Algirosphaera sp.*		x		
Pyramimonadophyceae	*Pyramimonas spp.*		x	x	x
Cryptophyceae	*Leucocryptos marina*		x	x	x
Dinophyceae	*Gymnodinium spp.*	x	x	x	x
Cryptophyceae	*Cryptomonas spp.*	x	x	x	x
Bacillariophyceae	*Unidentified pennate cells*	x	x	x	x
	Flagellates indet.	x	x	x	x

Table A 8. Number of taxa per station (RMF1, RMF2, VMF1 and VMF2) for each compartment (Ice, water column, and from the sediment trap) per ice core sections (cm) and depth (m).

		Nb taxa per station			
	Depth (m)/ Section (cm)	RMF1	RMF2	VMF1	VMF2
Ice core	0-3	7	3	28	27
	3-10	9	7	14	18
	10-20	6	10	20	13
	20-30/20-40	10	9		13
	30-TOP/40-60	15	6	12	14
	60-TOP			13	22
Suspended algae	1	18	17	20	30
	5	6	14	24	22
	15	7	13	8	11
	30	6	8	10	8
Sinking algae	1	5	6	15	19
	5	8	10	11	16
	15	6	9	8	16
	30	5	10	8	12